3D LiDAR POINT CLOUD PROCESSING USING STATISTICAL AND MACHINE LEARNING METHODS FOR PRECISION AGRICULTURE

A thesis submitted

in partial fulfilment for the degree of

Doctor of Philosophy

by

REJI J

Department of Earth and Space Sciences

INDIAN INSTITUTE OF SPACE SCIENCE AND TECHNOLOGY

Thiruvananthapuram – 695547

February 2023

CERTIFICATE

This is to certify that the thesis entitled **3D LiDAR POINT CLOUD PROCESSING USING STATISTICAL AND MACHINE LEARNING METHODS FOR PRECISION AGRICULTURE** submitted by Reji J to the Indian Institute of Space Science and Technology, Thiruvananthapuram, in partial fulfilment for the award of the degree of Doctor of Philosophy is a bona fide record of research work carried out by her under my supervision. The contents of this thesis, in full or in parts, have not been submitted to any other Institution or University for the award of any degree or diploma.

Dr. Rama Rao Nidamanuri

Professor (Remote sensing & Image processing)

Supervisor

Thiruvananthapuram

February 2023

Counter signature of HOD with seal

DECLARATION

I declare that this thesis entitled **3D LiDAR POINT CLOUD PROCESSING USING STATISTICAL AND MACHINE LEARNING METHODS FOR PRECISION AGRICULTURE** submitted in partial fulfilment of the degree of Doctor of Philosophy is a record of original work carried out by me under the supervision of Prof. Rama Rao Nidamanuri and has not formed the basis for the award of any other degree or diploma, in this or any other Institution or University. In keeping with the ethical practice in reporting scientific information, due acknowledgements have been made wherever the findings of others have been cited.

Thiruvananthapuram-695547 Reji J

December 2021 (SC17D029)

DEDICATION

This thesis is dedicated to my father

Late Shri R Devarajan

whose invisible presence made me strong at every point in my life.

ACKNOWLEDGEMENTS

It takes a lot of patience and perseverance to get a doctoral degree. I would like to express my gratitude to all the people who stood by my side during the course of the research and writing of the thesis.

I am very fortunate to have Prof. Rama Rao Nidamanuri as my supervisor. Thank you for the immense amount of patience you showed me at each step in my research, even if the results were not positive. Most importantly, the amount of time you have devoted to correcting the manuscripts, even during holidays and late nights. You have always guided me through the course of work, and when I was emotionally and mentally down, the kind of motivation you gave strengthened me to work more towards achieving the results.

Thank you for always being positive when I got the results, and thank you for answering those numerous emails for all my questions. Thank you for patiently correcting the thesis and the invaluable amount of your time you took for this. I would also like to express my gratitude to my supervisor's wife Mrs. Vijaya for her kind gestures and the love she gave me whenever I visited the house regarding the work.

I would like to thank my doctoral committee members Prof. Samir Mandal, Prof. Moosath, Dr. Gyanappazham, and Prof. Anandmayee Tej for their support and encouragement throughout my research. I am extremely grateful to Dr. A M Ramiya for her kindness and for teaching me the processing and managing of LiDAR data. I would like to thank my lab mates and friends, Mr. Sudhanshu Shekar Jha, Mr. Manohar CVSS, Mr. Gyaneshwar, Mr. Suraj Reddy, Mr. Nithin D Pillai, for the help and support they gave me whenever I needed it without any hesitation. I also thank the support provided by the department staff members Ms. Divya, Ms. Shalini, Ms. Aswathy.

The love and support of my family members, especially my mother and husband, gave me immense support to carry forward my work. My mother's motivation and my husband's continuous support have made it possible to carry out my research alongside my married life. Also, I would like to mention my little kid, Mr. Ilesh Panikar, who always made me cheerful and happy during this period. Without them, it would have been practically impossible. I am also thankful to my precious friends – Elizabeth, Dhanya, Anjali, Deepa, Thara, Amrita, Anagha, Chaitanya for always being there for me. I express my sincere gratitude to all my teachers throughout my journey in the teaching-learning process.

Finally, I thank God, the almighty, for His showers of blessings throughout my research work to complete the research successfully.

Reji J

ABSTRACT

Within the context of precision agriculture, site-specific crop management has been emerging as the globally relevant, environmentally sustainable and economically beneficial agronomic paradigm. In pursuing this, field-sensitive optimal agronomic practices related to crop monitoring, management, and intervention procedures are undertaken by acquiring spatially contextual information on inter and intra-field variability of crops' condition and growth. Field-level data on the crop type, growth status and potential trajectories of crops' traits form core information capsules in the decision-making process for arriving at responsive implementation strategies. Optical remote sensing data, both multispectral and hyperspectral, have been widely used for crop classification and biophysical characterization at various scales and spatial extents. However, the limited levels of diversity in the spectral characteristics and lack of structural features in optical remote sensing data constrain discrimination and biophysical characterization of crops with reasonably good accuracy and spatial scale.

LiDAR remote sensing is an evolving approach that offers distinct structural features of objects. Understanding the potential of LiDAR data (generally called point cloud) for discrimination and biophysical characterization of crops is vital for assessing its relevance in precision agriculture. Terrestrial laser scanner (TLS) offers the possibility of acquiring LiDAR point cloud at the plant scale in an agricultural field. With an overarching aim of estimating biophysical parameters (plant height, crown area, biomass), discriminating crops at plant level and predictive modelling of crop growth, the objectives of this research are (1) multi-temporal estimation of biophysical parameters of crops at different levels of nitrogen using TLS point cloud, (2) to develop a deep learning (DL) based methodology for multi-crop point cloud classification of crops, (3) examining the potential of fusing TLS point

cloud with high-resolution multispectral satellite data for crop discrimination at different N levels, and (4) to develop a DL based temporal framework for temporal prediction of crop structural parameters.

We have chosen three important vegetable crops that are consumed on a regular basis in India. The crops are considered with different height profile and potential horizontal spread due to lodging. Remote sensing based discrimination of crops with reference to nutrient level requires crops exhibiting differential growth profiles. We designed an experimental set-up for growing three different vegetable crops (tomato, eggplant, and cabbage) at different levels of nitrogen on the experimental station of the University of Agricultural Sciences, Bengaluru, India. TLS point clouds are acquired through the growing season. In addition, high-resolution multispectral satellite imagery from the WorldView-III is also acquired at a critical growth stage. The datasets are processed and analyzed using a host of statistical, conventional machine learning, and deep learning methods. The modelling frameworks involve estimating crown area, biomass, object-based crop classification using only LiDAR point cloud, the fusion of LiDAR point cloud and multispectral satellite imagery for crop classification sensitive to different nitrogen levels, and temporal prediction of plant height and crown area. The results are validated with reference ground truth measurements acquired throughout the crop growing season. Results suggest that TLS offers plant/patch level biophysical characterization of crops using LiDAR point cloud with 90% accuracy both by magnitude and direction. On the potential of LiDAR point cloud for crop discrimination, there are two possibilities observed. Point clouds analyzed with the deep machine learning method (CropPointNet) offers relatively high accuracy when the classification is not specific to the N level. The performance of the crop discrimination with explicit sensitivity to N level is reasonably good when the LiDAR point cloud and multispectral imagery are fused. The results from the deep learning model developed

(CropTemporalNet) for predicting the values of plant height and crown area based on the past growth stage(s) are promising. The predictions match well with the estimations from the TLS LiDAR point cloud.

Overall, the observations suggest the potential of LiDAR point cloud a general data source for precision crop discrimination and biophysical characterization. However, field conditions and environmental factors and the methods used for analyses sustainably affect the quality of retrievals. Further studies are recommended for evaluating the generalization potential across farmer's field, models, crops and geographic regions.

TABLE OF CONTENTS

LIST OF FIGURES

LIST OF TABLES

LIST OF ABBREVATIONS

2D	Two Dimension
3D	Three Dimension
3D-FCNN	3D Fully Convolutional Neural Networks
Aka	also known as
ASPRS	American Society for Photogrammetry and Remote Sensing
ASCII	American Standard Code For Information Interchange
BN	Batch Normalization
BNDVI	Blue Normalized Difference Vegetation Index
CHM	Canopy Height Model
ConvLSTM	Convolutional Long Short Term Memory
CNN	Convolutional Neural Network
CNN-LSTM	Convolutional Neural Network- Long Short Term Memory
CSM	Crop Surface Model
DL	Deep Learning
DCN	DeepCropNet
DCNN	Deep Convolutional Neural Network
DGCNN	Dynamic Graph CNN
DGPS	Differential- Global Positioning System
EVI	Enhanced Vegetation Index
3D-FCNN	3D Fully Connected Conditional Random Fields
FACT	Flexible Atmospheric Compensation Technique
FCC	False Colour Composite
FCN	Fully Connected Network
FN	False Negative
FP	False Positive
GPS	Global Positioning System
GKVK	Gandhi Krishi Vigyana Kendra
GNDVI	Green Normalized Difference Vegetation Index
GRU	Gated Recurrent Unit
IFOV	Instantaneous Field of View
IoT	Internet of Things

IoU	Intersection over Union
IR	Infrared
ITC	Individual Tree Crown
K	Potassium
LAI	Leaf Area Index
LASSO	Least Absolute Shrinkage and Selection Operator
LiDAR	Light Detection and Ranging
LSTM	Long Short Term Memory
MDG	Mean Decrease in Gini
ML	Machine Learning
MLP	Multi-layer Perception
MRS	Multi-Resolution Segmentation
N	Nitrogen
NIR	Near Infrared
NDVI	Normalized Difference Vegetation Index
NDWI	Normalized Difference Water Index
OOB	Out-Of-Bag
P	Phosphorous
PTD	Progressive Triangular Irregular Network Densification
R^2	Coefficient of Determination
ReLU	Rectified Linear Unit
RGB	Red-Green-Blue
RMSE	Root Mean Squared Error
RNN	Recurrent Neural Network
RF	Random Forest
SAVI	Soil-Adjusted Vegetation Index
SFM	Structure-From-Motion
SMAPE	Symmetric Mean Absolute Percentage Error
SVM	Support Vector Machine
SVR	Support Vector Regression
TLS	Terrestrial Laser Scanner
TP	True Positive
TIN	Triangular Irregular Network
UAV	Unmanned Ariel Vehicle
UTM	Universal Transverse Mercator
VRT	Variable Rate Technology

VI	Vegetation Index
VWF	Variable Window Filter
WGS	World Geodetic System
WDRVI	Wide Dynamic Range Vegetation Index
XGBoost	eXtreme Gradient Boosting

CHAPTER 1

INTRODUCTION

1.1 Precision agriculture and advances in remote sensing

With the beginning of the green revolution, farming practices in many developed and developing countries witnessed an increased use of chemical fertilizers resulting in adverse environmental conditions such as reduced soil fertility, soil erosion and environmental pollution. Thus a paradigm shift towards a sustainable and environmentally friendly farming practice turns out to be necessary. Site-specific agriculture, also known as precision agriculture, is an innovative approach to farm management that can encourage sustainable agriculture to improve crop performance and productivity. Site-specific farming offers a multi-dimensional approach to better farming practices regarding environment safety, food security, increased throughput, profit and economic growth.

With precision agriculture, the future farms are likely to be managed with much greater spatial and temporal resolution than the present. Precision agriculture needs the application of technologies, methods and principles to detect and manage spatial and temporal variability and simultaneously avoid the usage of chemical fertilizers and decrease environmental footprint and production rate incurred by less farm input (Figure 1.1). This mode of agricultural practice allows farmers to manage variability at scales within a defined farm unit (e.g. section, quarter section) and target specific spatial regions of the farm unit. Spatially variable crop yield can exist due to many factors such as soil nutrient, moisture content, topography, as well as insect and weed infestations that change over time. Site-specific agriculture requires spatial and

temporal management of crops which demand highly time and space sensitive information over large agricultural fields. In agriculture, plant structural and biophysical parameters such as height, crown area, canopy cover, and leaf area index (LAI) are important indicators for assessing crop status, nutrient requirements, and expected yield. Used often in combination, plant height and crown area are vital for estimating other crop parameters such as biomass, yield, stress, and nutrient status.

Traditional methods to retrieve crop traits are often destructive, invasive, and include a high manual amount of labour and are time-consuming. The computation of the above-ground biomass requires cutting the plant at ground level from an area of the plot and then oven-dried and weighted (Pask et al., 2012). These in-situ based measurements are limited to the number of samples that are considered. Also, sampling and the consequent procedures such as drying, manual intervention and transportation are labour intensive.

Figure 1.1: Precision farming depicting spot fertilizer application using sensors (source: www.google.com/images)

With the recent technological advancements encompassing IoT (Internet of Things) and wireless sensor networks in agriculture, variable rate technology (VRT) has enabled farmers to detect crop growth rate, soil health, and within-field crop variability. Even though these technologies are in their advanced stage, they are relatively expensive when the farming area increases to regional or national scale. The large volume of remote sensing data available from different platforms plays a promising role in helping the farmers implement sustainable farming practices for small and large areas.

Remote sensing is a geospatial tool often incorporated into a management strategy for the whole farm operation. It plays a significant role in the agriculture sector in providing crop information such as crop water stress, soil mapping and monitoring, nutrient stress, crop yield, crop growth, different pest and weed attacks in a non-destructive and cost-effective manner (Figure 1.2). Remote sensing data for retrieving different crop information can be collected by various sensors such as spectral sensors, viz hyperspectral and multispectral, laser scanners and radar imaging (Figure 1.3). At the regional to national scale, multispectral remote sensing has traditionally been used for crop mapping, monitoring, and yield predictions (Li and Chen, 2011). Over the last three decades, developments in imaging and sensing technologies have resulted in the operational launch of several sensors with higher spectral and spatial resolutions leading to the evolution of hyperspectral remote sensing. In contrast to multispectral imaging, hyperspectral imagery offers increased spectral definition with continuous and narrow-band spectral signals, capable of capturing information at a finer scale (Sahoo et al., 2015). Mounted on airborne platforms, compact hyperspectral sensors have been used for various applications at different altitudes (Nebiker et al., 2008; Adão et al., 2017). This approach has been extensively tested and applied and the accuracy and precision of various remote sensing-based crop information retrievals have increased continuously (Goel et al., 2003; Nidamanuri et al.,

2007; Nidamanuri and Zbell, 2011). However, contemporary demands for technological developments in agricultural infrastructure, machinery, cropping practices, and nutrient management are increasingly directed at the field and sub-field scale. Rapid developments in on-demand, low-cost data acquisition platforms (e.g. UAV) and miniaturised sensors have fostered remote sensing using close-range measurements (Whitehead and Hugenholtz, 2014; Van Der Meer et al., 2017).

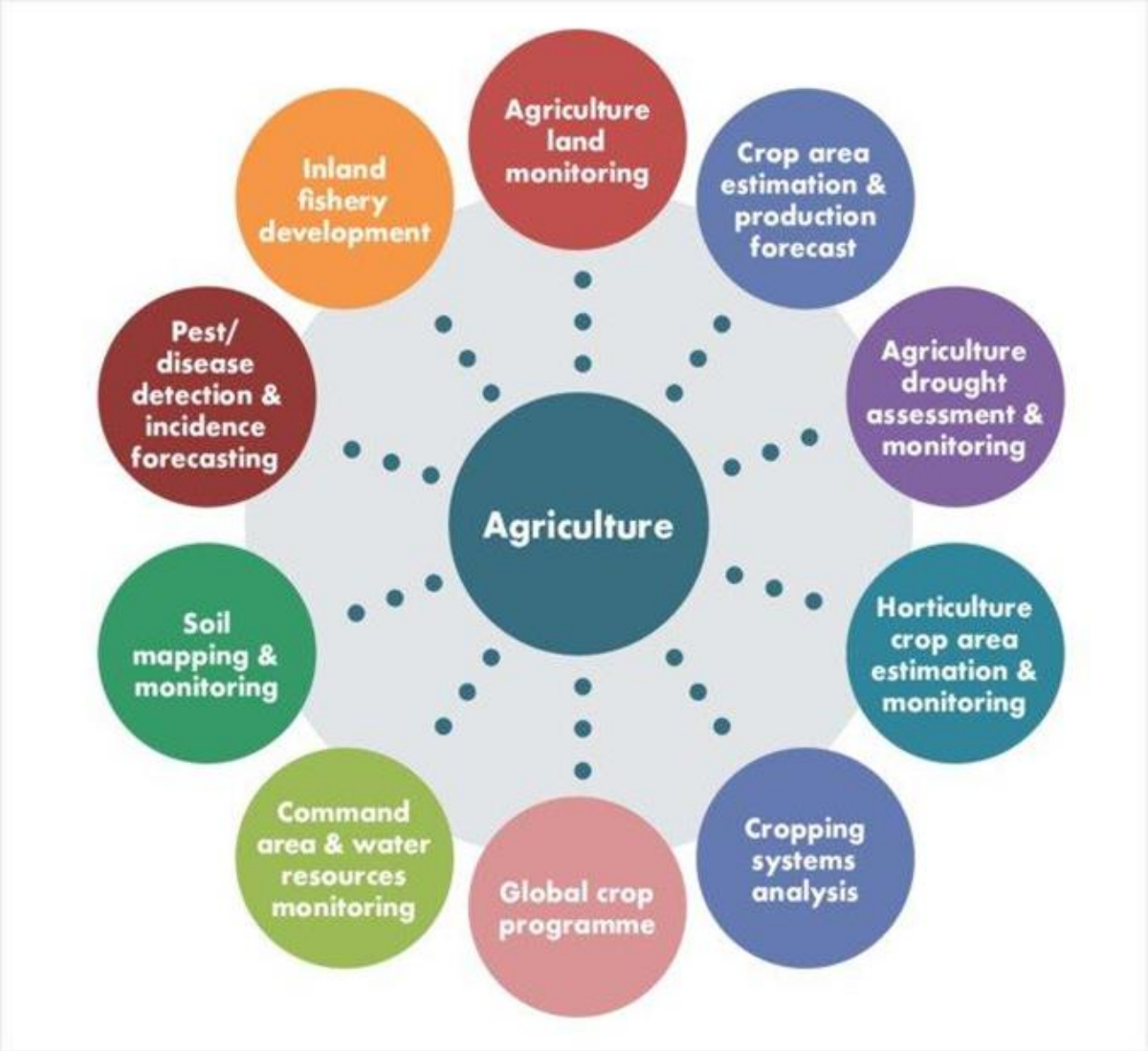

Figure 1.2: Various applications of remote sensing in agriculture (source: Tetteh et al., 2018)

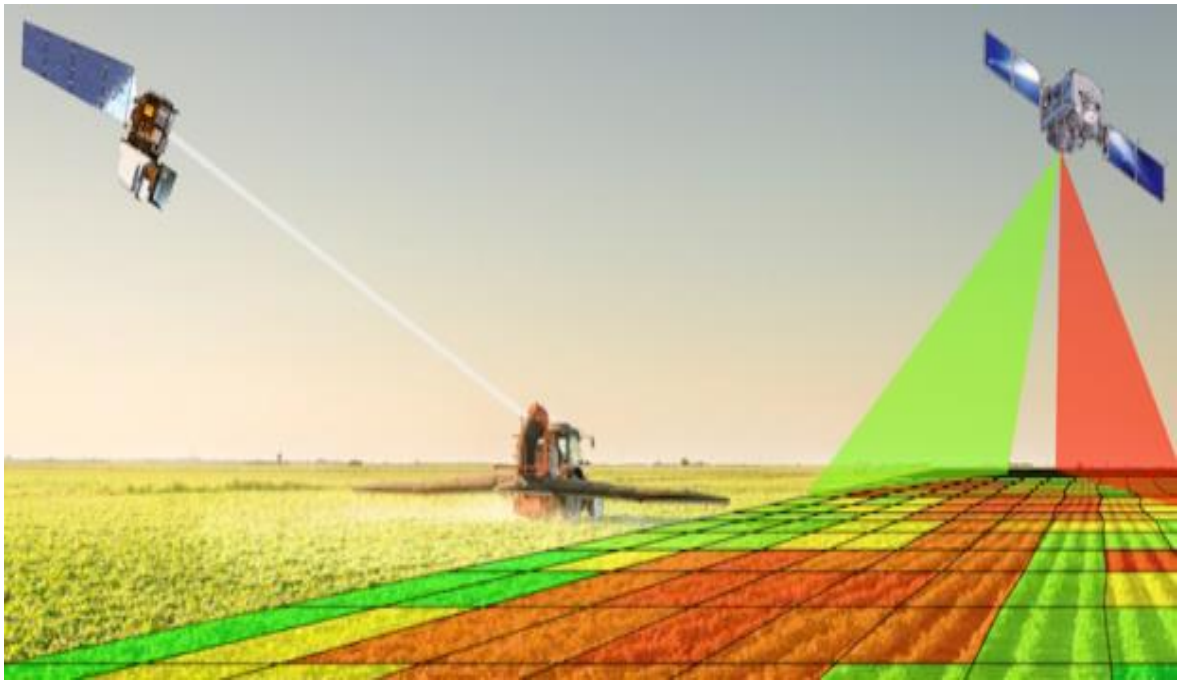

Figure 1.3: Example scenario of satellite-based remote sensing in agriculture applications (source:http://www.cleantechconcepts.com/2018/03/eye-in-the-sky-reduces-nitrogen-use-for-precision-farming/)

1.2 Structural features: 3D remote sensing

Many crucial tasks in agriculture such as fertilization, pest control, and irrigation can benefit from the knowledge of plant geometry (Lin, 2015). The structural attributes are obtained from the 3D information. Plant structural parameters are affected by various biological processes such as growth, photosynthesis, carbon sequestration. The importance of precise quantification of structural crop attributes has necessitated active sensing driven geometrical features in precision agriculture (Figure 1.4).

Although spectral remote sensing approaches are used to infer plant structural attributes, it has inherent limitations. Image is a 2D representation of the environment; therefore, when the 3D surface is converted to a 2D image, it results in the loss of the elevation information due to occlusion as the whole part of the plant is not visible. In order to mitigate this problem,

multi-view image capture (Klukas et al., 2014) at different angles are used to estimate leaf area and biomass using empirical relationships. But these methods pertain to only local application rather than a broader context.

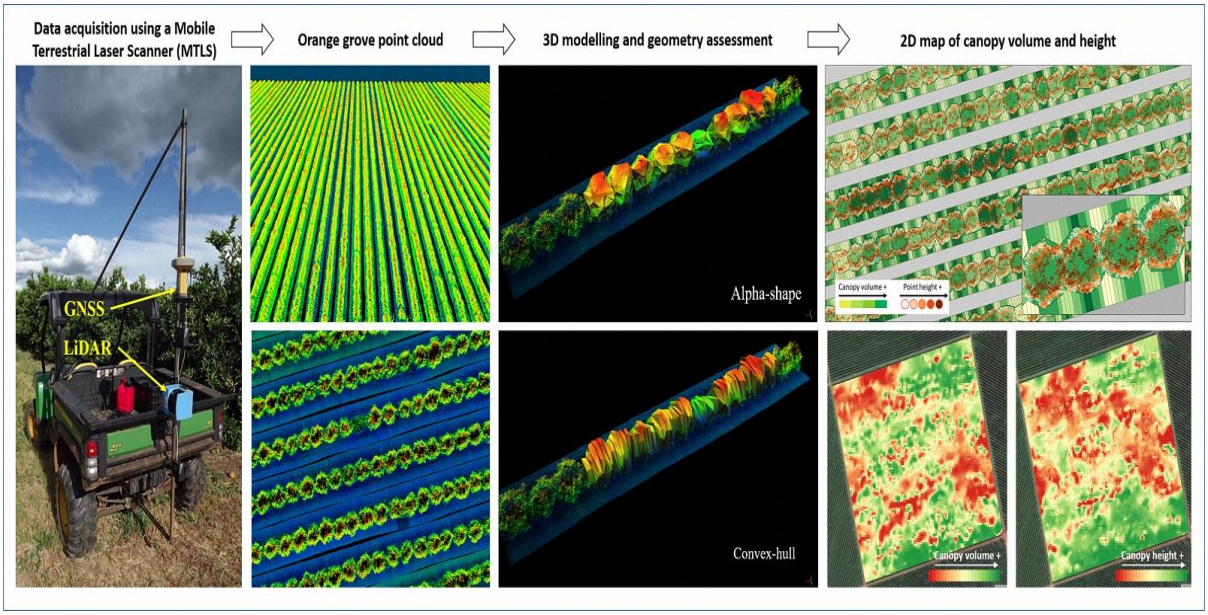

Figure 1.4: Canopy height model (CHM) of the orange orchard developed from the LiDAR data captured using a mobile laser scanner (source: Colaço et al., 2019)

1.3 Stereo imaging as the source of structural features

Multispectral stereo-imaging based remote sensing offers digital surface elevation modelling using the photogrammetry technique of matching stereo pairs and generation of orthophoto (also Structure-From-Motion, SFM) for the generation of 3D point clouds. This method has been used for plant phenotyping for the crops such as soya bean, rice and wheat (Biskup et al., 2007; Pound et al., 2014). The orthophotos are not error-free as they are limited in accuracy, are sensitive to environmental effects, and become computationally complex for big images (Li et al., 2014). Another serious limitation with stereo pair images is that they

cannot penetrate the canopy, hence limiting in providing height profile or local ground reference sensitive structural attributes.

1.4 LiDAR remote sensing data for computing structural attributes

The LiDAR technology, which operates in the near IR region of the electromagnetic spectrum using laser beams, can penetrate the vegetation canopy to certain levels of extent, enabling it to provide 3D information of the canopy. Complementing the spectral data, 3D laser scanning has emerged as the primary source of remote sensing data to directly estimate geometric attributes of land surface features (Lichti et al., 2002). Terrestrial or aerial LiDAR system finds applications in forestry, agriculture, urban mapping etc. (Figure 1.5). Several studies have detailed LiDAR applications in forest studies which include discrete return LiDAR, full-waveform LiDAR and fusion of LiDAR with other remote sensing data (Jones et al., 2010; Pirotti et al., 2010; Clark et al., 2011; Fieber et al., 2015; Nie et al., 2016; Lu et al., 2016). Some forest attributes such as individual tree characteristics (Figure 1.6), canopy height, topography, vertical surface attributes are directly measurable from LiDAR data. In contrast, canopy area, biomass, basal volume, and leaf area index (LAI) are derived from direct measurements.

Figure 1.5: Terrestrial laser scanner for characterisation of vegetable crops (field photographs)

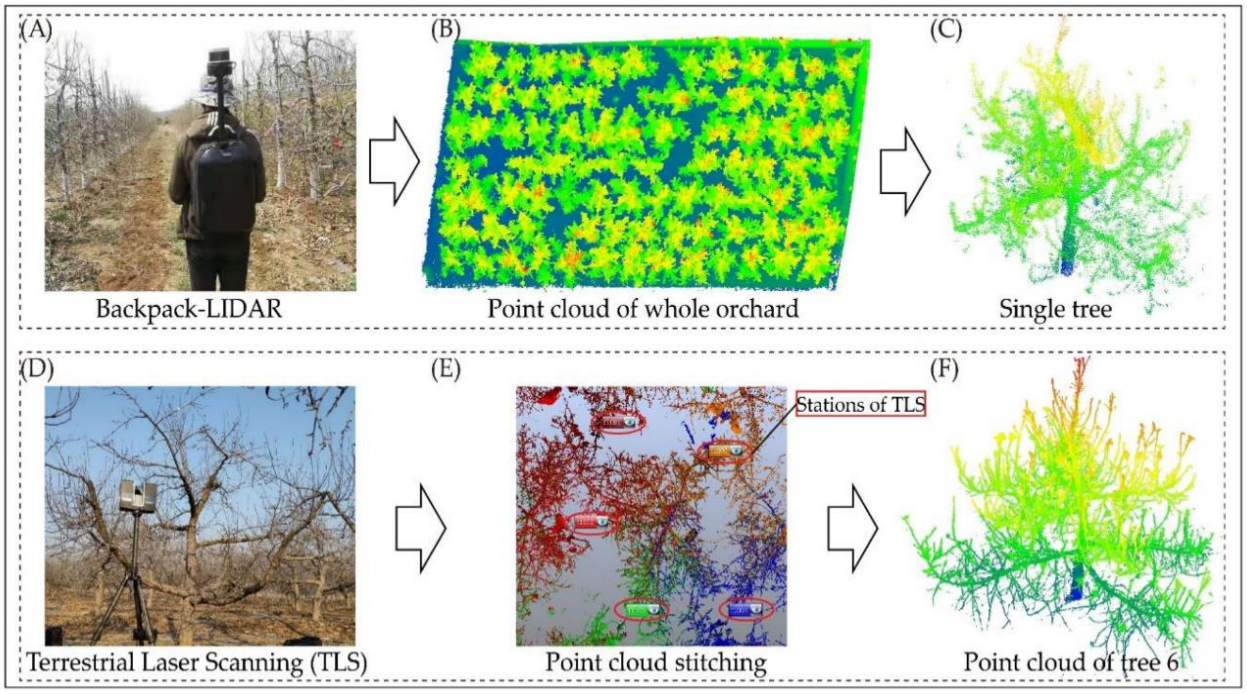

Figure 1.6: Individual tree identification using TLS (source: Zhang et al., 2020)

1.5 Fusion of multispectral and LiDAR point cloud for crop biophysical characterization

Despite having high spatial and spectral resolution, spectral features from optical remote sensing data are limited in providing quantifiable features 'within the field' scale with explicit reference to crop nitrogen (N) status. In a practical scenario, during the crop growth phase, the effects of differential N treatments on crops are observable in terms of differences in crop structural parameters such as height, crown area. The existence of inherent spectral similarities in crops and other vegetation types in the reflectance domain is present even in hyperspectral data. Complementary to the spectral features of multispectral imagery, the LiDAR point cloud offers geometrical features of objects. Precise crop discrimination and biophysical characterization can be achieved from the data level fusion of multispectral and LiDAR data.

1.6 Methods for processing 3D point cloud

Among the various approaches available for the analysis of various types of remote sensing data, supervised learning-based classification is the most comprehensive and broad-based method. Identification and discrimination of crops can be perceived as a classification problem. Given the availability of objective training data, multiple crops discrimination in the LiDAR point cloud can be approached as the supervised classification problem. While classifying point clouds, considerable time is devoted to engineering a reliable set of features which are then fed into a classifier of choice. Generally, such features are usually derived using the knowledge of local neighbourhood relationships. In the case of 3D point cloud data, different geometrical features such as normal, elevation etc., will be taken into account. While these features capture local information, the process is usually time-consuming and requires the application at multiple scales combined with contextual methods to describe the diversity

of objects within a scene adequately. Learning the features of these surfaces will help to retrieve the parameters essential for grouping similar objects successfully. In order to scale the semantic classification task to meet the demands of emerging data volumes – potentially at sub-meter resolution and global in coverage – an efficient, streamlined, and robust model that directly operates on 3D point clouds is needed.

Deep learning (DL) neural network has been evolving as a general method for predicting and labelling various types of data and applications. While the most contemporary deep learning models are amenable to ingest a rasterized point cloud directly, the unstructured nature of the 3D point cloud of natural landscapes limits the direct application of the DL architectures for classification or segmentation in a 3D perspective. Experiments on the adaptation, modification and improvement of sophisticated DL architectures for the classification of point clouds of crops are vital for enhancing the understanding and, potentially, developing generalizable models and methods.

1.7 Temporal prediction of plant parameters

The composition and quantity of nutrients to be supplied for a crop is directly related to the crop growth stage. An important scenario relevant in this regard is the ability of farmers to have the ex-ante prediction of their field crops. This capability helps farmers prepare for the crop growth trajectories and optimize the accumulation and application of interventional resources. Various plant and field level parameters such as nitrogen accumulation, potential crop yield, disease occurrence are key variables explaining the expected crop productivity from crop growth perspectives. Building automated systems for predicting plant parameters by

combining advanced remote sensing data and intelligent methods is gaining attention in agriculture practices.

Few studies have attempted this arena to analyse time-series UAV-based multispectral imagery using a host of machine learning algorithms to predict plant height, leaf nitrogen content, and potential yield (Marcial-Pablo et al., 2019; Zhou et al., 2017). However, these studies have relied upon spectral indices based correlation of plant parameters for obtaining reference data for building up the prediction models. Prediction of broad-based plant parameters such as plant height and the crown area forms a crucial knowledge base in the system for ex-ante assessment of crop growth trajectories. Because of its explicit nature of sensing, the TLS point cloud offers the possibility to compute reference plant attributes for further use by machine learning methods. Due to their vast potential for adaptation and generalizability across sensing mechanisms and parameter selection, DL methods seem the appropriate computational-methodological frameworks for evaluating the possibility of using TLS point cloud for developing a prediction system for ex-ante estimation of plant structural parameters.

Considering the utility of high-resolution TLS point cloud and the potential for model integration with multispectral imagery for crop discrimination, biophysical parameters estimation and the possibility for plant-level information retrieval, this thesis has attempted to address the following questions.

- What is the potential of TLS point clouds to discriminate crops and estimate biophysical parameters as a function of N level?
- How will the adaption of deep learning techniques to directly ingest the 3D LiDAR data for object-based plant level classification work?

- What is the potential to integrate 3D point cloud crop data with high-resolution multi-spectral imagery for crop discrimination at patch level with sensitivity to nitrogen level?
- Given the availability of crop structural parameters at one growth stage, what is the potential of the DL methods for predicting crop structural variables at a different growth stage?

1.8 Problem statement

Variability in plant growth, soil nutrition and expected yield exists within field. Depending upon the type of crop grown, the impact of variability can be seen at plant or patch level. Hence the within-crop diversity should be addressed at the plant or patch level for better crop throughput. For this purpose, the remote sensing data obtained should identify the crop at the patch or plant level. High-resolution optical remote sensing data is a partial solution for this, but at the same time, the need for structural features for crop modelling is equally essential. Thus utilizing LiDAR to capture crop geometry is critical for crop modelling. We have considered three essential vegetable crops consumed by the people daily: cabbage, eggplant, and tomato. The prospect of remote sensing based crop monitoring for these vegetable crops has not yet been explored from the 3D perspective. A distinctive feature of these crops is their height concerning the ground surface, which is in the order of a few centimetres compared to cereal crops. This further complicates crop characterization and extraction of the crop traits such as canopy height and crown area. To automate the semantic classification task for meeting the growing volume of LiDAR point cloud, an efficient model is to be developed that functions directly on the LiDAR point cloud. The amenability of deep learning architectures for direct ingestion of LiDAR point cloud for semantic classification is still in its infancy. Development of a deep learning technique that can effectively be adapted to process 3D data from a terrestrial

laser scanner for horticulture crops at a multi-temporal scale has largely been an unexplored arena. Also, the change in classification accuracy when satellite-borne multispectral data is integrated with the LiDAR data for horticulture crops is also studied in this thesis. Using 3D LiDAR data, the crop structural parameter prediction is not yet investigated. These are some vital tasks involved in crop monitoring which helps in site-specific farming. At the same time, the irregular and unstructured nature of the 3D LiDAR is quite challenging to be considered from the deep learning perspective. Thus, how the LiDAR data (Figure 1.7) is amenable to all these goals is investigated in this research.

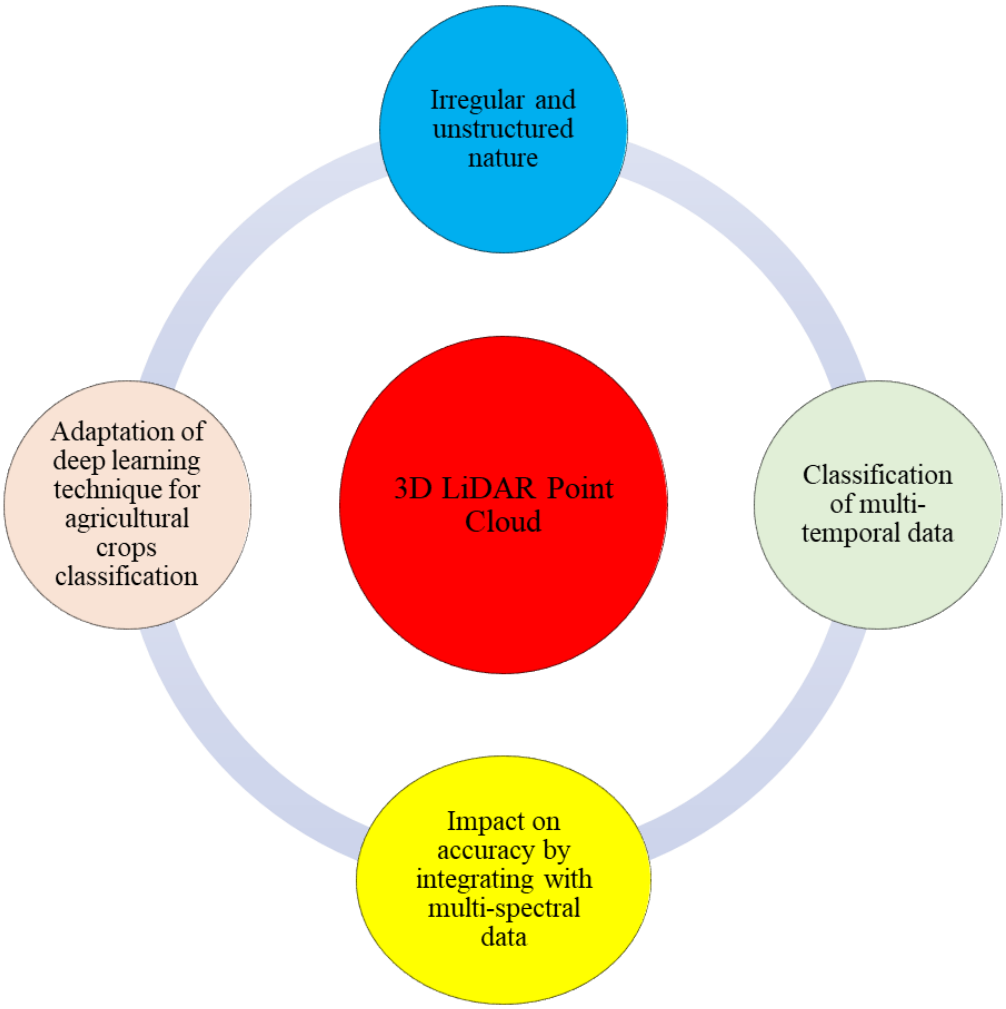

Figure 1.7: Problem statement

1.9 Research Objectives

The overall aim of this is to explore LiDAR point cloud for crop parameters estimation, prediction and discrimination of crops at plant/patch level. This has been expressed in the form of the following four specific objectives.

- Multi-temporal estimation of biophysical parameters of agricultural crops at different levels of nitrogen using TLS point cloud
- To develop a deep learning-based methodology for multi-crop point cloud classification of agricultural crops
- Examining the potential of integration of TLS point cloud with high-resolution multispectral satellite data for crop discrimination at different N levels
- To develop a DL based temporal framework to predict crop structural parameters

1.10 Organisation of the thesis

This thesis is organized into six chapters. Chapter 1 introduces the subject, describing the relevance of the topic and the scientific issues addressed in this thesis, including listing the thesis's objectives. Chapter 2 presents the relevant literature organized by the nature of objectives and the sub-tasks involved in each of the objectives. Considering the facts that (i) remote sensing is not new and that it has become part of the standard tools and technologies for agriculture, and LiDAR remote sensing has been explored reasonably well across different disciplines in vegetation research, a basic textual introduction of the LiDAR remote sensing is undesirable. Hence, to preserve the study's focus and make the thesis report sharp, conscious efforts have been made to avoid basic level descriptions and elaborations.

Chapter 3 details the study site, the various types of remote sensing datasets acquired, and the in-situ measurements. Chapter 3 further describes pre-processing and detailed methodological approaches and the validation methods adapted for each objective. In Chapter 4, results and their interpretations are presented. A comprehensive discussion of the results and observations are presented in Chapter 5. Chapter 6 contains summary of the results, major observations and conclusions drawn. Finally, though not meeting the definition of a regular chapter, we present the major contributions and scope for future research in the form of a micro chapter, Chapter 7.

CHAPTER 2

LITERATURE REVIEW

***Prelude**: In this chapter, a review of literature pertaining to the various objectives are presented concisely. For ease of readability, the chapter's content is organized into four sections relating to the objectives of the work. The first section presents relevant literature on the estimation of biophysical parameters of various crops at various levels of nitrogen (N) fertilizer. This section also contains an overview of the methods used for generating a canopy height model at different crop growth stages and the various geometrical parameters that are used for the estimation of biomass. The second section describes the methods of crop discrimination based on the deep learning technique. Traditional machine learning techniques for crop discrimination as well as deep learning techniques utilised in the computer vision tasks are also reviewed in this section. The third section is related to the object-level classification of crops sensitive to N levels based on the integration of high-resolution multispectral satellite imagery and TLS point cloud. The final section describes the evolving method of advance prediction of plant parameters using DL approaches.*

2.1 Multi-temporal estimation of biophysical parameters of agricultural crops at plant level using TLS point cloud

In the agriculture context, plant structural and biophysical parameters such as height, crown area, biomass, and leaf area index (LAI) are important indicators for assessing crop status, nutrient requirements, and expected yield. Used in combination, plant height and crown

area are vital for estimating other crop parameters such as biomass, yield, stress, and nutrient status, which are not directly measurable. The 3D structure of plants helps understand the plant functions and structure. That is why it is important to obtain 3D information about crops. This information also helps in understanding plant stress and stress responses. Recent studies indicate that crop height can be directly estimated from terrestrial laser scanner (TLS) point clouds (Ehlert et al., 2009; Jimenez-Berni et al., 2018). However, compared to the estimation of tree height in a forest environment, plant height estimation in an agricultural context is complicated because of the lower ratios of plant and soil surface variance and the magnitude of the crop height versus the accuracy thresholds TLS point clouds.

A few studies have attempted using TLS point clouds to estimate plant height and growth patterns in agriculture (Lumme et al., 2008; Hosoi and Omasa, 2009; Hoffmeister et al., 2013; Kjaer and Ottosen, 2015). Friedli et al. (2016) used high-density TLS point clouds for the classification of barley (Hordeum vulgare L.), oat (Avena sativa L.) and wheat (Triticum aestivum L.) and estimated temporal increases in canopy height. Tilly et al. (2014) generated a digital crop surface model (CSM) for paddy rice (Oryza sativa L.) to track plant height over time as a means to predict fresh biomass. In a related study, Tilly et al. (2015) combined spectral vegetation indices with the TLS height measurements for the estimation of barley biomass. Based on the voxel-based canopy profiling method, Hosoi and Omasa (2006) measured wheat canopy's vertical plant area density profiles at different growth stages using portable scanning LiDAR. With the LiDAR-derived plant area density, the area of each type of organ (stem, leaves and ears) was compared with the actual dry weight of each organ type.

Luo et al. (2021) have estimated crop heights of maize and soybean using two approaches: CHM based estimation and LiDAR variables using UAV based LiDAR system. The LiDAR variables were obtained by calculating the difference between the DEM elevation model and elevation from the laser point. The study showed that LiDAR variable based height

estimation gave better result when set side by side to CHM based method. Moreover, the combined height estimation model of maize and soybean is more accurate in comparison to individual estimate models.

Friedli et al. (2016) have used TLS point cloud to track the increase in canopy height of a few crop species under field conditions. They have estimated canopy height at various growth stages for wheat, maize and soya bean crops. In addition, they have also evaluated three different types of point cloud filtering approaches considering different statistical quartiles of point cloud by choosing data distribution over a specified area of interest. Using height estimates at different statistical quartiles, they have derived biomass estimates suggests a strong correlation between the point cloud and biomass with a coefficient of determination of 0.8. Forming the part of the first line of studies using the TLS point cloud for agriculture, Tilly et al. (2014) have developed a crop surface model visualizing the height of rice crop during the single crop growth stage of maturity. The CSM generated for multi-temporal dates was further analysed to infer the rice crop's growth profiles. Study of vegetative growth in fruits using LiDAR such as strawberry has been carried out by Saha et al. (2022) where plant geometrical parameters such as number of points per plant, height and area and volume where extracted from LiDAR scanner based on time of flight measuring principle. The obtained measurements were correlated with LAI, which exhibited a linear relationship with the LiDAR derived parameters. At the same time the work has reported uncertainty in measurements where the canopy was dense.

There have also been efforts to estimate the dry biomass of crops using the TLS point cloud. A dry weight estimate is an indicator of the growth condition of the crops. The capability of TLS for biomass estimation is explored in the studies conducted on the wheat crop (Jimenez-Berni et al., 2018), sagebrush (Olsoy et al., 2014), and barley (Tilly et al., 2015). Walter et al. (2019) have carried out biomass and crop height estimation of wheat fields across different

environments using TLS and analysed the efficiency to extend its application within a breeding program. Jin et al. (2020) evaluated different regression models and derived plant traits of maize crops using TLS based LiDAR data and examined the suitability among these for biomass estimation. The estimation was carried out at four different levels, such as individual plot, plant, leaf group and individual leaf and stem levels. Their study concluded that simple regression technique is the suggested method for biomass estimation using TLS derived plant traits and height related variables gave robust biomass prediction. However, the estimates of dry biomass correlate very poorly with the reference biomass values suggesting that wet biomass is the representative of crop growth and a stable parameter for estimation using TLS point cloud.

2.2 Crop classification using 3D point cloud- deep learning approach

Identification of crop type and delineation of field boundaries broadly referred to as crop discrimination is the first task of technology application in agriculture. Thanks to the vertical geometrical feature retention capability of the LiDAR point cloud, it is possible to identify crops based on the geometrical distribution and assign labels for each crop. However, this discrimination can be done at two different levels: (1) Discrimination w/o any reference to management factors such as nutrients and (2) Crop discrimination with specific reference to management factors. Crop discrimination is generally achieved through the supervised classification of the point cloud. Semantic labelling and classification is the general framework for the analysis of LiDAR point cloud for crop discrimination. The classification methods used for point cloud traditionally utilises the custom-made feature extraction methods in which (Guo et al., 2014; Niemeyer et al., 2014; Hackel et al., 2016; Zhongyang et al., 2018), the class

labelling procedure is usually achieved by supervised or unsupervised learning approach. The supervised methods often used are machine learning-based involving the training of different classifiers with extensive training data. Weiss et al. (2011) carried out plant species classification with a 3D laser scanner using agriculture robots for the application of crop scouting. In a machine learning framework, 83 features are extracted from the 3D point cloud and are fed to different state-of-the-art classifiers to compare the classification accuracy across the classifiers.

Based on the nature of ingestion, machine learning approaches for point cloud labelling can be grouped into direct and indirect methods. The direct methods operate on the point cloud without changing the 3D structure of the data. The state-of-the-art in classification is the deep learning-based methods. In the case of 2D images in computer vision, the deep learning model convolution neural network has reached new heights in terms of performance. Deep learning neural network has been evolving as a general method for the prediction and labelling of various types of data and applications. The Convolutional Neural Network (CNN) based deep learning model has recently been successfully used for semantic segmentation of 2D imagery (Liu et al., 2019; Varfolomeev, Yakimchuk, and Safonov 2019). Deep learning techniques can directly operate on point clouds and avoid the need for an analyst-level conversion of 3D point clouds into an ordered representation such as an image or a volume. A view-based method is one of the indirect methods in deep learning, which can be applied for the conditioning and processing of 3D imagery and point cloud. Su et al. (2015) proposed a multi-view based CNN for 3D shape identification which was acquired by placing cameras at different view angles around an object. These approaches of transforming the original 3D data to a 2D Euclidian space suffers from the loss of the information contained in the third dimension. Huang et al. (2016) devised a volumetric approach, where an occupancy voxel grid was generated on the LiDAR point cloud. For training, each voxel was labelled according to the label of the centre

point of the voxel grid, and the rest of the points were given the labels obtained from the prediction using CNN on these voxels. Tchapmi et al. (2017) proposed a voxel-based 3D Fully Convolutional Neural Networks (3D-FCNN) named "SegCloud" along with trilinear interpolation and fully connected Conditional Random Fields (FC-CRF) to perform point level semantic segmentation. Compared to the image-based method, voxelization offers better results but at the cost of overhead incurred during the data conversion, which might affect the invariance of data (Qi et al., 2017). While the deep convolutional neural network (DCNN) model is amenable to ingest a rasterized point cloud as input directly, the unstructured nature of the 3D point cloud of natural landscapes limits the direct application of DCNN for classification or segmentation in a 3D perspective. When it comes to the point clouds of the natural landscape, the unstructured and non-uniform nature of the point cloud poses a challenge for the direct application of DCNN (deep convolutional neural network) for classification or segmentation procedures.

A significant development that makes the possibility of applying point cloud directly into deep CNN framework is presented by Qi et al. (2017). The CNN model, popularly known as PointNet, is a unified architecture amenable for the exploitation of 3D features in a semantic classification framework. The distinct advantage of PointNet architecture is the usage of shared Multi-layer perceptron (MLP) which converts the input to a set of features in space for each point. The critical element of the architecture is the use of max-pooling layer that acts as a symmetric function capable of handling the permutation invariance. A joint alignment network, T-net designed for classification, gives a canonical representation of the input similar to the spatial transformer network introduced in 2D images (Jaderberg et al., 2015). In the case of semantic segmentation, in addition to the generation of global features from the max-pooling layer, the shared MLP is used to produce per-point features. However, PointNet architecture fails to capture the local information of its immediate neighbourhood. Similarly, Yousefhussien

et al. (2018) proposed a fully-convolutional network for semantic segmentation of areal 3D point cloud. Further, they have integrated aerial multi-spectral imagery with the point cloud at point level. The spectral information from the IR-R-G imagery was added to the 3D point cloud using bilinear interpolation. Similar to the PointNet, the global features were obtained through max-pooling and are combined with the local per-point features to generate per class scores. For semantic segmentation, in addition to the generation of global features from the max-pooling layer, the shared MLP is used to produce per-point features. The wide popularity of CNN in computer vision, especially for 2D images, relies on interaction with the local neighbourhood pixels in the defined kernel filter and extracts information as features, giving more meaning to the image. This helps in identifying objects with some similar and varied properties. These properties can be distinguished through the details extracted hierarchically from the image. This same concept of hierarchical feature learning has been extended to point clouds by Li et al. (2018) and named the deep learning network as Pointnet++, which is an extension of PointNet.

Improvements of extending the architecture of PointNet to processing point clouds of individual buildings have also been reported (Soilán et al., 2019). Semantic segmentation of LiDAR point cloud of vegetable crops in 3D perspective is a challenging task due to the complex object-background interactions and thresholds of height differences required for normalization and filtering of LiDAR point cloud. There are no studies that assess CNN-based deep learning approaches' potential for semantic segmentation of crops.

2.3 Discrimination and biophysical parameter estimation with reference to nutrient level: combining high-resolution multispectral imagery and LiDAR point cloud

Crop discrimination at the plant/patch level requires micro-level information; the spectral information available from multispectral imagery alone is insufficient to differentiate different plants with an almost similar spectral response. Also, the same crops can exhibit variability in their reflectance across different fields. Spectral and spatial variance within a field limits the use of spectral imagery independently for crop discrimination. In such cases, the similar spectral responses of crops could be discerned with the structural parameters obtained from LiDAR point cloud ranging from plant to patch level.

Spectral tracking of the distinct phenological features at different growth phases has been the general method employed for crop discrimination using multispectral imagery. Doing away the necessity of using multi-date datasets for crop discrimination using multispectral imagery, single date hyperspectral data acquired from in-situ spectral measurements, airborne and space borne hyperspectral imaging sensors have been demonstrated for multiple crops discrimination (Nidamanuri et al., 2007, 2011). Depending upon the crop types and spatial resolutions, accuracies of 60 to 90% have been reported.

The current suite of remote sensing satellites provides high-resolution data at spatial resolutions amenable to discriminate crop patches and estimate biophysical (e.g. biomass) at the field scale. Most of the current generation remote sensing satellites such as GeoEye-1, WorldView-2, WorldView-3, WorldView-4 offer multispectral data at spatial resolution from 1m to 5m indicating the potential to capture within-field variability. Several studies have applied high-resolution remote sensing data for crop discrimination and biophysical

characterization (Camps-Valls et al., 2010; Claverie et al., 2012, Shwetank et al., 2012; Thenkabail et al., 2013; Battude et al., 2016; Thenkabail et al., 2016).

Even with the increased spatial-spectral resolution in the current scenario, crop characterisation and biophysical parameter estimation at different N applications at patch level in a field are not yet attempted. As the crop grows and matures, the N nutrient's significant effect is observed mainly through its structural developments such as height and crown area. The delicate greenness and vigour sensitive spectral features of the multispectral data of crops with different N treatments at the ground or airborne level lose sensitivity in the multispectral data or at the satellite level. The discernible features for crops discrimination and biophysical characterization at different N levels are mainly from crops' structural-geometrical attributes. The optical remote sensing (both multispectral and hyperspectral) data have serious limitations in proving crop structural attributes such as height, crown area. The state-of-the-art studies in the literature are limited to crop discrimination and biophysical characterization under laboratory conditions or at a large area level (Mutanga and Skidmore, 2004; Mariotto et al., 2013; McNairn et al., 2014; Khan et al., 2016; Skakun et al., 2017). Therefore, remote technologies for sub-field or patch level crop discriminations or biophysical characterization are crucial for site-specific within-field level predictions of crop growth.

Complementary to the spectral features of multispectral imagery, the LiDAR point cloud offers geometrical features of objects and has the potential to provide information on canopy structural parameters such as crop height, canopy area, etc., at a finer spatial scale, potentially with explicit reference to nutrient status such as N level. Precise crop discrimination and biophysical characterization can be achieved by combining multispectral and LiDAR point clouds. Therefore, it is a potential approach for simultaneous crop discrimination and biophysical characterization tasks with specific re6ference to N levels. However, due to crop plants' low heights and complex background soil interactions, geometrical characterization of

crops requires very high-density LiDAR point cloud and scans from multiple facets. The geometry of data acquisition, the influence of prevailing weather and environmental factors and the point density required for modelling the generally small and shorter crop plants pose greater challenges. Terrestrial laser scanner (TLS) offers the possibility to acquire LiDAR point cloud at high density retaining the plant level structural features of crops. High-resolution multispectral imagery, preferably better than 1m, provides the patch level spectral features useful for crop discrimination. Therefore, a fusion of data from TLS and the high-resolution multispectral sensor is a viable strategy for high-resolution crop discrimination and biophysical characterization for crops and to integrate the data and model from ground level to satellite level.

2.4 Methods of integration

Assimilation of vertical and spectral aspects of the data from multi-sensor for crop discrimination at varied nutrient contents has not yet been reported in the literature. Integration of multi-sensor data provides a consistent and accurate baseline dataset for recognising and characterising land surface objects. Integration can be performed at three different levels: (1) pixel level, (2) feature level, and (3) decision level. Here the LiDAR and WorldView-III sensor data have been integrated at pixel level, and feature level. Fusion has been carried out using handcrafted features derived from both the datasets and applied to machine learning techniques; where as a pixel-level approach was followed for crop classification using deep learning methodology.

2.5 Temporal based prediction of plant-level crop structural parameter

Availability of ex-ante information related to crop dynamics helps to achieve a better quality and throughput, which is beneficial for farmers. Advanced remote sensing techniques coupled with precision agriculture practices provide temporal crop information at the farm level for better crop management. One of the necessary tasks in precision agriculture is to automate the assessment of growth and discrimination of the different crops to take a suitable decision for a better profit and yield at the individual plant level. It is important to understand the plant phenology to gain a better yield. The 2D image-centered time-series-based crop phenotyping has been advancing faster due to the technological developments of the sensors and their associated processing. However, these assessments are carried out mainly for a single plant/species or large scale.

Focusing on individual plant growth patterns and knowing ex-ante information about crops is vital for precise farming practices. Determining the plant growth response to various input parameters such as nutrient application and water uptake require information in hand to make appropriate decisions. Therefore, to understand the plant growth trajectory, the availability of prior knowledge regarding plant traits is necessary.

Traditional machine learning and statistical model-based methods have demonstrated their ability to predict the yield and biomass and learn the complex pattern of plant growth temporally. Numerous tools and techniques exist for building plant growth models. These models produce 2D/3D plant simulations. Moreover, predicting the growth of crops helps to examine the growth pattern in future. However, these approaches have considered single crops for forecasting over a large area based on spectral indices and other quantitative parameters. Predicting geometrical crop growth parameters such as height and crown area of the crops

holds the potential to evaluate the crop throughput. Recent advances in computer vision have triggered the progression of applying deep-learning methods to measure crop traits effectively.

Over the past years, remote sensing data has been utilized for crop estimation and yield (Huang et al., 2019). Many studies have used remote sensing data coupled with smart technologies in agriculture paving the way to effectively manage the crops and monitor their growth pattern over time based on temporal information. Still, satellite-based crop growth analysis is limited in terms of low spatio-temporal resolution and weather effects (Becker-Reshef et al., 2010). Due to this, accurate yield estimation, growth monitoring, and prediction/forecasting are challenging tasks for individual field or plant levels. Therefore, a better remote sensing technique should capture the phenological traits of the crops based on spatio-temporal analysis throughout its growing period.

Understanding the plant's health and growth in various environmental conditions needs beforehand agronomic inputs to compare and take necessary actions (Großkinsky et al., 2015). Therefore, the availability of plant growth statistics at a particular time is vital (Chawade et al., 2019). In addition to that, the precise agronomic parameters on a temporal scale produced from the individual plant across the field assist in providing more information associated with crops. Crop yield prediction using various machine learning techniques from UAVs and space-borne based imagery have been able to produce results more accurately than statistical-based models (Khaki et al., 2020). Singh et al. (2020) assimilated crop phenology using monthly NDVI time series derived from Sentinel and Landsat data for some croplands in Russia. Their study area covered cash crops such as sunflower, sugar beets, wheat, maize, onion etc. With the NDVI profile, they have to tracked the status of the crop’s different growth stages. Using the UAV, Nevavuroi et al. (2020) collected RGB and weather data collected from nine crop fields in Finland. This study examined the feasibility of time series based spatio-temporal crop yield prediction using different spatio-temporal deep learning architectures such as CNN-LSTM,

ConvLSTM, 3D-CNN. The temporal RGB images were evaluated with the models, among which 3D-CNN architecture outperformed the other two architectures with a coefficient of determination (R^2) 0.962. By the RMSE percentile, CNN-LSTM was able to generalize more to the unseen data. Lin et al. (2020) proposed a deep learning architecture, DeepCropNet (DCN), for a county-level corn yield estimation in the USA from 1981 to 2016. The DCN model has been applied to establish a relationship between different meteorological factors that affect the crops with the corn yield. DCN achieved a better RMSE compared to LASSO and Random Forest algorithms. For capturing the temporal features, an attention-based LSTM is designed, and for spatial features, multi-task learning layers were developed. Ienco et al. (2019) performed crop type mapping for multi-temporal and multi-sensor-based data viz Sentinel-1 and Sentinel-2 for the area of Nebraska, US. In their work, an object-based RNN Land cover classification was performed to account for the data from the two different sensors. A growth prediction model employed by Chang et al. (2021) has used XGBoost for multiple reduced time steps forecasting the growth prediction of Arabidopsis with a limited number of crops using the extracted projected area obtained from segmentation of plants.

Most of the studies cited and other works broadly related to this topic have considered the prediction of yield or crop growth stages for a limited number of plants or a large extent, for a single crop. Therefore, an appropriate approach for forecasting crop growth for different crops at a field scale with different crops needs to be addressed.

2.6 Chapter closing remarks

The literature review presented in this chapter pertains to the general nature of the work that has been formulated in the form of different objectives stated in section 1.9. Since the

LiDAR technology has matured through the past two decades, we have presented the literature survey selecting the studies that are primarily relevant to the scope of the research work of the thesis. This chapter has also addressed the application of deep learning for LiDAR point cloud processing using various direct and indirect methods. The studies reviewed have shown how the LiDAR point cloud can be used via deep learning for various segmentation and classification tasks. Further, the integration of LiDAR point cloud and multispectral imagery for crop identification and its impact on accuracy has been explored. Also, a temporal based crop structural parameter predicted for its different growth stages is also deliberated.

Vegetable crops cultivation includes irrigation, applying the right amount of fertilizers, protecting from disease and pest infestation, and requiring intense soil care. The literature survey indicated that the past studies have not evaluated the possibility of temporal estimation of biophysical parameters of vegetable crops such as tomato, cabbage, and eggplant. Further, the potential of the TLS point cloud to discriminate plant biophysical parameters as a function of various levels of N application has not been studied. Additionally, these crops exhibit different complexities of growth patterns and profiles, canopy shape and directions of temporal biomass accumulation. Finally, it has been observed that the temporal prediction of structural based biophysical parameters is not yet tried for crops.

CHAPTER 3

MATERIALS AND METHODS

Prelude

This chapter provides information on the study area and the experimental setup designed for conducting the research. It contains a brief narrative of the geographical location, data capture mode, and data acquisition procedures and the different data and sensors used in the study. Further, the chapter describes the methods used to achieve the objectives. The various steps followed to realize each objective are discussed in detail in the subsequent sections. This includes the detailed methodology adapted for each objective and the pre-processing steps before further data processing.

3.1 Study area

As part of a larger perspective work aimed at studying the effects of rural-urban transformation on soil productivity, nutrient cycling, and ecosystem services, a drip-irrigated factorial field experiment was established in 2017 (January – May). To this end, agricultural plots were set up at the University of Agriculture Sciences (UAS), Bengaluru, India (Figure 3.1) with the coordinates 12°58’20.79’’N, 77°34’50.31’’E. The climate of Bengaluru is mild, with a mean temperature of 29.2°C with annual precipitation of 873 mm.

3.2 Data used

The data used for this research has been collected from multiple sources that include 3D LiDAR point cloud, satellite imagery, and in-situ geometrical and biophysical measurements of the crops. Data acquired using the sensors and the sampling dates are shown in Table 3.1.

Table 3.1: Data acquisition dates and type of remote sensors

Data	Sensor	Date of acquisition
Optical satellite imagery	WorldView – III	19 May 2017
Terrestrial laser scanner	Faro Focus^S 350	18 May 2017, 4 May 2017, 22 May 2017, 14 June 2017

Table 3:2: Properties of TLS and WorldView - III sensors used for the experiment

Properties	Specifications
TLS sensor	
Wavelength	1550 nm
Positional accuracy	2 mm for every 10 m
Coverage	Horizontal: 360
	Vertical: 300
Camera	165 megapixel RGB inbuilt camera
Scanning speed	976 pts/s
WorldView - III sensor	
Number of bands considered	4
Bands	R, G, B, NIR
Panchromatic spatial resolution	0.31 m
VNIR spatial resolution	1.24 m
Temporal resolution	Less than a day

3.3 Experimental design

The crop cycle was planned to mimic a typical crop rotation of southern India with its two distinct crop seasons Kharif (June to October) and Rabi (January to May). The results of this study pertain to the summer (Rabi) season. The cultivars used correspond to those typically used by local farmers in the Bengaluru area. The experiment field consisted of 12 main plots of 12m × 18m size, each of which was further subdivided into three subplots yielding thus a total of 36 subplots of area 6m × 12m with four replications. Sub-plots were randomly assigned to three levels of mineral (N) fertilizer. Corresponding to the 'medium' N level referred to in this work, 46 kg N ha^{-1}as urea for tomato, 60 kg N ha^{-1} for cabbage, and 50 kg N $ha^{-1}$for eggplant. 'High N' referred to 50% more and 'low N' to 50%. Apart from the N fertilizer, a blanket application of phosphorus (P) and potassium (K) at the rate of 17.5 kg P $ha^{-1}$and 19.9, 41.5, and 16.6 kg K $ha^{-1}$for tomato, cabbage, and eggplant was blanket-applied at sowing. To reduce potential leaching of nutrients due to heavy rainfall, the N fertilizer was applied in two instalments. The rate of N fertilizer for different treatment levels was calculated on a per-row basis. During the monsoon season, some surface N transport may have occurred in some of the plots due to intensive rainfall events during early crop stages, but this did not happen during the Rabi season. For acquiring reference biophysical measurements (e.g. biomass), each sub-plot was divided into two parts: one was used for destructive sampling (S-plot; Figure 3.1) and the other for non-destructive sampling (H-plot; Figure 3.1).

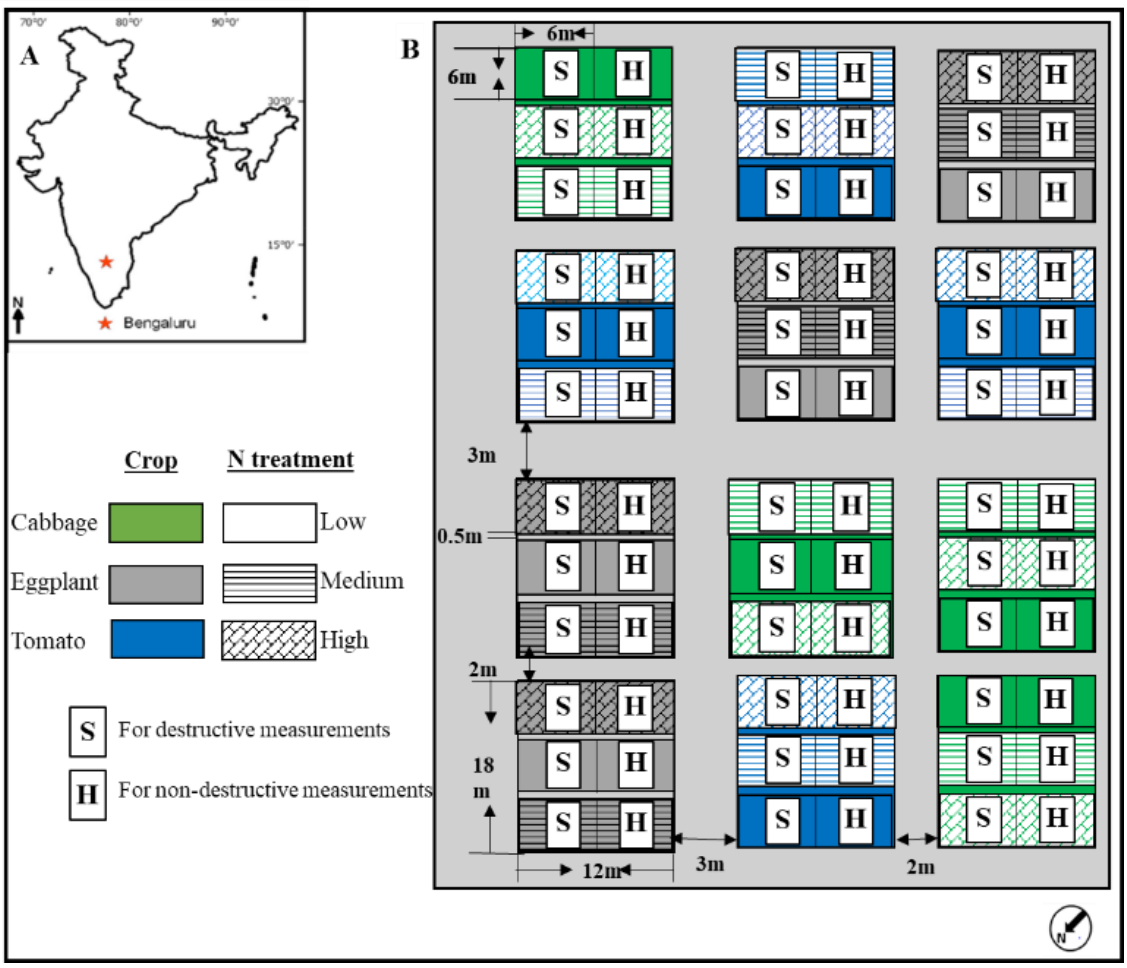

Figure 3.1: (A) Location of Bengaluru in India and (B) layout of the experimental setup. Sub-plots marked S and H indicate sub-plots used for destructive and non-destructive sampling, respectively.

3.4 In-situ measurements

For the sampling and measurement of crops, plant height was determined with a ruler to the nearest 0.01m. Average crop height was calculated from heights of 30 plants in each sub-sub-plot marked S and H. Total fresh biomass was measured by random harvesting and on-site weighing of three plants in each S sub-sub-plot. All the plant-level biomass measurements were averaged for each field and expressed in t ha^{-1}. Destructive yield measurements were taken at five sampling dates during the season. Crop area measurements were obtained from digital

reconstruction of plants from the periodic digital photographs acquired by adapting the methodology proposed by Phattaralerphong and Sinoquet (2005). A further extension of introducing guided image rectification and segmentation to yield individual results plant crown areas. At discrete locations, distance measurements of plant crowns in the N-S and E-W directions were also taken. The images of the various modes of data acquisition is shown in Figure 3.2.

Figure 3.2: Different data acquisitions in the experimental plot GKVK, Bengaluru

3.4.1 WorldView – III satellite imagery

With the increased availability of high-resolution optical satellite imagery, detailed mapping of topographic features of the earth's surface has become easier. The WorldView – III satellite is operated by Digital Globe at an altitude 617 km of in the sun-synchronous orbit. The sensor provides high spatial resolution imagery in panchromatic band (450 – 800 nm) with a spatial resolution of 0.31m (at nadir) and multispectral imagery in eight spectral bands at spatial resolution 1.24m (at nadir). The mmultispectral satellite imagery used in this work was

acquired on 19 May 2017 in both multispectral and panchromatic modes. The spatial resolution of the imagery in multispectral and panchromatic mode is 1.24 m and 0.5 m, respectively, as supplied by the imaging agency as per government regulation. However, for data integration component of the work, we used multispectral imagery in four spectral bands (R, G, B, NIR) only. A false colour composite (FCC) of the satellite imagery is shown in Figure 3.3.

Figure 3.3: WorldView-III imagery of the experimental plot in the false colour composite.

3.4.2 TLS point cloud acquisition

Compared to the woody trees, the acquisition of laser measurements for vegetable crops is complicated because the vegetable plants are generally shorter, and the presence of soil ridges complicates the height contrast. To mitigate these problems and reduce the impact of

wind, the experimental plots were scanned from multiple view angles and positions (Figure 3.5).

Concurrent to the dates of biophysical sampling measurements, TLS measurements were acquired for three different sampling dates (4 May, 22 May, and 4 June of 2017) using a 3D terrestrial laser scanner (FARO 350^S, FARO Technologies Inc., USA). The data capture on 18/04/2017 was acquired using a different TLS instrument (Riegl sensor) due to the non-availability of the sensor; however, the scan density and the associated scan parameters were similar to other dates. For tomato, the TLS measurements were not acquired on 4 June 2017 as the crop was harvested by then. The TLS operates in the near-infrared region (at 1550nm) and has a maximum range of 350m. The data capturing involving the TLS scanner requires the scanner to be placed at multiple scan positions in order to cover the entire agricultural field. The TLS was placed at 16 positions around the experimental field. DGPS (Differential-GPS) was used to improve the positioning information of the target. Further, for precise registration of data from multiple scans, four checkerboard target boards were used. For each scan, four targets (checkerboard) were placed at a distance not more than 15m according to the selected scan resolution. This ensured minimal error during scan co-registration. The data was collected during March - June 2017 in the experimental agricultural plots containing three vegetable crops- tomato (*Solanum lycopersicum* L.), eggplant (*Solanum melongena* L.) and cabbage (*Brassica oleracea* L.) using FARO $Focus^S$ 350 terrestrial laser scanner. The data were collected at four different periods representing the various growth stages of the crop.

3.4.3 LiDAR point cloud description

The acquired LiDAR point cloud was in the .laz format. The dataset contains geo-referenced LiDAR point cloud data in .laz (ASPRS compressed LiDAR storage format) collected from the experimental agricultural plots. Along with the range information from the sensor (X, Y, Z), spectral information (R, G, B) was also captured using the in-build camera (Figure 3.4). The same procedure was repeated for all the subsequent scan dates and laser scans pertaining to each scan date. Each data file was geo-referenced to World Geodetic System (WGS)-84 datum with UTM projection.

Figure 3.4: Shows the images captured from the inbuilt RGB camera of the TLS and the target used.

3.4.3.1 Parameters for LiDAR data collection

A minimum of 20-25% overlap was maintained between successive scans for proper registration. Checker board targets were placed around the scanning area to ensure precise co-registration of the scans. Spectral measurements using the integrated camera were also captured along with the range information. Inbuilt GPS was enabled to capture the data in the world coordinate system. The height of the tripod was adjusted to 1.5 - 2m depending on the growth stage of the crops, and the scan duration was set to 10 minutes with a scan density of 6.1mm in 10m to ensure highly dense point cloud data. Figure 3.6 shows a sample visualization of a fully co-registered LiDAR point cloud acquired on 22/05/17.

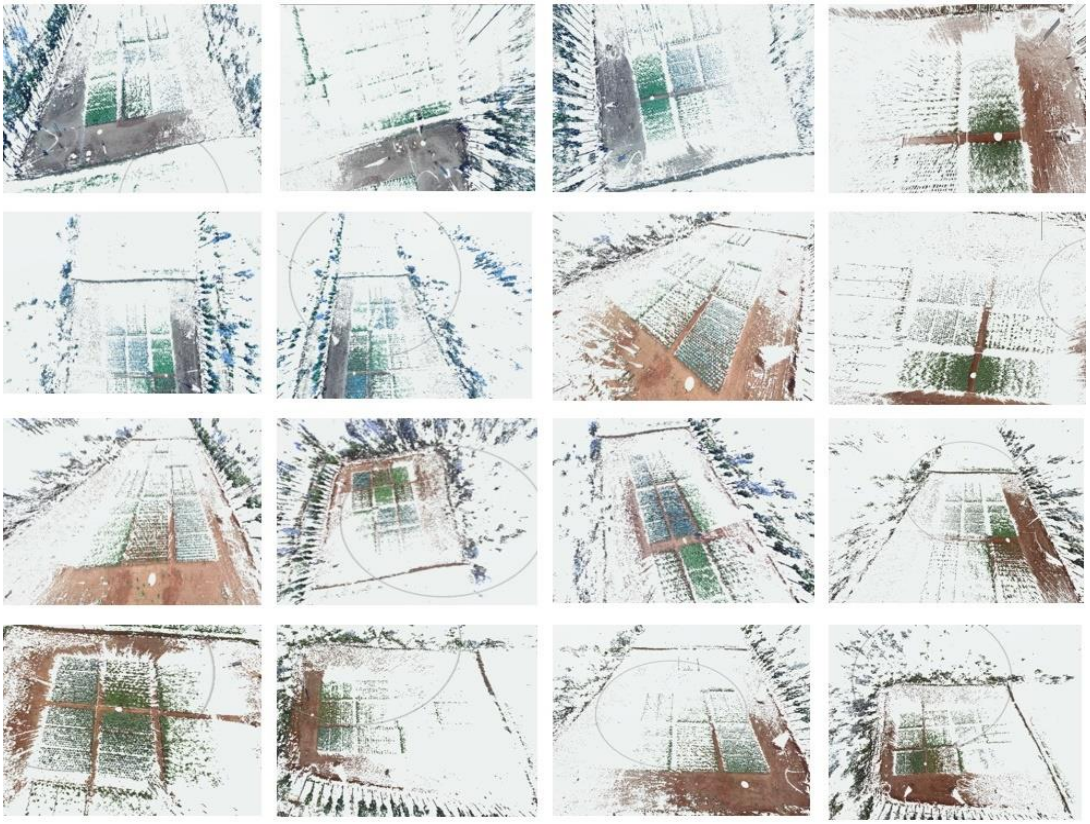

Figure 3.5: Visualization of the point cloud from TLS measurements in the experimental plots. These point clouds were acquired from different positions to capture the crop canopy structure from different perspectives.

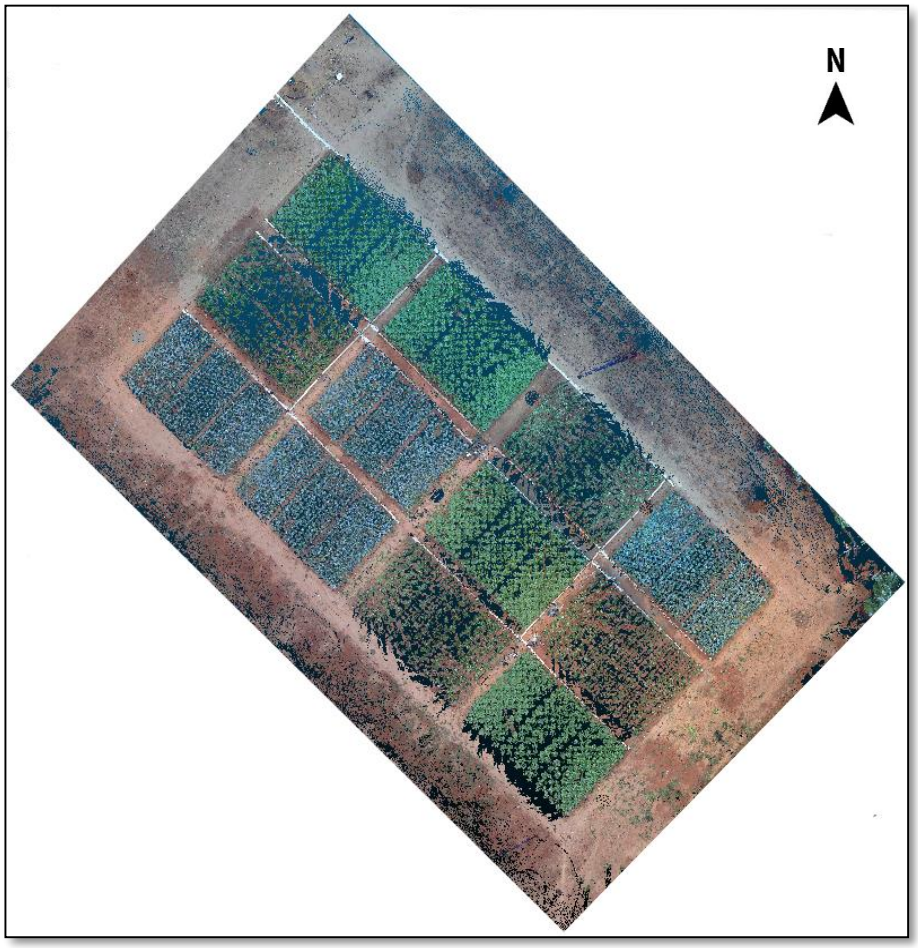

Figure 3.6: The co-registered geo-referenced 3D LiDAR point cloud data captured on 04/05/17.

3.5 Methodologies

Broadly expressing the various methods and algorithms adapted and developed in this study, an overall view of the methodological process flow is shown in Figure 3.7. Detailed processing steps which were undertaken to realize each objective are presented in the following subsections in the order of the objectives of the work described. Some processes such as filtering and basic processing of LiDAR data, co-registration of satellite imagery are common for more than one objective.

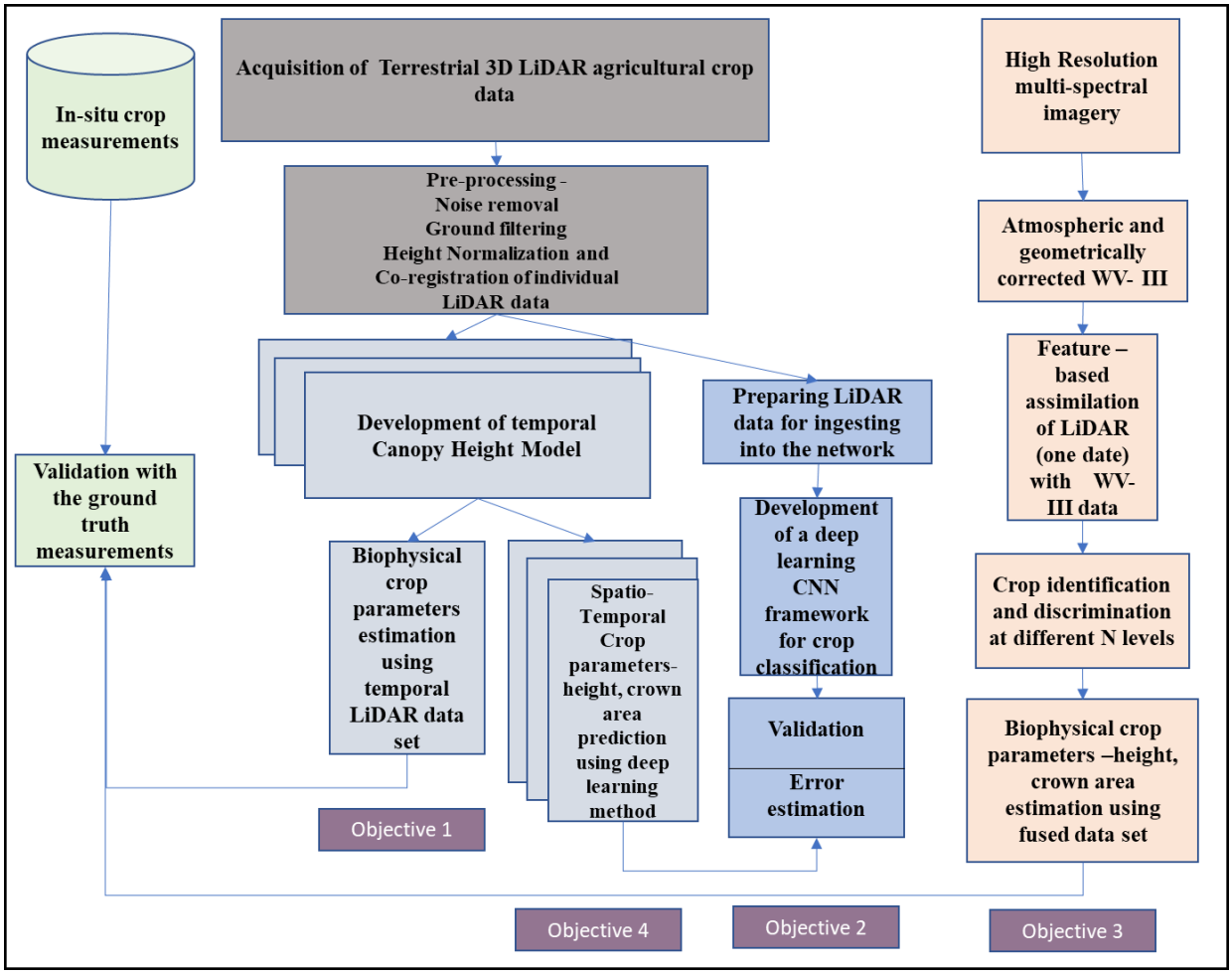

Figure 3.7: Top-level methodological process flow developed for the thesis.

3.5.1 **Methodology for realizing Objective 1** (multi-temporal estimation of biophysical parameters of agricultural crops at different levels of nitrogen using TLS point cloud)

The methodology developed for realizing this objective consists of tasks such as filtering, crop height modelling, and crown area estimation culminating with the estimation of biomass as a function of different levels of N using a machine learning-based approach. A Detailed methodological process flow is presented in Figure 3.8.

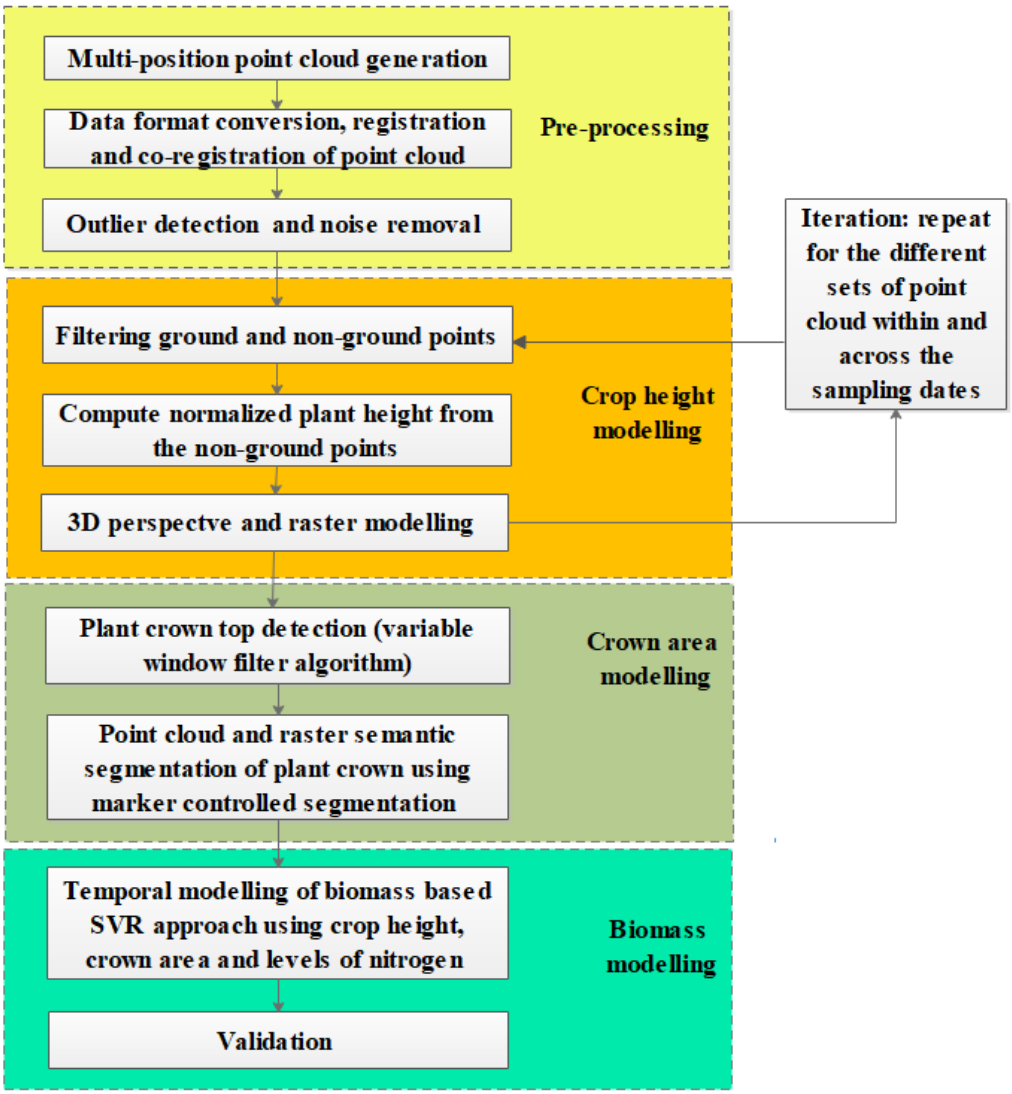

Figure 3.8: Outline of the methodological process flow from point cloud acquisition until estimation of the biophysical parameters of the factorial vegetable experiment at GKVK Campus, Bengaluru, India.

3.5.1.1 Pre-processing of 3D LiDAR point cloud

The acquired sets of point clouds were subjected to preliminary processing such as change of data format into a generic data format such as ASCII text format and integration of the ancillary high-resolution gray scale optical imagery obtained simultaneously with the point cloud acquisition. Since the work involved temporal series of the point cloud, numerous

different scans demand accurate registration from a single sampling date and multi-date integration perspective. We performed the registration of sets of point clouds by slightly modifying the semi-automatic method suggested by He et al. (2017). The soft nature of vegetable plant material and unpredictable occurrence of winds over the plants cause the scans of point clouds to lack sturdy geometric corners. Therefore, the registration procedure was modified to generate tie points for matching points based on the manual-guided sphere fit algorithm, and the 2D intensity imagery acquired. Local neighbourhood threshold algorithm based on the grid cell dimension of 3 x 3 x 3 was applied on the registered point cloud to remove outliers.

3.5.1.2 Computation of crop height model (CHM)

The co-registered, noise removed point cloud was further processed to compute a plant level crop height model (CHM). To this end, we first extracted the point cloud pertaining to only the crops by spatial and vertical filtering of the total point cloud into a ground and non-ground point cloud (Figure 3.9). We adapted the grid simplification based progressive triangular irregular network (TIN) densification (PTD) method proposed by Axelsson (2000). In this algorithm, the first step was to divide the dataset into a number of tiles and search for the lowest points in each tile. These lowest points were considered as the initial ground points. Then, for the reference surface construction, a triangular irregular network (TIN) was built. In each triangle of the TIN, one of the unclassified points was added to the set of ground points following two criteria: the point's distance to the TIN facet and the angle between the TIN facet and the line connecting the point with the closest vertex of the facet must not exceed given thresholds. All the classified ground points were appended to the TIN, and the next iteration started. The triangulation was carried out progressively till all the points were classified as

either ground or non-ground. However, the point cloud filtered for further modelling in this process contains elevation in the global reference coordinate system with elevation referenced to mean sea level. In order to enable the possibility of plant level and temporal crop traits estimation, the elevation attribute of the point cloud was normalized to reflect plot surface level referencing. This was approached by generating a TIN model of the ground point cloud filtered and subtracting from the filtered point cloud of the plants. After normalization, only the non-ground point cloud was considered for computing the raster canopy height model (CHM). This was calculated by rasterization of the elevation normalized non-ground point cloud. For the rasterization process, an n x n area of the data points was gridded on one raster, where the n (n = 0.02 was used for the experiment) represents the step size used for gridding (Khosravipour et al., 2014).

3.5.2 Modelling of the crown area

The estimation of the plant-level crown area involved two distinct steps: (1) the identification of plant crown top, and (2) the segregation and delineation of plant crown area (Figure 3.8). The crown tops were identified using the variable window filter (VWF) method proposed by Popescu and Wynne (2004). The VWF is an adaptive filtering technique that finds the local maximum within the window size of variable length, which is used to delineate individual vegetation crowns. This method was used in a forestry environment for tree top identification using point cloud. We applied this algorithm because of its ability to handle within-tree crown elevation and uneven morphology of the crown. We expanded the application of VWF to identify potential crop plant crown top adaptive change in the window radius. Corresponding to each height value of the CHM, the window size was computed to find the local maxima within that window. The size of the window changed depending on the height

value of the cell on which it was centred. If the pixel under consideration was the highest value, then it was identified as the crop crown top. We devised a simple linear equation (Equation. 3.1),

$$a*b+c \quad (3.1)$$

where a represents the radius of the window, b and c are the fractional values, to serve as the function that defines the dynamic window size considering the cell value from CHM and return the radius of the search window. Based on the heuristics, we estimated the values of b and c as 0.2 and 0.3, respectively. After the computation of the radius and the window size, the minimum crop height was also included as a segmentation input.

Image segmentation approaches can be applied on the processed point cloud with the crown top identified for delineation of the plant crown. The watershed segmentation (Vincent and Soille, 1991) algorithm can be used to segment crowns from a canopy height model. The watershed segmentation algorithm has been widely used in topographical analysis and in various image processing techniques. Given the morphological similarity between an inverted canopy and a terrain model, this method has the potential to detect plant crowns. The over-segmentation of the raster point cloud is typical of the watershed segmentation algorithm, making it complicated to retrieve plant crowns. Especially in the case of fully grown eggplant and tomato crops, small branches and other spurious crown tops of individual plants were considered as different segments. A modified form of this algorithm, known as marker-controlled watershed segmentation (Beucher, 1993), was used to circumvent this problem, considering the crown tops as markers. This segmentation algorithm assumes that the input raster image is based on a topographic model. The marker-controlled watershed segmentation algorithm takes a height value, which will be lower than that assigned to VWF. For the VWF, minimum height defines the lowest possible crown top, but for segmentation it defines the

height above ground of the fringes of the lowest crop top. The point locations detected using the VWF algorithm were used as the sources for segmentation yielding crown outlines as polygons. When compared to raster crown map, polygons need more disk space and take more time to process. Furthermore, segments without an associated crown top were removed (Figure 3.10). The area plants' crowns thus obtained were validated with in situ measurements.

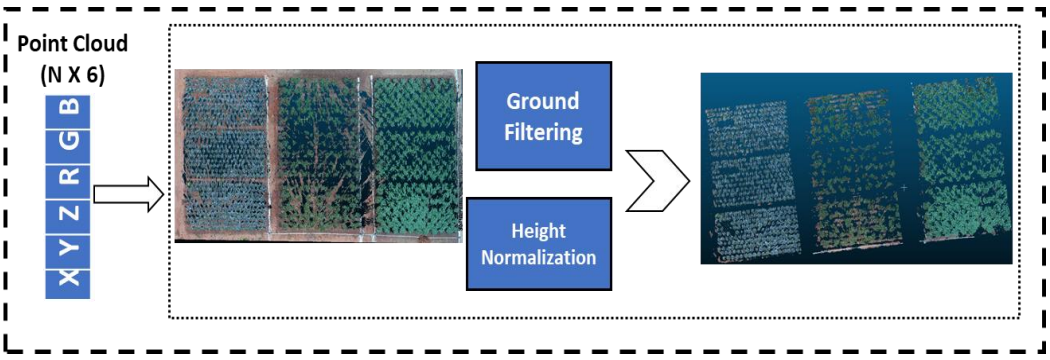

Figure 3.9: Visualization of spatial filtering of TLS point cloud for segregating point cloud of crop plants

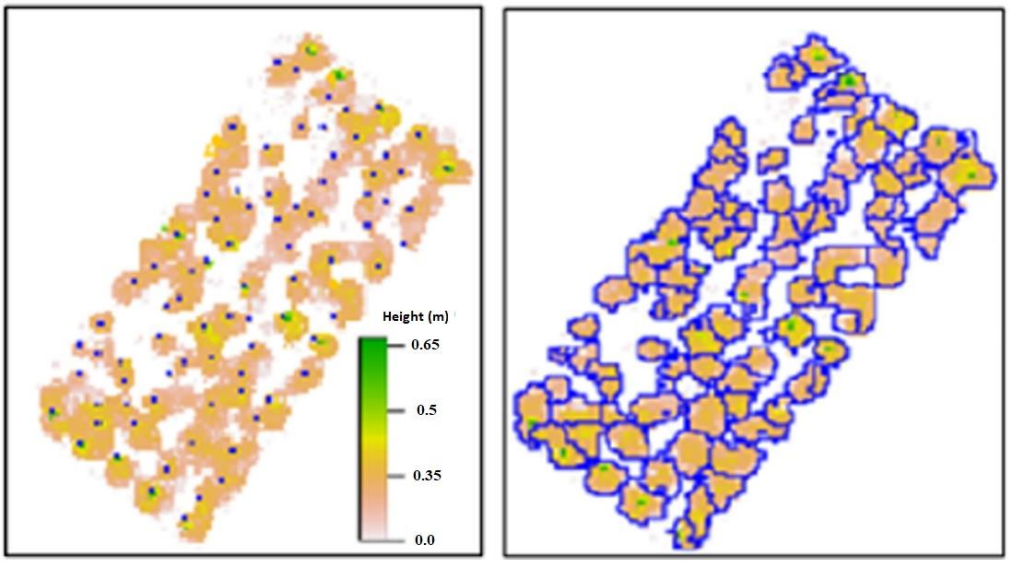

(a) (b)

Figure 3.10: (a) Crown top identification, (b) crown delineation for a subplot with tomato crop for 4 May 2017 in a factorial vegetable experiment at GKVK campus, Bengaluru, India.

3.5.2.1 Estimation of biomass

Most studies that reported retrieving crop plant traits from TLS derived height have used simple regression techniques with linear or exponential functions. Bendig et al. (2014) and Moeckel et al. (2018) have predicted crop biomass using crop height derived from 3D point clouds retrieved from UAV based stereoscopic RGB imagery. Plant height is frequently used as an estimator for biomass; however, the relationship is no longer linear for dense mature crop stands. Introducing crown area in the prediction models, in principle, has the potential to substantially enhance the precision and accuracy of estimations of biophysical parameters such as biomass for vegetable crops. The prediction of biomass with two independent variables (i.e. crown area, and plant height), which exhibit complex linear and non-linear relationships, respectively, can be best handled with non-linear regression approaches. For this, we used a support vector machine (SVM) for predicting biomass. SVM is one of the most popular statistical machine learning-based algorithms for pattern classification (Vapnik, 1998). SVM is a nonparametric classifier, insensitive to data dimensionality, and has the inherent ability to handle nonlinear and complex data relationships. Extending the functional applications with minor modifications of the architecture to handle real numbers, SVM has also been used for regression problems (Shim and Chang, 2011) and is typically called support vector regression (SVR). The quality of regression by SVR depends upon setting proper tuning parameters, the loss function ε, and the error penalty factor C and the kernel function. Following heuristics and cross-validation procedures, we estimated values for these parameters choosing polynomial function as the kernel function.

3.5.2.2 Statistical analyses of estimations and validation

The quantification of accuracy and relative performance of the retrievals from TLS point cloud vis-à-vis reference measurements is generally based on computing statistical error

metrics and coefficient of determination. Among several error metrics, root mean square error (RMSE) coupled with relative error has been widely used for assessment of the model accuracy of statistical predictions of biophysical variables (Whiting et al., 2006; Bellocchi et al.,2010; Forkuor et al., 2017). The computation, and interpretation of RMSE are easy for discrete random variables. However, because the RMSE is the square root of the average squared errors, larger errors in predictions result in disproportionately larger RMSE values. Further, because RMSE is a scale-dependent measure, it is not appropriate to compare estimates from different types of datasets. As quantitative measures of estimations and direction of deviations, we used two accuracy measures which are unbiased, symmetric and are easier to analyze statistically: (1) symmetric mean absolute percentage error (SMAPE), expressed in Equation 3.2, in conjunction with the coefficient of determination (R^2), and the logarithmic deviation (L_d) of the accuracy ratio as shown in Equation 3.3. The second measure is useful for estimating the direction of change of deviation relative to the one-to-one line and further assessing the level of underestimation or overestimations of predictions made.

$$\text{Symmetric mean absolute percentage error, SMAPE} = \frac{100\%}{n}\sum_{i=1}^{n}\frac{|y_i - x_i|}{|y_i|+|x_i|} \quad (3.2)$$

$$\text{Logarithmic deviation, } L_d = \sum_{i=1}^{n}\log\left(\frac{y_i}{x_i}\right) \quad (3.3)$$

Where y_i is the estimated parameter, x_i is the measured parameter for the measurement pair i.

3.6 Methodology adopted for the realization of Objective 2 (to develop a deep learning-based methodology for multi-crop point cloud classification of agricultural crops)

A detailed methodological process flow in the Figure 3.11.

The methodology developed follows point cloud filtering, removal of ground points, outlier detection and removal and preparing the data ready to be fed into the CropPointNet preceded by a random sampling-based selection of points to the DNN network. An outline of the methodological process flow is shown in Figure 3.11. In the subsequent sections, the DNN architecture and the validation of the classification with the reference measurements are described.

3.6.1 Point cloud processing and reference data generation

The input for the realization of the objective is the filtered point cloud pertaining to three chosen crops and the associated field infrastructure.

Based on expert analyses, six information classes were identified for the 3D segmentation and classification - three types of crop plants and three types of field infrastructure (pipes, sticks, and residual soil ridges) elements. While our aim was to classify the point cloud for crops only, the categories of field infrastructure were also included in the classification to account for the overlapping and height confusion in the laser returns of crop plants and field infrastructure.

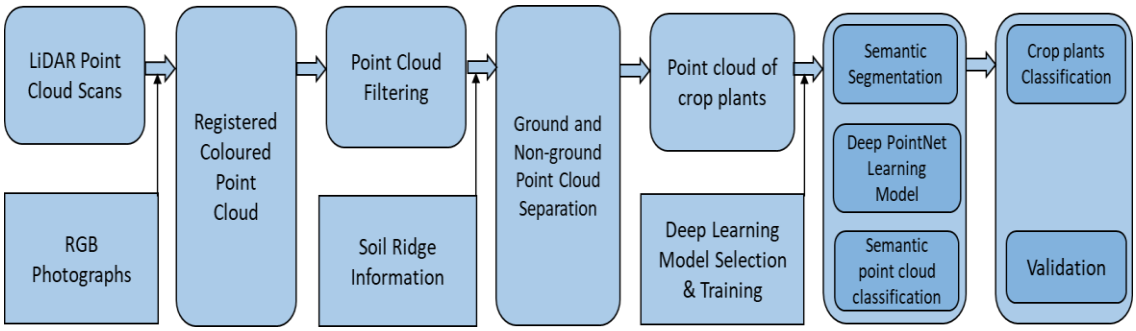

Figure 3.11: Outline of the methodological process flow

3.6.2 Segmentation classification using deep learning methods

An outline of the deep learning architecture adapted for point cloud classification is shown in Figure 3.12. The methodological architecture has two functions: segmentation and classification. For the segmentation, the PointNet deep learning architecture was modified to enhance object representation and learning and feature derivation for handling the discrete TLS point cloud. The PointNet is a recent deep learning neural network model with a unified architecture for various applications in segmentation, object classification, scene semantic parsing using point cloud (Qi et al. 2017). The PointNet network learns a collection of point functions that selects representative points by randomly picking a set of point functions from and visualising their activation regions. The classification was done by the fully connected layers of the network by aggregating the optimal values into global descriptors for predicting per point labels. The PointNet has been applied for successful indoor scene segmentation, urban scene segmentation, using the point cloud produced from Kinect and airborne laser scanner (Lowphansirikul et al., 2019). In contrast, the TLS point clouds of crop plants lack regular and well quantifiable shape and their related geometrical attributes. Further, the plant height and ground surface profile changes are comparable with the minimum measurement range of the

laser scanner. Combined with the possibility of ground interference and the shorter plant height, 3D segmentation of crops is a challenging task, and the inferences and methodological procedures from other application domains may not be directly applicable. Therefore, the architecture of the PointNet model for enhancing the learning of local and overall crop structure in the TLS point cloud was modified and named the improved model as 'CropPointNet' in this thesis.

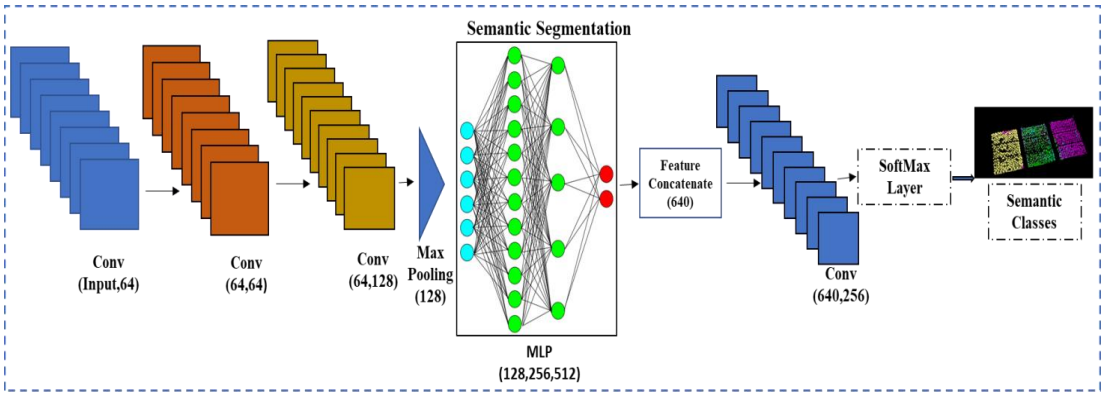

Figure 3.12: The deep neural network architecture for semantic crop segmentation

A k-dimensional LiDAR point cloud represented as $X= \{x_1, x_2,\ldots x_n\} \subseteq R^k$, where k = 6 represents the 3-dimensional coordinates of the point cloud (x,y,z) and colour intensity (RGB) of each point is the input for the deep CNN model. The rationale behind the exclusion of the normalized position coordinates, unlike the PointNet, is that in the case of 3D agricultural LiDAR point clouds, this mode of representation does not enhance the semantic interpretation of the LiDAR point cloud. The point cloud was fed into the CropPointNet model by random sampling of the point cloud.

Like the image domain, where the convolution process extracts the features building up a denser feature map, the point cloud convolution in the CropPointNet generates a feature map

with more features extracted in the forward pass. The input point clouds were given to a convolutional neural network that produces 64-dimensional features. These features were further given to the convolutional layer resulting in 512-dimensional feature extraction. In each layer before the activation function, batch normalization (BN) was performed (as shown in Equation 3.4), which can work around the covariance shift to reduce the overfitting of the data and dispense an implicit effect regularisation. When the pointwise convolution occurs, the output of each mini-batch of the previous layer was scaled with a mean-centred towards the standard deviation. Thus, batch normalization adds standard deviation and mean as two trainable parameters to the layer. During training time, a batch normalization layer calculates the mini-batch mean (μ_{MB}) and variance (σ^2_{MB}). Accordingly, the layer inputs were normalized using the expression

$$\bar{u_i} = \frac{u_i - \mu_B}{\sqrt{\sigma_B^2 + \epsilon}} \tag{3.4}$$

where, u_i is the mini-batch during training. Finally, a scale and shift is applied to equation 2 to obtain z_i, the output from the layer i,

$$z_i = \gamma \bar{u_i} + \beta \tag{3.5}$$

with the γand β learned during the training process with the other parameters in the network. To handle non-linearity in the network, a computationally efficient activation function - rectified linear unit (ReLU) was used, defined as

$$f(x) = \max(0, x) \tag{3.6}$$

Mathematically, the CropPointNet network can be represented as:

$$Y_{i=} \text{Conv}^{(i)}(X_j) \in R^K \quad (3.7)$$

$$Y_i^{F_i} = \max(0, \text{BN}(Y_i)) \quad (3.8)$$

where Conv refers to the convolutional layers, i refers to the i^{th} layer of the network, j denotes the j^{th} 3D point of the point cloud, BN refers to the batch normalization, max is the activation function after the convolution and $Y_i^{F_i}$ refers to the feature map generated from the i^{th} layer. The CropPointNet network was designed to learn both the point level features and the features obtained from the pooling layer. The max-pooling method was used to project the most stimulated presence of a feature. Following this, the MLP (multi-layer perceptron) maps the features to the next level of 512 dimensions, where the same weights are shared. This is the subsequent step for the extraction of global features from the point cloud. The point level features and the features from the max pooled layer were concatenated together to obtain rich contextual and denser feature representations. These concatenated features form a robust map for further semantic interpretation of the data. Finally, all the points in the dataset were labelled with a SoftMax activation layer, which varies from 1 to 6.

3.7 Methodology adopted for implementing Objective 3 (examining the potential of the fusion of TLS point cloud with high-resolution multispectral satellite data for crop discrimination at different N level)

Exploiting the distinct features of traditional machine learning (ML) and recent advancements in deep ML, we carried out fusion-based crop discrimination and biophysical parameter estimation using two distinct approaches. The first approach is a non-parametric decision tree-based approach (RF) which has advantages of simple model development and faster implementation of requirements. The second approach is a deep ML-based approach,

wherein the two distinct datasets are fused based on automatic feature generation and model predictions.

The methodology process flow adopted for fulfilling the two distinct perspectives of the goal of this study is shown in Figure 3.13. Overall, the methodology adopted consisted of ground filtering, canopy height modelling and crop area segmentation as discussed in the section 3.5.1.1, object-based classification, and biomass estimation as a function of different levels of N using appropriate machine learning-based approaches using the LiDAR point cloud, multispectral imagery and the fused dataset. In the following subsections, the various processes and approaches used are described in detail.

The multispectral imagery was acquired in all the spectral bands of the sensor operating. The inherent radiometric and atmospheric dictions were removed using the FACT atmospheric correction process (Jha et al., 2021). As indicated in the methodological process flow, the LiDAR point cloud and multispectral imagery were fused at the feature level. To enable this, the spatial resolution of the multispectral imagery was enhanced to 0.5m by using the Grand-Schmidt image fusion method (Maurer et al., 2013). The resulting high-resolution imagery was co-registered with the LiDAR point cloud to remove residual geometrical inconsistencies and pixel-point positional misalignments.

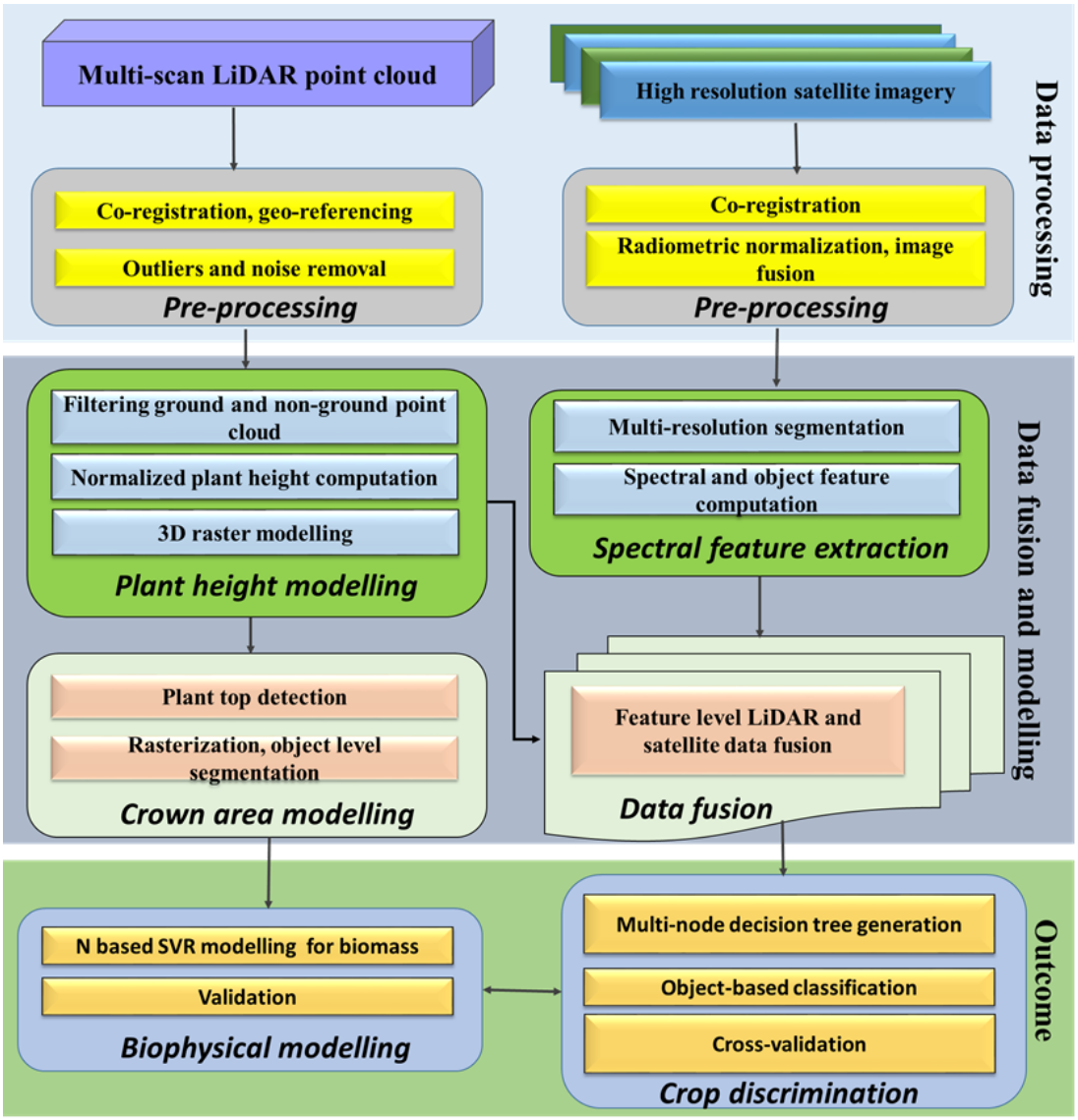

Figure 3.13: Methodological process flow indicating key steps from the datasets acquisition to the crop discrimination and biophysical characterization.

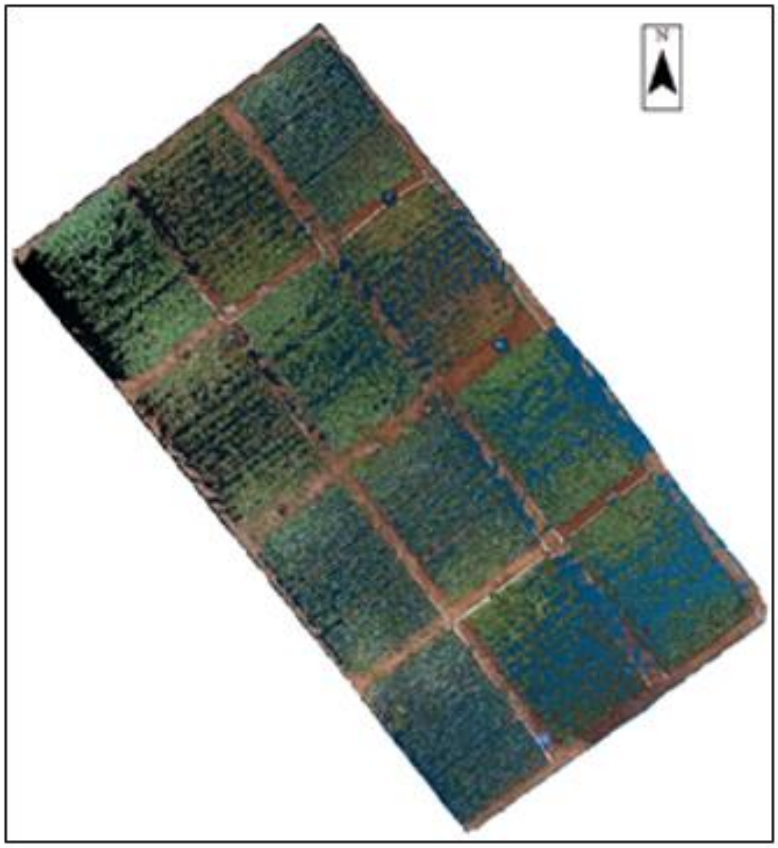

Figure 3.14: Visualization of the co-registered point cloud for the entire experimental setup for the sampling date of 22 May 2017 at GKVK Campus, Bengaluru, India.

3.7.1 Crop discrimination

With explicit reference to different N levels, crops were discriminated by supervised classification of two datasets: very high-resolution WorldView-III imagery independently and data generated from the fusion of LiDAR point cloud and very high-resolution WorldView-III imagery. Multi-modal data fusion can be achieved at various abstraction levels of data - pixel, feature, and decision. Compared to the raster imagery, the LiDAR point cloud is unorganized and is spatially discrete. The unique geometrical features of the LiDAR point cloud are best retained in the 3D perspective of the point cloud. A visual perspective of the co-registered, filtered (only non-ground points are retained) and normalized LiDAR point cloud for the entire

experimental set-up is shown in Figure 3.14. We, therefore, adopted a feature fusion approach for fusing LiDAR point cloud and multispectral imagery. Geographically meaningful object-based image classification is the apt technique for exploiting the rich spatial features of high-resolution remote sensing data (Blaschke, 2010) and enhancing data-interoperability compliance for operational use of remote sensing data-based products in agriculture. Since the spatial resolution of the datasets is very high (0.5 m for imagery and plant level for LiDAR point cloud), we opted for object-based image classification rather than the classical pixel-level classification. The object-based classification has two critical tasks – image segmentation and supervised classification.

Multi-resolution segmentation (MRS) (Baatz, 2000) has been one of the widely used approaches at the operational level in many remote sensing applications (Nidamanuri and Zbell, 2011). The MRS algorithm, a region-based image segmentation technique, produces object-level image segments by user-dependent iterative optimization of hyper-parameters – scale, shape, and compactness, which control the spectral variance, heterogeneity, and boundary adherence. Image objects are created by grouping spatially contiguous pixels until reaching a threshold (scale parameter) representing the image object's upper level of spectral variance. To eliminate noise and for minimizing the fractal borders, the image object's spectral variance at various levels of approximation was weighted with the image object's shape parameters. The quality of image segmentation varies substantially with the changing values of the user-dependent hyper-parameters. To ensure model convergence and avoid subjective segmentation, we applied a supervised method for hyper-parameter optimization and selection suggested by Tong et al. (2012). The test object boundaries required for evaluation were extracted from the ground truth map. The LiDAR point cloud and multispectral imagery were fused by pairing up plant height and crown area with geographically corresponding image

segments. This feature level fusion enables the computation of a range of crop plants' spatial, spectral, and geometrical features.

3.7.2 Supervised classification

Fusion of the LiDAR point cloud and multispectral imagery enables the generation of high dimensional feature space containing linear and non-linear variables of spectral and geometrical relevance. The effective volume of the feature space, spatial aggregation and numerical range of features call for supervised classifiers with adaptive architectures. We applied an ensemble classification method, Random forest (RF) (Breiman, 2001), on the remote sensing datasets at two different levels of data aggregation: (i) at sub-plot level with explicit reference to different N levels, and (ii) at crop plot level without reference to the N level. About two-thirds of the samples (referred to as in-bag samples) were used to train the model, with the remaining one third (referred to as out-of-the bag samples) used for cross-validation for estimating the quality of the model's performance. Each decision tree is independently produced without any pruning, and each node is split using a user-defined number of features (M_{tree}), selected at random. The algorithm creates trees with high variance and low bias by growing the forest up to a user-defined number of trees (N_{tree}). The final classification decision is taken by averaging (using the arithmetic mean) the class assignment probabilities calculated by all produced trees. The unlabelled data input is thus evaluated against all decision trees created in the ensemble, and each tree votes for class membership. The membership class with the maximum votes will be the one that is finally selected.

3.7.3 Feature importance

During recent years there has been an increased interest in additional RF functions, such as using the variable importance (VI) to optimize feature space (Corcoran et al., 2013; Pedergnana et al., 2013; Belgiu et al., 2014), measuring the correlation between high dimensional datasets on the basis of internal proximity matrix measurements (Peerbhay et al., 2015), or identifying outliers in the training samples by explorative analysis of sample proximities (Corcoran et al., 2013). The VI can be calculated internally in a number of different ways, such as using the Mean Decrease in Gini (MDG) or the Mean Decrease in Accuracy (MDA) (Breiman, 2001). The MDG measures how much a variable reduces the Gini Impurity metric in a particular class. At the same time, the MDA takes into account the difference between the OOB error resulting from a data set obtained through random permutations of the values of the different variables and the OOB error resulting from the original data set (Breiman, 2001). Most studies reported in this review used the MDA to determine the VI.

The fused features serve as a basis for the random forest classification. Random forest is an ensemble decision tree-based learning method for classification, that construct numerous decision trees during training and takes the mode of classes while testing. The principle behind such an ensemble model is that a multitude of decision trees for classification can run over the problem of overfitting caused by a single decision tree classifier. Thus a mixed bag of uncorrelated trees having the same distribution without any pruning, when formed, will outperform an individual decision tree, where the low correlation between the trees is the key factor. The selection of attributes plays a pivotal role in random forests. The most considered attributes are the Information Gain ratio criteria and the impurity index calculation viz Gini Index. As a classifier, random forest devises an automatic feature selection, leading to superior classification performance. This serves as an indicator for feature relevance known as Gini

importance. This feature importance provides a relative ranking of the features. The Gini impurity G(n) decides the ideal split considering how efficiently it separates the samples of two classes for each node n in the trees of the random forest.

Out of the total n features/samples at each node n, with $P_j = n_j/n$, P_i is the fraction of features/samples from class c. The Gini impurity is calculated as:

$$GI(\psi) = \sum_{i=1}^{T} \sum_{j=1}^{N} GI_{\psi}(T, N) \quad (3.9)$$

Due to the optimum split caused by the Gini impurity, reduction in Gini impurity will be amassed over all the nodes in binary tree in the forest for all the variables/features. Considering that, in many cases, crops are classified without reference to the nutrient status, the potential LiDAR point cloud and multispectral imagery were assessed at two levels of data representation – fine and coarse level. At the fine level, the classification was done at the individual sub-plots with explicit reference to the different nutrient treatments of the crops. Therefore, the purpose of the classification was to know whether the LiDAR point cloud or multispectral imagery offers crop discrimination maintaining the sensitivity to different nitrogen levels of crops. At the coarse level, the purpose of classification was mainly to obtain the benchmark crop discrimination results from LiDAR point cloud or multispectral imagery without reference to the nitrogen status of the different vegetable crops considered. The results of the classification were validated by 5-fold cross-validation.

3.7.4 Biophysical characterization

3.7.4.1 Crown area estimation using multispectral imagery

Plant crown area is a vital structural parameter that exhibits a linear relationship with growth and biomass accumulation across the phenological cycle. Estimating tree crown area

using high-resolution remote sensing data has been well documented under individual tree crown detection (ITC) (Wang et al., 2004; Otsu et al., 2019). Amenable to the specific context of the surface objects being short the height of vegetable crops, we have extended the application of the "valley following" method of image segmentation and ITC for crown area estimation for the crops considered. To match the location-sensitive spatial resolution and comparison with the LiDAR point cloud-based estimates, we resampled the multispectral imagery to 10cm resolution and applied a super-pixel based spatially continuous clustering algorithm for the initial candidate plant objects generation. The possibility of within-canopy gaps induced soil pixels in the plant-context image object was reduced by histogram thresholding of the spectral indices. The boundaries of plant-location sensitive crowns generated thus were filtered for spatial continuity and connectivity using morphological operators.

3.7.4.2 Biomass estimation using multispectral imagery

Similar to the scheme implemented for crop discrimination, biomass was estimated using multispectral imagery and LiDAR point cloud independently and with the fused dataset. The spectral attributes capturing the crop structural and biophysical features are indirect. They are mainly embedded in the differential reflectance features in various spectral bands across the optical range of the electromagnetic spectrum. Different spectral indices highlight the nature of the crop response in the recorded spectral radiance in the multispectral imagery. Therefore, we estimated biomass from multispectral imagery using various spectral indices as surrogate variables for biomass modelling. Based on the sensitivity to the vegetation structure and seven standardized and derived spectral indices, namely, enhanced vegetation index (EVI), soil-adjusted vegetation index (SAVI), normalized difference vegetation index (NDVI),

normalized difference water index (NDWI), green normalized difference vegetation index (GNDVI), blue normalized difference vegetation index (BNDVI), and wide dynamic range vegetation index (WDRVI) were computed from the multispectral imagery biomass (Adam et al., 2014; Ramoelo et al., 2015; Wang et al., 2017; Chlingaryan et al., 2018; Chao et al., 2019; Kayad et a., 2019; Guan et al. 2020). A detailed mathematical formulation of these spectral indices is available in Thenkabail et al. (2018). In conjunction with reference ground truth measurements of the biomass, the spectral indices and crown area were used as the predictor variables in the SVR based regressing modelling for estimating the crop biomass. The high-density capability of the TLS used enables acquiring LIDAR point cloud retaining the individual plant structures in the data. However, the size of vegetable crop plants, expressed by canopy extent and height, is smaller than the resolution spatial resolution of most high-resolution multispectral imagery, including the WorldView-III, distinct retention of crop plant structure is not functionally possible, per se. Most remote sensing studies attempting to retrieve canopy area and height are directed at natural vegetation such as a forest. In contrast, the LiDAR point cloud enables retrieval of canopy area and height as direct variables. Hence, we retrieved only the biomass from the multispectral imagery for further comparison with the estimations from the LiDAR point cloud.

3.7.4.3 Biomass estimation using LiDAR point cloud and the fused dataset

Plant height has a direct linear relationship with biomass for a range of standing crops (Franco and Kelly, 1998; Poorter et al., 2012). For many vegetable crops, also applicable in several other crops, plant height saturates at maturity, and the further accumulation of biomass, and hence responses to different N levels, is reflected mainly in the form of the lateral expansion of plant components characterized by crown area. The non-linear relationship

between N levels and biomass response can be modelled better with plant crown area. Considering the synchronized existence of linear and non-linear patterns of N levels, biomass response and plant height and crown area as predictor variables, we applied a non-parametric machine learning model, support vector regression (SVR) (Shim and Chang, 2011), for modelling the crop biomass for various levels of N. Based on the cross-validation and heuristics, the hyper-parameters of the SVR algorithm - loss function ε, error penalty factor C, and kernel function were estimated. Adapting a similar methodological framework used for estimating biomass from the LiDAR point cloud, the fused dataset, which contained spectral attributes appended to each discrete point in the point cloud, was used for biomass estimating through the SVR algorithm. As the dimensionality of the feature space was higher for the fused dataset, the divergent set of features was optimized by an iterative forward feature selection method to choose the most influential variables.

The validation of the biophysical parameters follows the same procedure as described in section 3.5.1.5.

3.7.5 Deep learning-based fusion of LiDAR point cloud and WorldView – III imagery

The filtered point cloud and the corrected WorldView-III imagery are input to the model. The point cloud was further rasterized and resampled to a spatial resolution of 0.5m to match with a spatial resolution of WorldView-III imagery (Figure 3.15). For performing the classification of crops, we designed a 2D deep convolutional neural network for crop classification. For ingesting the fused dataset into this DL framework, the data has to be prepared. The classification has been performed at three different levels of N: medium, low and high for each crop considered. For plant level training patches, a subset of 7x7x5 was

extracted from the fused imagery and referred to each class for classification, thus totalling nine different classes. For each crop, 140 patches were extracted for each training set. To satisfy the training needs of deep CNN, the original training patches were used for data augmentation, thereby increasing the number of training data samples sufficient to cater for the learning training requirement of DCNN. Data augmentation in computer vision refers to increasing the size of the data set by creating modified image versions through various geometrical transformations such as shift, rotation, flip, zoom etc. Thus before augmentation, the intensity values of the spectral bands were normalized to meet the intensity range across different bands of the dataset.

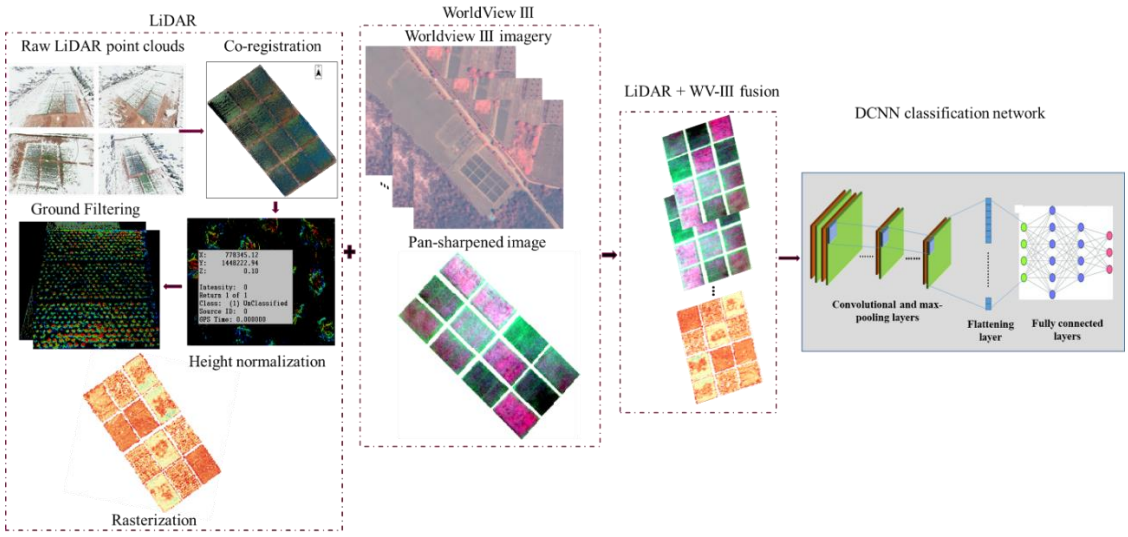

Figure 3.15: Overall methodology flowchart adopted for deep learning based classification of crops at different levels of N.

Outline of the architecture of DCNN for classification is shown in Figure 3.15. the fused dataset represented as image patches of size nx7x7x5 was given as input to the 2D convolution layer. 2D convolution understands the spatial context of the input imagery and can produce better classification results compared to the individual–pixel level approach. There are three convolution layers of size as described in Figure 3.15, where each convolution layer is given

the activation function ReLu (Rectified Linear Unit). In contrast to the traditional way of applying max-pooling after each convolution layer, we performed feature aggregation after all the convolution layers. The layers were flattened into a single dimension as a latent representation and fed into the fully connected layers to produce the results of crop classification.

To prevent the problem of over-fitting typical to learning algorithms, dropout with probability 0.5 and exponential decay based learning rate techniques were applied to generalize the loss function. For optimization of the loss function, an adaptive moment estimation (adam) optimizer was used, which has a faster convergence rate.

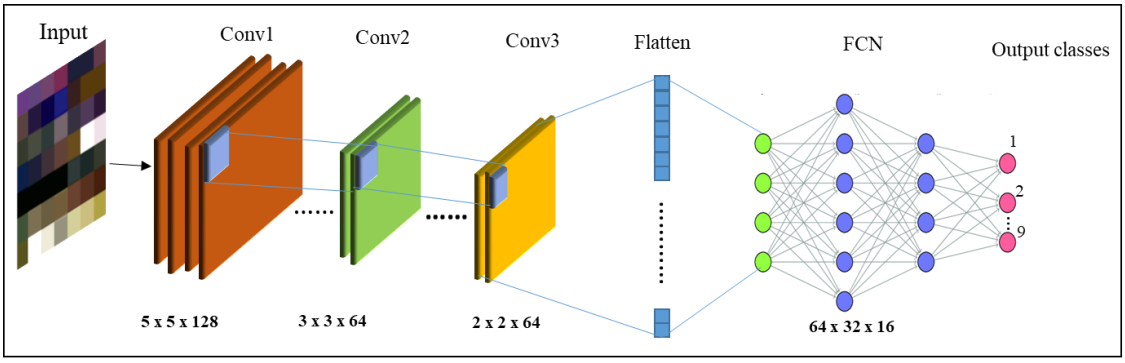

Figure 3.16: Top-level overview of DCNN architecture designed for crop classification with specific reference to N levels

3.8 Methodology developed for implementing Objective 4 (to develop a DL based temporal framework to predict crop structural parameters)

Figure 3.17 shows the overall methodology flow developed to implement this objective. The basic DL architecture adapted is a variant of the recurrent neural network (RNN), where a stacked model of LSTM (Long Short Term Memory) and GRU (Gated Recurrent Unit) networks are used. We named the deep learning model developed for this specific purpose as

'TemporalCropNet'. Figure 3.17 depicts the TemporalCropNet architecture. Unlike the feed-forward neural networks, recurrent neural networks use their internal state memory to process the data sequences. To overcome the drawbacks of RNN, such as vanishing gradient or exploding gradient problem, two variants of RNN such as LSTM and GRU, were developed. A single LSTM unit is composed of a cell, an input gate, an output gate, and a forget gate, which facilitates the cell to remember values for an arbitrary amount of time. The gates control the flow of information in and out of the LSTM cell.

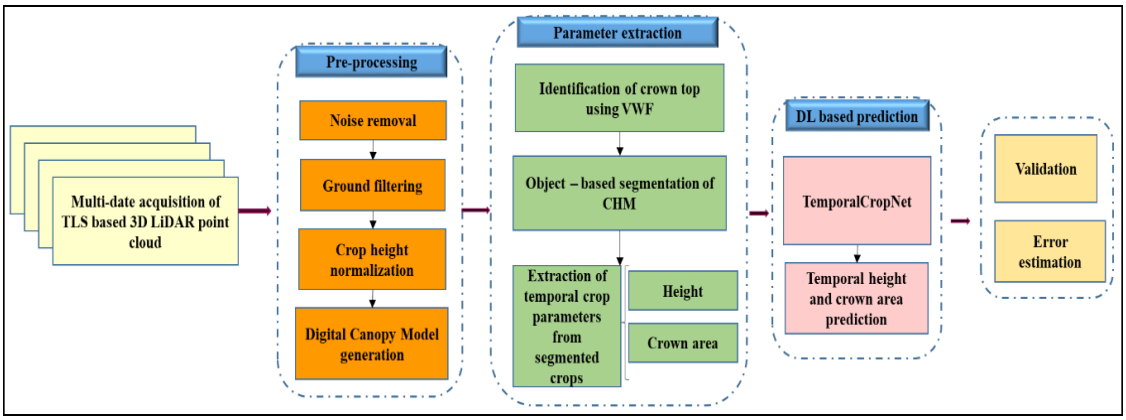

Figure 3.17: Flowchart depicting the steps involved in the prediction of crop parameters.

A brief description of recurrent neural network (RNN), long short term memory (LSTM), gated recurrent unit (GRU) is given below.

3.8.1 Recurrent neural network

Unlike the feed-forward neural network such as CNN that has only a finite receptive field, a recurrent neural network (RNN) can process sequential data using the internal state memory. This dynamic nature of RNN finds application in audio, speech analysis and several other temporal based applications. The recurrent state is achieved by connecting the time steps'

output as input to the network and using the same weights to back propagate through time. Therefore, RNN is a neural network that uses the shared weights for each time step. At the same time, RNN suffers from short-term memory when the sequence length becomes larger and suffers from vanishing gradient problems during backpropagation. Neural network weights are updated using gradients while back propagating. The issue of vanishing gradient produced leads to minimal gradients and contributes nothing to the learning process, thus leading to short-term memory. LSTM (Long Short Term Memory) and GRU (Gate Recurrent Unit) are proposed as a solution to the short term memory problem. These variants of RNN have gates in the internal memory cell that can retain the data sequence and thus regulate the information flow. In the following sections, we briefly describe the two variations of RNN, namely LSTM and GRU. A top-level architecture of stacked LSTM-GRU adapted for the proposed 'TemporalCropNet' as shown in Figure 3.18.

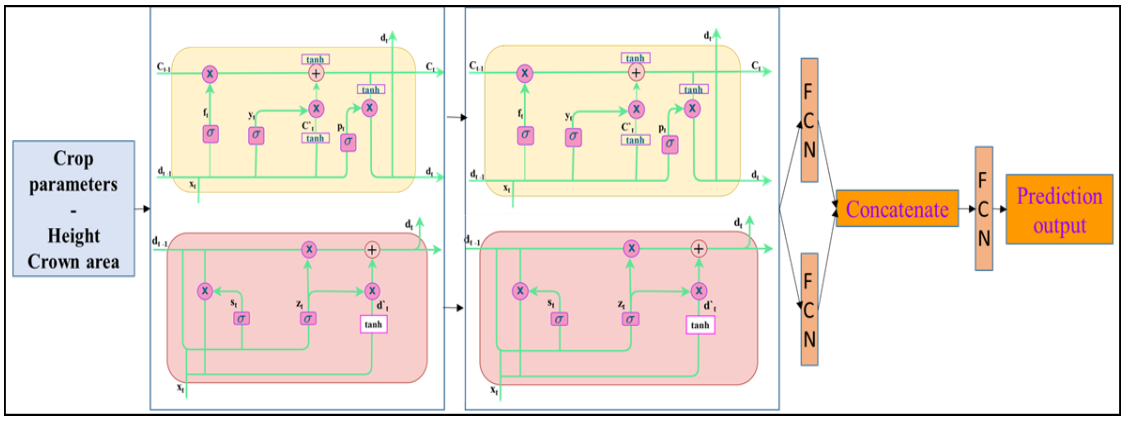

Figure 3.18: Stacked LSTM-GRU architecture of TemporalCropNet

3.8.2 Long Short Term Memory (LSTM)

The cell state and the gates are the core structural elements of the sequential network, LSTM. A high-level representation of LSTM is similar to that of RNN but differ in terms of

the internal representation of the memory cell. The input to the sequential network is a sequence of vectors (x_1, x_2,… x_n), where x_t is the input at time t. The three basic units of the LSTM are forget gate (f_t), input (y_t), and output gate (p_t). The forget gate determines to keep or discard the information from the previous time step. From the input gate, LSTM learns new information that enters the cell. The output gate passes the updated information in the cell from the present time-step to the next. Similar to RNN, LSTM also has hidden state d_t, d_{t-1}, representing the current and next step's hidden unit. Also, the cell state is represented by c_t and c_{t-1} for the current and next time step, respectively. The cell state and hidden states are the two states of LSTM. All the gates undergo the sigmoid activation function, which gives the output value for each state and gate ranging between 0 and 1. In addition to that, LSTM also has a temporary cell state $C`_t$, where the hyperbolic tangent activation function is applied that outputs values between -1 and +1. In The final cell state C_t, the forget gate f_t and input gate y_t determines how much information should be kept in the current time step. The new hidden state h_t for the next time step is determined by C_t and p_t, which determines the amount of information the memory cell have at the output step. For all cell states and gates, in addition to the weight parameter, bias value is also added to each equation from (1) - (5).

As represented in Figure 3.18, the hidden state d_t and the cell state C_t for an LSTM cell can be calculated as follows:

$$y_t = \sigma(x_t T^y + h_{t-1} W_y) \tag{3.10}$$

$$f_t = \sigma(x_t T^f + h_{t-1} W^f) \tag{3.11}$$

$$p_t = \sigma(x_t T^p + h_{t-1} W^g) \tag{3.12}$$

$$\tilde{C}_t = tanh(x_t T^g + d_{t-1} W^g) \tag{3.13}$$

$$C_t = \sigma(f_t * C_{t-1} + y_t * \tilde{C}_t) \tag{3.14}$$

Here, y, f, p is called the input, forget, and output gates, respectively. W is the recurrent connection at the previously hidden layer and current hidden layer, T is the weight matrix connecting the inputs to the current hidden layer. The GRU, known as the Gated Recurrent Unit, is an RNN architecture and is similar to LSTM units. The GRU comprises of the reset gate and the update gate instead of the input, output and forget gate of the LSTM. The reset gate determines how to combine the new input with the previous memory and analyses how much information is to be embedded with the current information. The update g ate defines how much of the previous memory to keep around.

3.8.3 Gated Recurrent Unit (GRU)

LSTM has a number of parameters which resulted in a number of operations to be performed. Thus, the variant of LSTM, GRU, is a simplified, compact representation of LSTM in terms of the parameters and operations performed. Unlike LSTM, GRU has only two gates: reset (s_t) and update (u_t), instead of input, output, and forget gate of LSTM and a hidden state h_t. The reset gate determines how to combine the new input with the previous memory, and the update gate defines how much of the previous memory to keep around. Also, the two gated combine the input x_t and d_{t-1} (information from previous state t-1). Since GRU has lesser tensor operations, it is faster to train the network than LSTM. The computation of z_t, d_t is given in equations (6) - (9) expressed below:

$$u_t = \sigma(x_t T^u + d_{t-1} W^u) \tag{3.15}$$

$$s_t = \sigma(x_s T^s + d_{t-1} W^s) \tag{3.16}$$

$$\tilde{d_t} = tanh(x_t T^d + (s_t * d_{t-1} W^d)) \tag{3.17}$$

$$d_t = (1 - u_t * d_{t-1} + u_t * \tilde{h_t}) \tag{3.18}$$

In this work, we used a stacked representation of LSTM and GRU. Combining multiple LSTM layers leads to greater model complexity and high-level time dependency. Stacked LSTM provides output for each time stamp and not the single output for all time steps. Similar is the case of GRU. Thus, stacking the LSTM and GRU and a combined model helps improve the projection of information in latent dimension space, giving better prediction results. The crop parameters– height and crown area pertaining to different dates of data acquisition are given as input to the TemporalCropNet. Here the LSTM and GRU layers are stacked together to form a hierarchical model. This stacked model was then fed to an individual fully connected layer (FCN) and then combined and given to the final FCN, where the feature concatenation occurs, and the parameters are predicted.

For the validation of the predicted values with the TLS measurements, SMAPE, as discussed in section 3.5.1.5 is used. The training, test and validation datasets were taken as 60, 20, 20 % of the total dataset.

Chapter closing remarks

Studying the changes in spatio-temporal characteristics is necessary as it plays a vital role in precise agricultural farming practice. The dataset used in this study contains high-density ground-based laser measurements of three agricultural crops viz, cabbage, eggplant, and tomato (scientific names) captured using a Terrestrial Laser Scanner. This dataset helps to characterize the crops at various growth stages at varying nitrogen levels and derive the biophysical crop parameters. The data can also be used as a reference for understanding the potential of LiDAR for precision farming practices.

Identification, classification and estimation of biophysical parameters of the vegetable crops have been carried out using TLS LiDAR point cloud, WorldView–III imagery and a combination of both the datasets. The crown area and biomass at different N levels have been assessed using SVR. An improved version of PointNet based on DCNN has been proposed for the classification of crops by directly ingesting 3D LiDAR data to the network. Further, at varied N levels, a feature-based fusion of LiDAR and WorldView –III imagery using random forest classifier has been used to classify the crops at the patch level. A deep learning-based pixel-level classification approach has also been followed using DCNN for this fused dataset. Finally, the prediction of structural parameters of the crops using DL based method named TemporalCropNet has been proposed that predicts the height and crown area during the crop growth stage.

CHAPTER 4

RESULT AND ANALYSIS

Prelude

This chapter presents the results of all the experiments and methodologies implemented for all the objectives of the thesis. The results are presented in the same order to maintain the order of tasks in each objective. The first section presents the results of the estimation of the biophysical parameters at different levels of nitrogen using the LiDAR point cloud. The second section's content is related to objective 2, the deep CNN-based object-level classification of LiDAR point cloud for crop discrimination at the plant level. Results of the third objective - RF-based classification of the crops by the fusion of WorldView-III and LiDAR point cloud and further extension of the data fusion with deep learning approach has been described in the third section of the chapter. Finally, the fourth section presents the results of exploring the deep learning approaches for the temporal prediction of crop structural parameters using LiDAR point cloud. Further, this chapter presents the analysis of the results for ease of readability and organization. A detailed discussion of the results is presented as a standalone chapter (Chapter 5).

4.1 Multi-temporal estimation of biophysical parameters of crops at different levels of nitrogen using TLS point cloud (Objective 1)

4.1.1 Estimation of plant height and the effect of nitrogen (N) levels

The combined use of plant height and crown area estimations allowed the accurate and consistent biomass across growth stages and N fertilization levels. The relationship between measured versus estimated plant height as a function of the different levels of N fertilization is shown in Figure. 4.1. For high N, plant height discrimination derived from the TLS point cloud allowed distinguishing between tomato and eggplant. A low percentage of deviation error (SMAPE < 5), coupled with strong correlations ($R^2 \geqslant 0.96$ across crop species and N level), and a compact spread of estimations around the one-to-one line indicate that the plant height retrievals are accurate for all crops (Figure. 4.1).

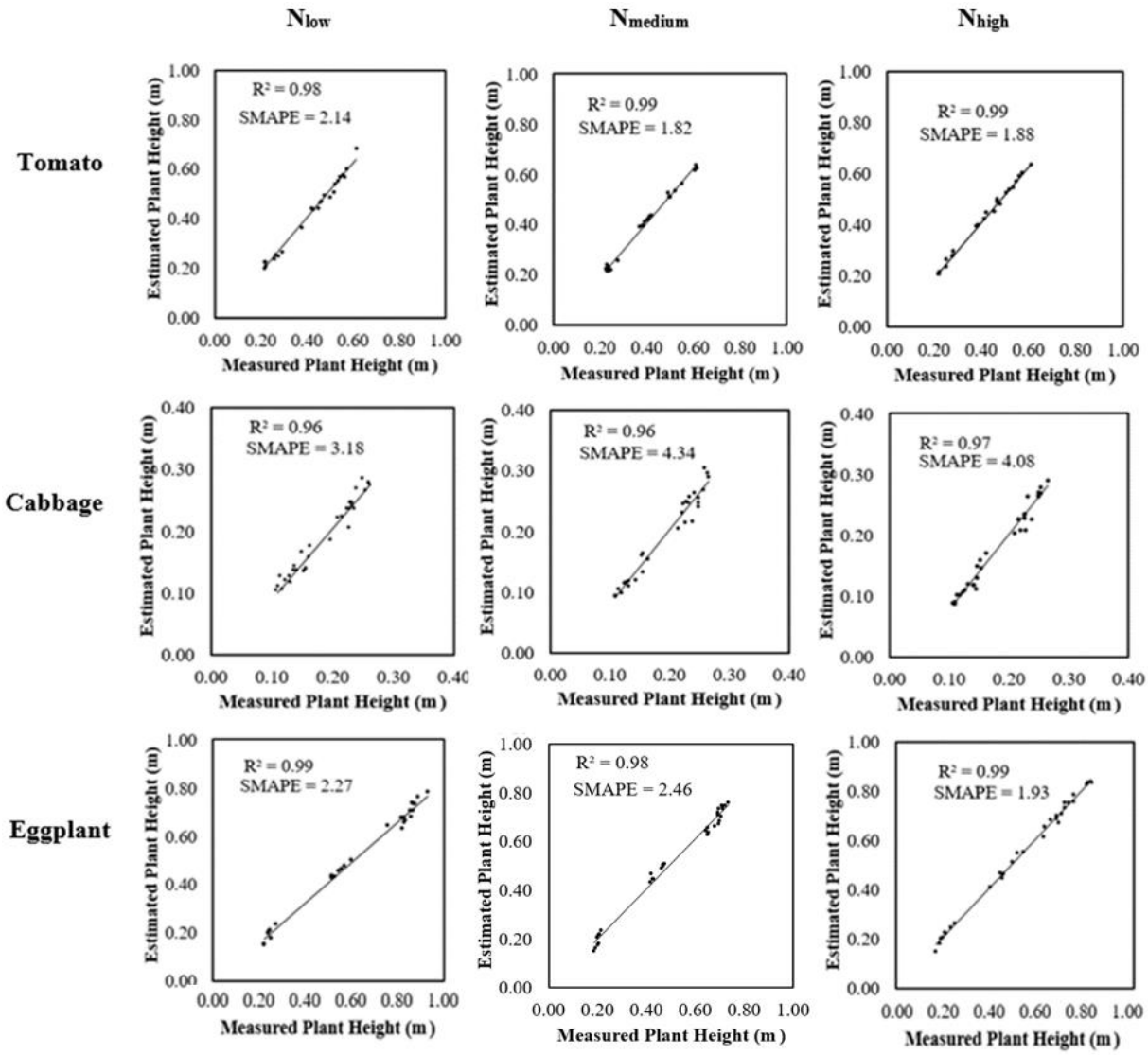

Figure 4.1: Correlation between ground-based (measured) and TLS-based (estimated) plant height of tomato, cabbage, and eggplant across the growing period for low, medium, and high levels of N. The coefficient of determination (R^2) and symmetric mean absolute percentage error (SMAPE) are given.

Both the overestimation and underestimation of plant height were observed. A visualization of the deviation of estimated plant height with reference to the measured height is presented in Figure 4.2. Based on the patterns in the temporal-logarithmic deviations, plant height estimations based on the TLS point cloud were equally prone to positive and negative bias during early growth stages. However, after the height of the crops, especially for eggplant and tomato, exceeded 25 cm (sampling date 2), there was a decrease in the incidences of

underestimation and a comparable increase in the frequency of overestimations was observed. The data show that overestimation occurred more frequently at sampling date 2 than on date 3. Based on the crop-wise logarithmic deviation, the plant height of cabbage was more substantially overestimated compared to the other two crops.

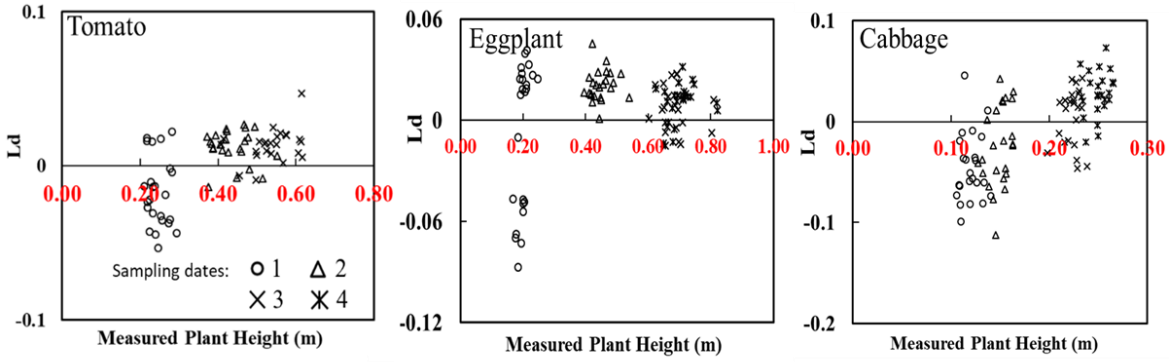

Figure 4.2: Directional variation, given as the logarithmic deviation (L_d), between measured and TLS-estimated plant height for eggplant, tomato, and cabbage, at four different sampling dates in a factorial experiment at the University of Agricultural Sciences (GKVK Campus), Bengaluru, India.

The analysis of the variation of plant height (Figure 4.3) for 15 medium N plants sampled along a transect within a sub-plot indicates substantial within-plot variance. These within plot height variations were consistent for sampling dates indicating a localized N effect on the plant growth profile.

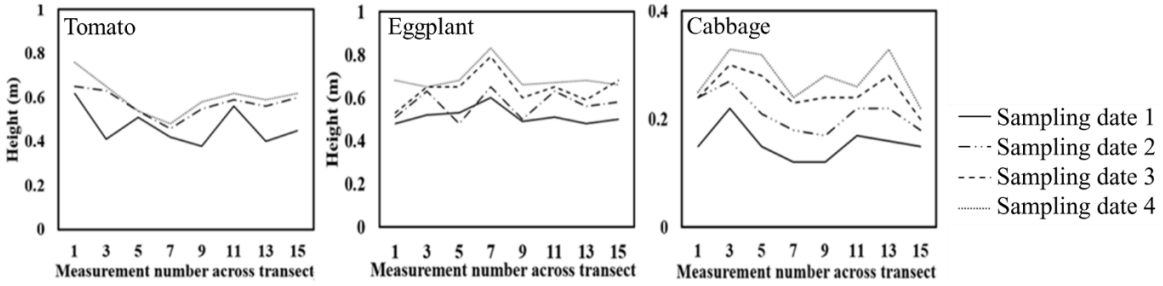

Figure 4.3: Spatial variation of plant height for four dates within a single plot (medium N level) in a factorial vegetable experiment at GKVK Campus, Bengaluru, India. Sampling date 1, sampling date2, sampling date 3, and sampling date 4 correspond to 18 April 2017, 4 May 2017,22 May 2017, 14 June 2017 respectively.

4.1.2 Estimation of plant crown area

The results of crown area estimation using the TLS point cloud indicate remarkable consistency in the prediction accuracy for all the three crops considered (Figure 4.4). The crown area estimations indicate accurate retrievals for all three crops, with even the poorest performing treatments achieving a maximum SMAPE of 13.63 (tomato with medium N fertilization) and a minimum R^2 of 0.81 (cabbage with cabbage medium N fertilization).

The estimated and measured crown area samples were distributed compactly around the one-to-one line, indicating the closeness of the predicted and measured crown area for all three crops (Figure 4.4). Compared to estimated plant height, the crown area estimations spread widely at medium N. Besides, the examination of the range of crown area estimations across N fertilization levels for tomato and eggplant indicated a pattern of higher N fertilization producing a larger crown area. As evident from the relatively low SMAPE values compared to other crops, crown area estimation for cabbage presents a rather complex scenario of similarity of measured and estimated crown area with large ranges within N fertilization treatments. For tomato, the range of predicted crown area indicates a progressive accumulation with increasing N. As for plant height estimations, the linear accumulation of crown area across growth stages and its estimation by a TLS point cloud are promising.

The majority of the deviations of crown area predictions for eggplant indicate slight overestimations (Figure 4.5). For tomato, the deviations between measured versus estimated tomato crown area indicate both overestimations and underestimations throughout the growing season (Figure 4.5). In the absence of apparent crop-specific patterns in the deviations between measured and estimated crown area, as well as crop height, the setup of the TLS point cloud measurements and transient micro weather patterns (e.g. wind, moisture) control the direction of estimation deviations.

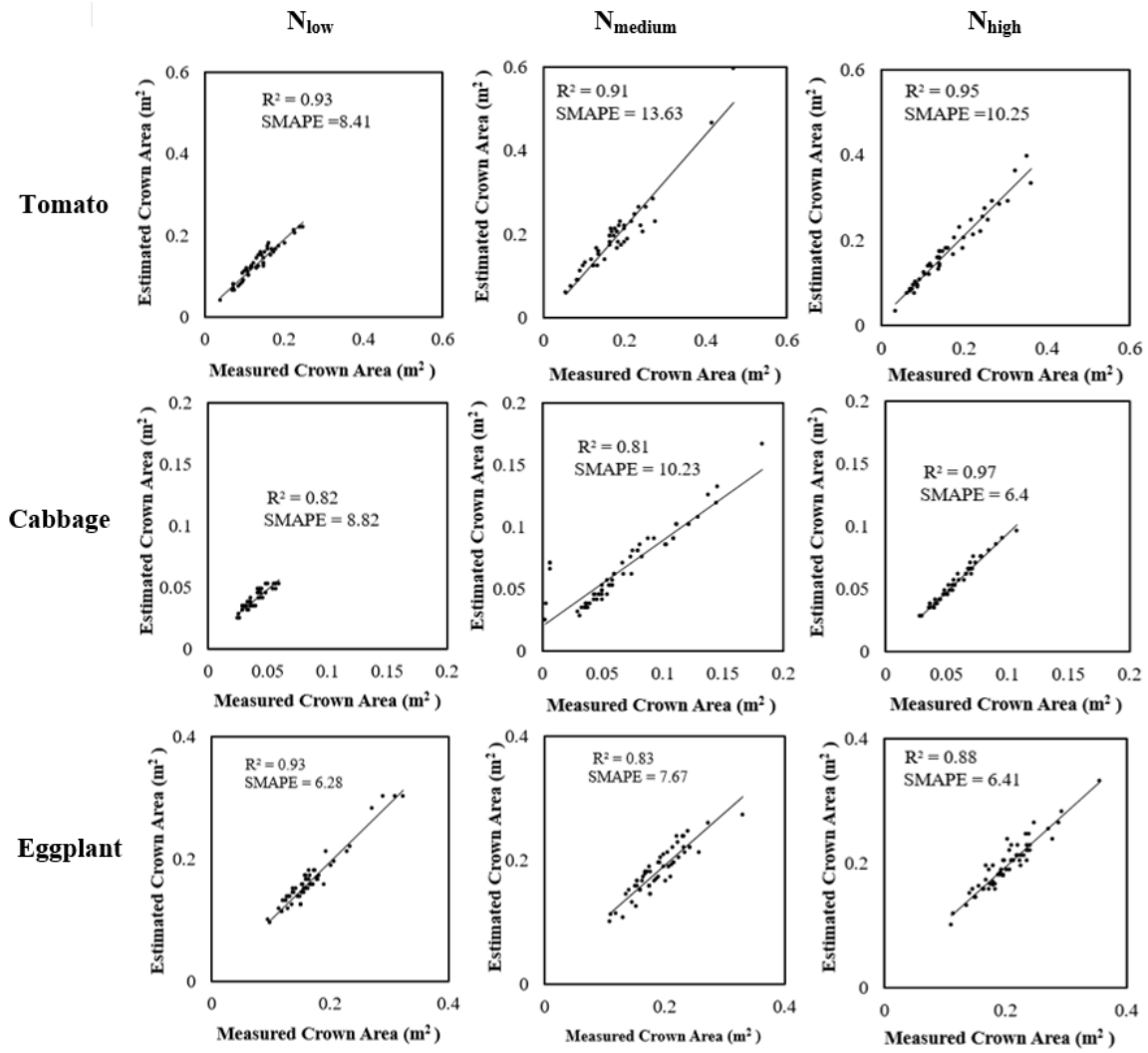

Figure 4.4: Correlations between ground-based (measured) and TLS-based (estimated) crown area for tomato, cabbage and eggplant crops across the growing season for low, medium, and high N fertilization levels. The coefficient of determination (R^2) and symmetric mean absolute percentage error (SMAPE) are given.

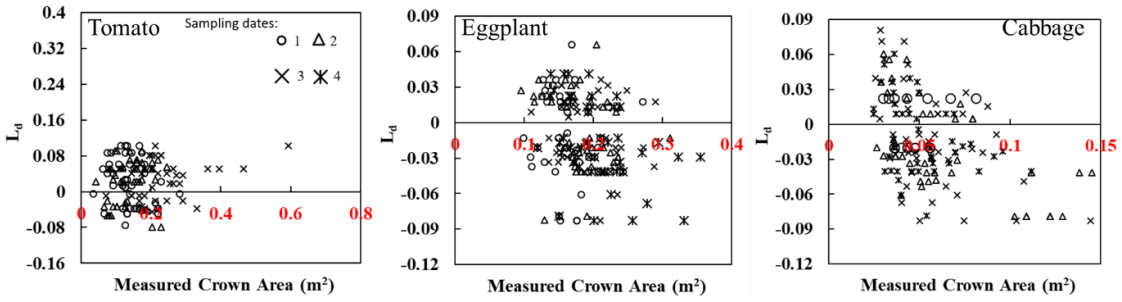

Figure 4.5: Directional variation, given as the logarithmic deviation (L_d), between measured and TLS-estimated crown area for eggplant, tomato, and cabbage at four different sampling dates.

4.1.3 Estimation of biomass

Our premise was that the precise estimation of plant biomass ought to consider the complex relationship between canopy patterns and distributed structural parameters such as the crown area. As evident from Figure 4.6, there is a consistent and robust relationship between the predicted and measured biomass for all three crops throughout the growth period (R^2 = 0.92 for tomato, 0.96 for cabbage, and 0.98 for eggplant). The SMAPE for tomato, cabbage, and eggplant was 7.53, 5.46, and 3.96, respectively, indicating consistent agreement between predictions and the reference biomass measurements. Examination of the vertical spread and distribution of the biomass for the three N fertilization levels suggests the lack of unambiguous discrimination between biomass estimations at different N levels (Figure 4.6).

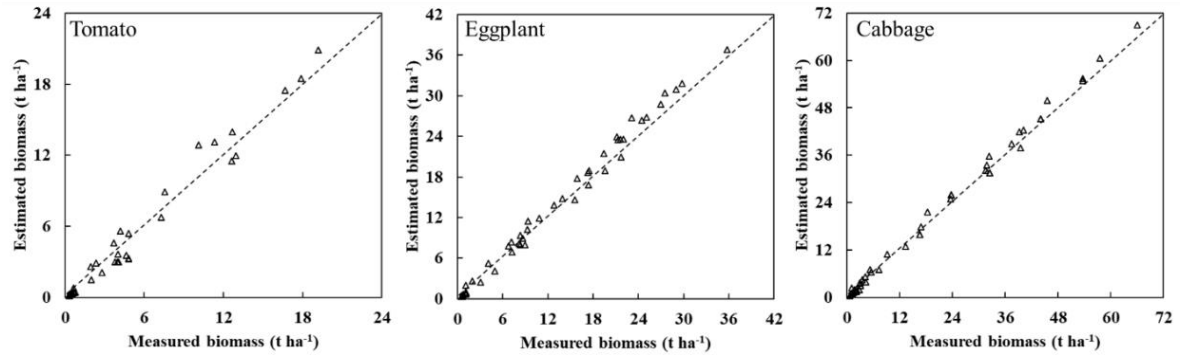

Figure 4.6: Correlation between ground-based (measured) and TLS-based (estimated) biomass for eggplant, tomato, and cabbage for three N levels across the growing season.

For eggplant and cabbage, the estimated and measured biomass values spread across the biomass range, indicating the confusion of samples across the different N levels (Figure 4.7). However, biomass estimations for high and medium N are discernable for tomato, especially at the stage of higher biomass, even though confusion prevails at lower biomass levels. Biomass estimations of the three crops show two distinct patterns (Figure 4.7). At the first sampling date, crop biomass was underestimated substantially, followed by moderate overestimation as the crops grew (from the second sampling date onward).

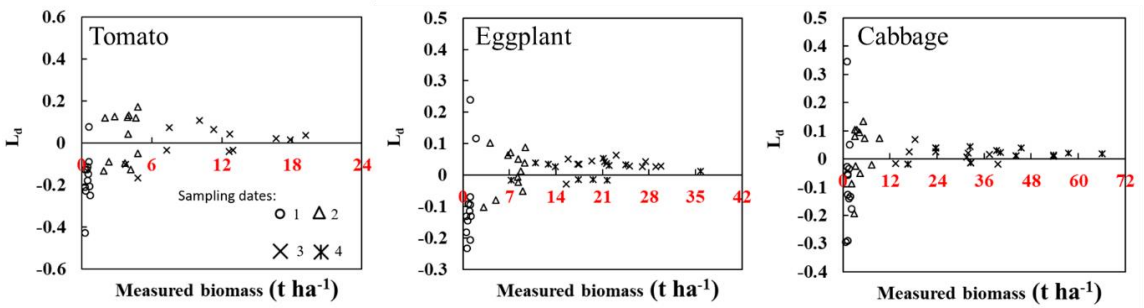

Figure 4.7: Directional variation, given as the logarithmic deviation (L_d), between measured and TLS-estimated biomass for tomato, cabbage, and eggplant at different sampling dates.

The initial sampling dates occurred during the emergence and vegetative development of the plants. At this time, canopy cover was generally lower, and soil exposure was relatively high. As a result, the probability of receiving laser pulses returned from the plants is leading to less underestimation or overestimation. As the crops grow, the underestimation of biomass changes to overestimation at biomass > 6 t ha^{-1}. The second pattern is stable and indicates a higher level of consistency in matching estimated and measured biomass for all three crops. Manual validation of the plant count using high-resolution digital pictures captured concurrently indicated accuracies of > 85% (Table 4.1).

Table 4.1: Measured versus terrestrial laser scanning (TLS) based estimates of plant counts at the plot level on sampling date 1 in a factorial vegetable experiment at University of Agricultural Sciences (GKVK Campus), Bengaluru, India.

Crop name	Plot number	Number of plants		Nitrogen treatment
		Plant Enumeration	TLS Estimated	
Eggplant	1	101	94	Medium
	2	102	93	Low
	3	103	90	High
Cabbage	10	200	186	High
	11	191	183	Medium
	12	190	185	Low
Tomato	22	100	86	High
	23	97	83	Medium
	24	97	91	Low

4.2 Deep learning-based methodology for multi-crop point cloud classification of agricultural crops (Objective 2)

Results of the object-based point cloud classification of the vegetable crops using the CropPointNet deep learning architecture are presented in Figure 4.8 and the corresponding accuracy estimates in Tables 4.2 and 4.3. As evident from Figure 4.8, the individual plant level discrimination of the tomato, cabbage, and eggplant is unambiguous. The crop objects in the point cloud were classified with the best overall accuracy of 81.5% by the CropPointNet model. The PointNet and DGCNN models yielded an overall accuracy of 55% and 66.5%, respectively (see Table 4.2). However, the quality of discrimination varied by the crops and the model. Cabbage and eggplant crops were discriminated accurately by the CropPointNet and DGCNN models (see Fig. 4.8(a), (c)). The discrimination of tomato crop was very low by all the three models, despite very high inter-crop discrimination. Most of the tomato crop discriminations are underestimations with the apparent confusion with residual soil ridges (see Fig. 4.8(b)). Results from the PointNet model show a substantial misclassification wherein the cabbage crop was overestimated at the cost of eggplant followed by tomato.

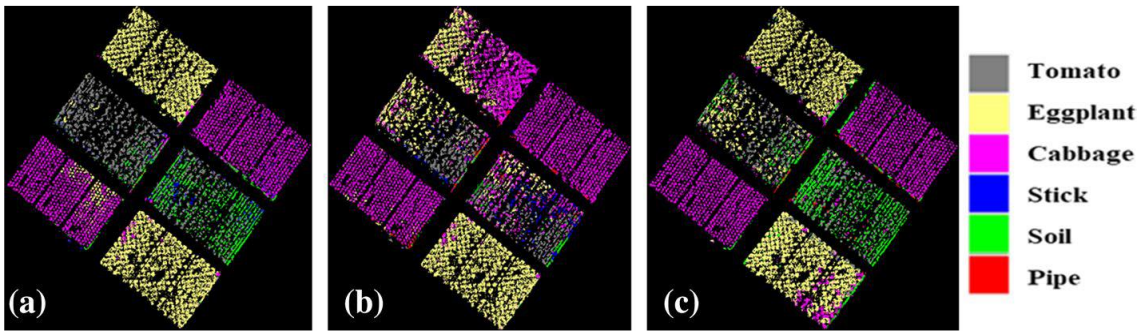

Figure 4.8: Semantic segmentation using (a) CropPointNet (b) Pointnet and (c) DGCNN

Cabbage and eggplant crops are discriminated with the highest accuracy of 91% and 88%, respectively (see Table 4.3). For the non-crop classes (residual soil ridges, pipe, and

stick), the CropPointNet model yielded relatively higher per-class accuracies (about 70%) even though substantially lower than the accuracy of the crops. The discrimination of non-crop classes by the PointNet model is negligible (see Table 4.3). Cabbage and eggplant were classified with a marginal difference of accuracy (3%). However, the Precision scores of cabbage and eggplant differed substantially (12% and 21%) from the CropPointNet model and PointNet model, respectively. Eggplant and cabbage were classified with Precision of 91% and 79%, respectively. Compared to the accuracy metric, the Precision score matches closely with the quality of crop classifications accounting for the false positives in the cabbage. The Recall and F1 Scores substantiate the matching of crop classifications with the ground truth data. Overall, the scores of Precision, Recall, and F1-Score are very closer to the overall and per-class accuracies estimated from the k-fold cross-validation. Compared to the PointNet model, results from the CropPointNet model are much superior by magnitude and consistency of all the accuracy metrics across the crop and non-crop classes (see Tables 4.2 through 4.5). The results of the statistical z-test computed between the performance of the CropPointNet with PointNet and DGCNN models yielded a z-score of 6.31 and 3.81, respectively. At the 95% confidence interval, the computed z-scores are higher than the tabulated value of 1.96, confirming that the superior classification performance of the CropPointNet is not by chance. This observation confirms the potential impact of the point cloud sampling strategy introduced in the training stage of deep learning networks in the CropPointNet architecture.

Table 4.2: Per-class accuracy estimates (%) for crop and non-crop categories in the LiDAR point cloud from all three deep learning neural network models.

Class	CropPointNet	PointNet	DGCNN
Tomato	65	60	61
Eggplant	88	69	83
Cabbage	91	72	82
Stick	79	21	00
Soil	72	41	81
Pipe	70	50	76

Table 4.3: Overall accuracy (%) of the classification of point cloud for vegetable crops from all the three deep learning neural network models.

Models	Overall Accuracy (%)
CropPointNet	81.5
PointNet	55.2
DGCNN	66.5

Table 4.4: Object-to-object comparison of CropPointNet model predictions and ground truth for accuracy estimation - Precision, Recall, and F1-score.

Class	Precision	Recall	F1 Score
Tomato	0.79	0.85	0.81
Eggplant	0.91	0.88	0.89
Cabbage	0.79	0.91	0.85
Stick	0.79	0.79	0.79
Soil	0.71	0.76	0.73
Pipe	0.91	0.70	0.79

Table 4.5: Object-to-object comparison of the reference PointNet model predictions and ground truth for accuracy estimation - Precision, Recall, and F1-score.

Class	**Precision**	**Recall**	**F1-Score**
Tomato	0.69	0.60	0.64
Eggplant	0.48	0.69	0.56
Cabbage	0.38	0.90	0.54
Stick	0.84	0.21	0.33
Soil	0.95	0.41	0.57
Pipe	0.72	0.50	0.59

The discrimination of the non-crop geometrical objects (return pulses from irrigation pipes, support sticks, and residual soil ridges) from the crop plants in the scene is a vital requirement for automatic crop scene analysis. Figure 4.9 visualizes the segmentation of a sub-plot for each crop. The crops are segmented at the plant level, exhibiting distinct separability with other geometrical features such as support sticks. Segmentation results from the CropPointNet model (Figure 4.8(a)) are unambiguous compared to the relatively confused discrimination of tomato plants (Figure 4.8(b, c)).

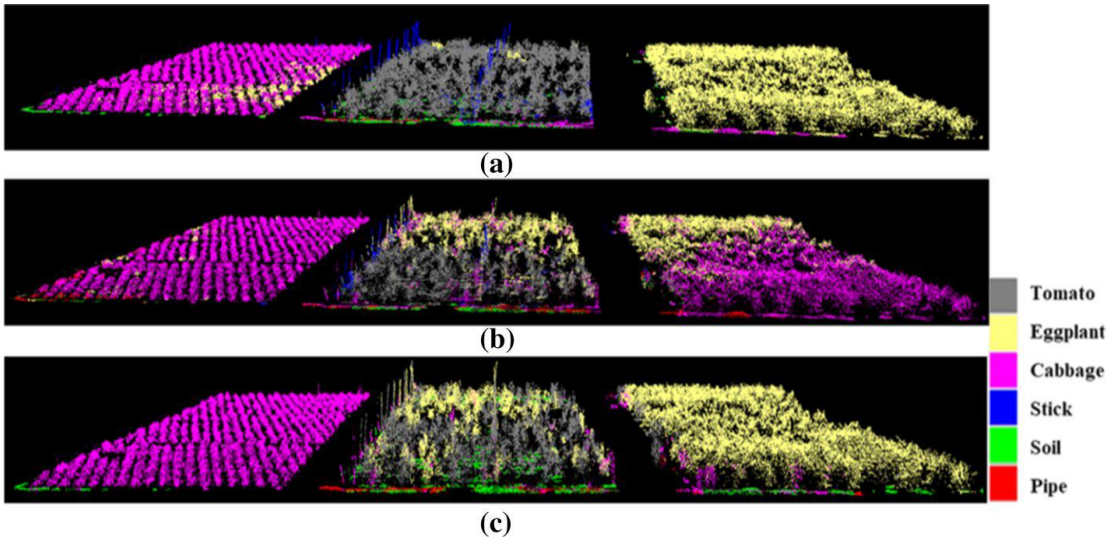

Figure 4.9: Visualization of the crop segmentation at a sub-pot level depicting the separation of crop plan9ts from the non-crop geometrical features from the models (a) CropPointNet, (b) PointNet, and (c) DGCNN.

4.2.1 Spatial conformity of the predicted crop plant objects

The statistical accuracy metrics analyses for assessing the performance of the crop discriminations show consistently good accuracy in the point cloud classification for crop discrimination at the semantic point labelling level. However, as the deep learning model architectures implemented in this research are object-based segmentation and classification approaches, in principle, it is possible to evaluate the accuracy by matching at crop plant object level. The level of completeness and correctness of the object-based labelled crop plants was assessed using a matching area-based accuracy metric, Intersection over Union (IoU) expressed as

$$\text{IoU} = \frac{\text{Area of Overlap}}{\text{Area of Union}} = \frac{\text{TP}}{\text{TP+FP+FN}}, \tag{4.1}$$

where FN is false negative, FP is false positive, and TP is true positive for the respective information classes considered. The mean IoU (mIoU) was computed from the IoU values of

all the six classes. The IoU values of the crop and non-crop information classes are shown in Table 4.6. The IoU values of each information class and the mIoU exceed the threshold (Meng et al. 2019) IoU value, indicating the consistency of plant-to-plant level classification results.

Table 4.6: Estimates of the per-class and mean IoU of object-oriented classification of vegetable crops. Values greater than 50% indicate consistent matching of predictions of crop plants with ground truth.

Class	**CropPointNet**	**DGCNN**	**PointNet**
Tomato	80.66	70.71	59.74
Eggplant	81.58	80.42	68.07
Cabbage	83.54	90.47	74.27
Stick	65.88	0.00	25.65
Soil	63.68	74.01	41.26
Pipe	61.32	70.10	48.68
mIoU	**72.78**	**64.28**	**52.94**

4.3 Examining the potential of integration of TLS point cloud with high-resolution multispectral satellite data for crop discrimination at different N levels (Objective 3)

4.3.1 Crops discrimination with explicit reference to the nitrogen status

The results of the classification of the vegetable crops for three different cases of data aggregation: LiDAR point cloud, multispectral imagery and the fused data at the fine and coarse level are presented in this section. The results of classification for the fine level depicting the discrimination of the vegetable crops with reference to nutrient level are shown in Figure 4.10 and the corresponding statistical measures of accuracy: confusion matrix, Kappa coefficient and the overall accuracy obtained from the cross-validation in Figures 4.11 and 4.12. As evident from the accuracy metrics (Figures 4.11 and 4.12) and the spatial diffusion of segments of two different crops visible in Figure 4.10, the quality of crop discrimination from the multispectral imagery is poor.

Multiple inter-crop confusion cases led to misclassification of a crop sub-plot (e.g. cabbage) wrongly labelling as another crop (e.g. tomato), explaining the lowest accuracy of about 68% by kappa coefficient (see Figure 4.12). Compared to the results from only multispectral imagery, the results obtained from using only the LIDAR point cloud are relatively better. The overall accuracy is about 79%, indicating a 10% higher accuracy than the multispectral imagery results (see Figure 4.12). This improvement can be ascribed to the apparent reduction in the mislabelling of the whole sub-plot to partial sub-plot, indicating the dominance of structural features in the discrimination. The classification results from the fused datasets are distinct (92% accuracy) and significantly higher than the results (20% improvement) obtained from the multispectral imagery or the LiDAR point cloud, supporting the hypothesis is that spectral and structural features are vital for discriminating different crops with reference to nutrient level. However, a few sub-plots are wrongly labelled by nutrient

level, even though classifying was correct by crop type (see Figures 4.10b, 4.11a). For example, a sub-plot of cabbage with medium N was classified as a sub-plot of cabbage with low N.

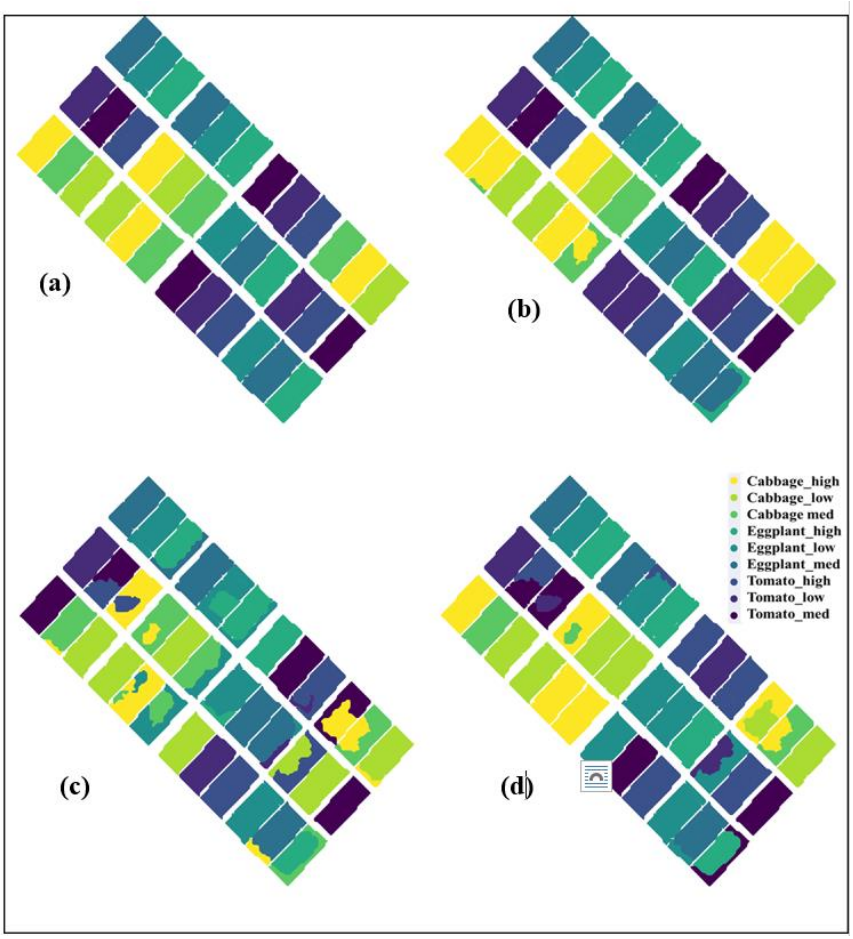

Figure 4.10: Classification map obtained using different sensors (a) Ground truth, (b) WorldView-III and LiDAR classification, (c) LiDAR classification, and (d) WorldView-III classification.

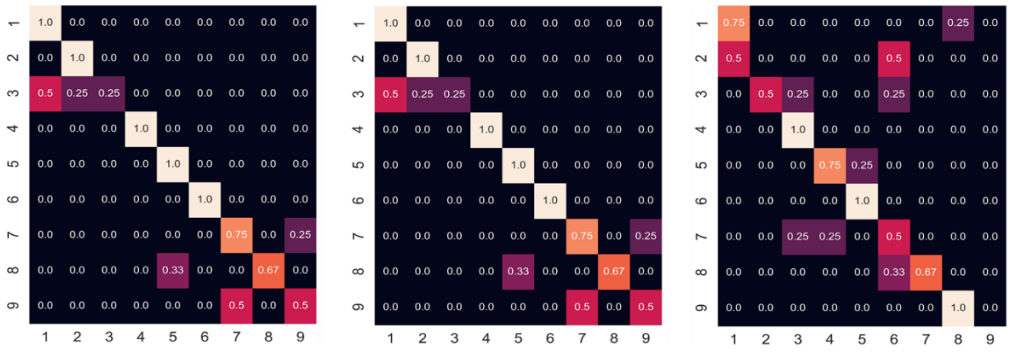

Figure 4.11: Confusion matrix of three different sensor combinations for classification (a) WorldView-III and LiDAR, (b) LiDAR, and (c) WorldView-III.

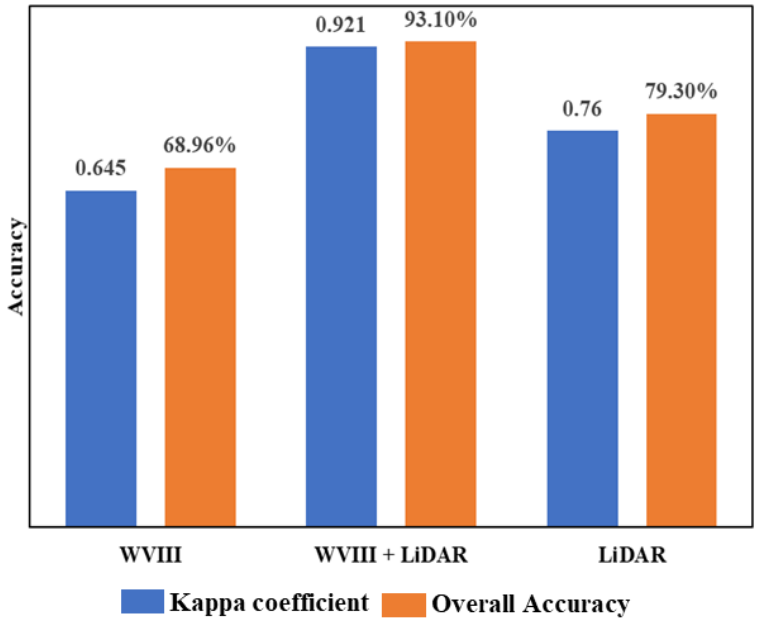

Figure 4.12: Bar plot showing Kappa coefficient and overall accuracy of classification with N reference for the case of data WorldView-III only, WorldView-III +LiDAR combined, and LiDAR point cloud.

4.3.2 Crops discrimination without reference to the nitrogen status

The results of the classification model that was trained with reference crop patches extracted from different locations in the scene, without specifying the nitrogen status, are presented in Figures 4.13 and 4.14. As evident from Figure 4.14, the quality of crop discrimination with the multispectral imagery is reasonably good, with an overall accuracy of about 88% (see Figure 4.14). The significant performance gap (about 20%) observed between the multispectral imagery and the LiDAR point cloud for the case of classification with explicit reference to nitrogen level has reduced substantially. Indicating the continuance of the dominance of structural features, compared to the results from multispectral imagery, the classification results from using only the LiDAR point cloud are still better, even though the margin of accuracy difference reduced to only 5%. In both cases, a few patches of cabbage

were wrongly classified as tomato or eggplant. The crops are discriminated in the fused dataset with close to 100% accuracy. However, the margin of accuracy improvement is only 7% indicating that either of the spectral or geometrical features alone can differentiate the crops without reference to the nitrogen status of crops.

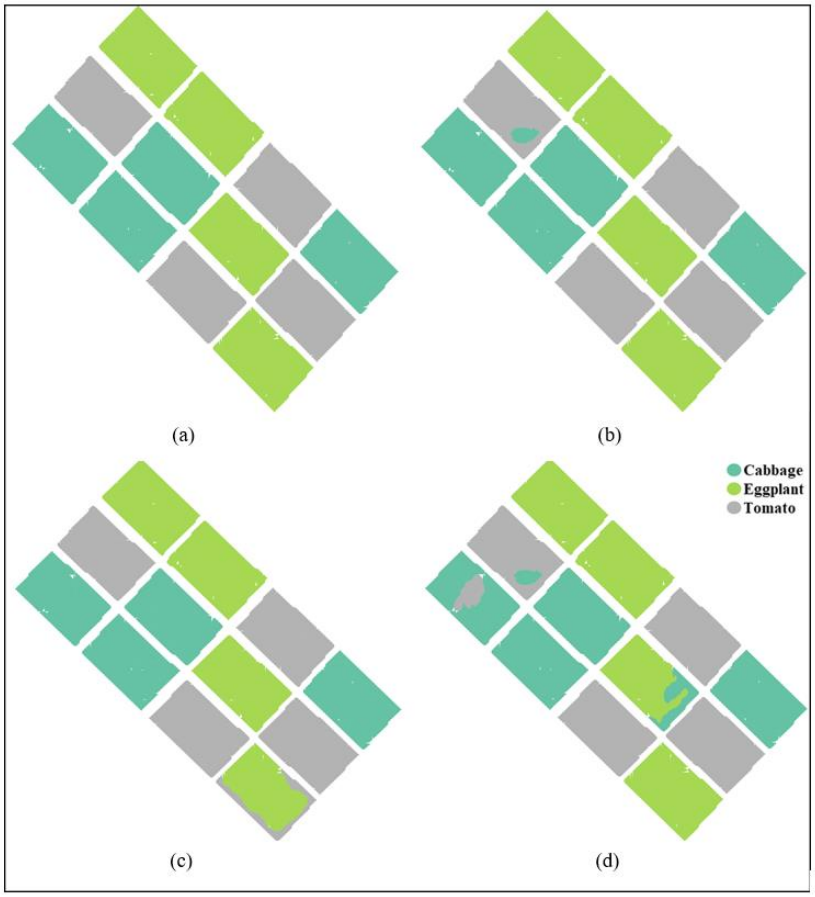

Figure 4.13: Classification results without reference to N treatment obtained from (a) ground truth, (b) from the fused dataset generated from multispectral imagery and LiDAR point cloud, (c) from LiDAR point cloud, and (d) from multispectral imagery.

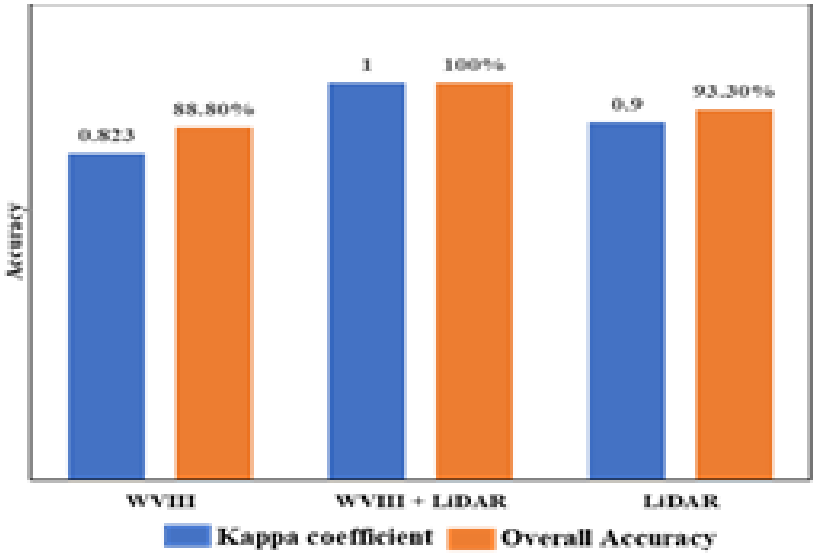

Figure 4.14: Overall accuracy and Kappa coefficient of classification without reference N from multispectral imagery (WorldView-III), fused dataset (WorldView-III +LiDAR), and LiDAR point cloud (LiDAR).

4.3.3 Feature importance

Gini index indicates the importance of spectral and structural features. The relative importance of different features computed from the fused dataset is shown in Figure 4.15. the variation of the Gini index across different features indicates the relative importance of different of different features. Thus, the Gini index is the deciding factor for variable importance.

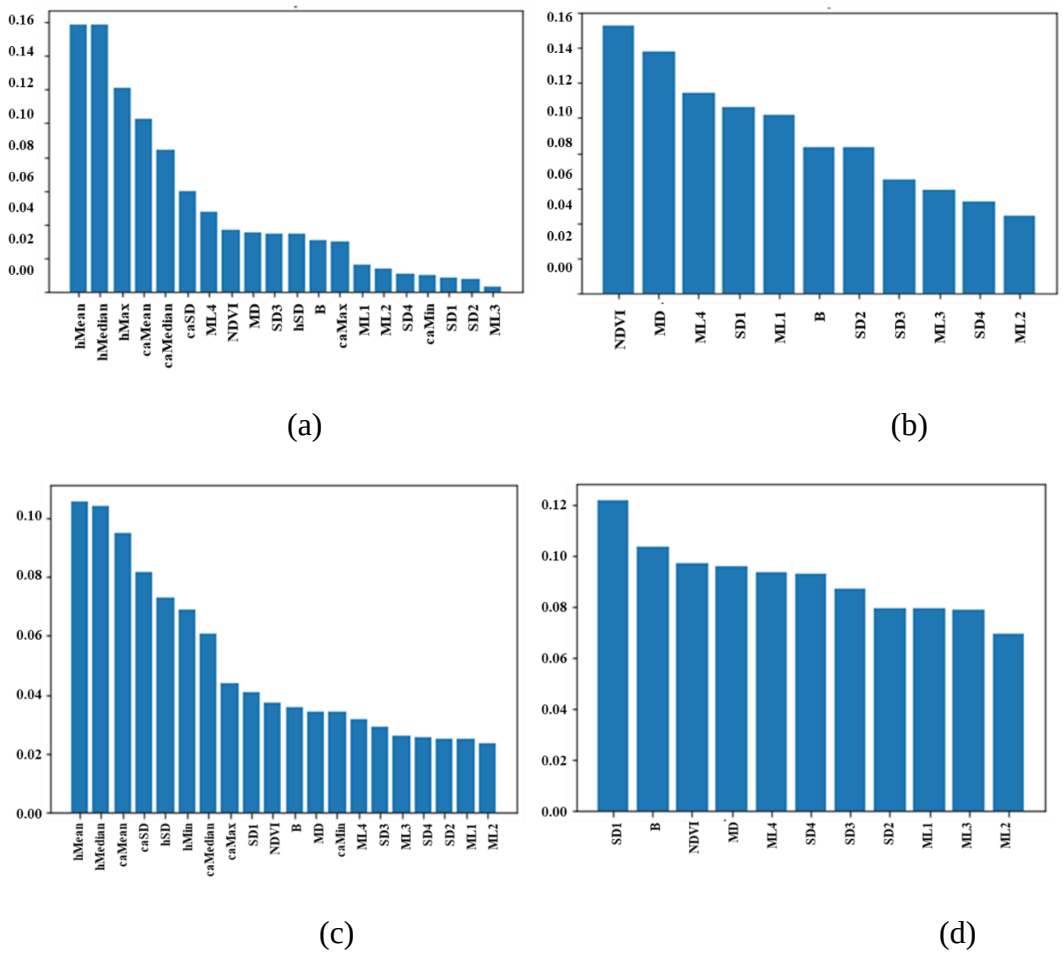

Figure 4.15:(a) Feature importance without explicit reference to N (a) WorldView-III and LiDAR, (b) WorldView-III, (c) WorldView-III and LiDAR, and (d) WorldView-III

The Figure shows the feature importance based on Gini impurity index for explicit reference to N and without N reference. Figures 4.15 (a) and 4.15 (c) represents the feature importance of combined WorldView-III and LiDAR-based classification. Figures 4.15 (b) and 4.15 (d) represents WorldView-III based classification. The height measurements and crown area measurements are LiDAR-derived estimates. The Gini impurity index is relatively for most of the LiDAR-based features indicating the dominance of structural attributes in the crop classification.

4.3.4 Estimation of biophysical parameters

There are two types of biophysical parameters relevant to crop phenotyping. The first category is directly measurable tangible primary plant parameters (e.g. height, canopy area) and forms the primary determiners of crop physical and functional attributes. The second category is intangible and are not directly measurable (e.g. yield, biomass, vigour) but are derived based on the primary parameters. Both the category of parameters is required for functional descriptions of crops from the precision agriculture perspective. We, therefore, assessed the potential of LiDAR point cloud vis-a-vis multispectral imagery independently and in combination by the fusion of the datasets (Figures 4.16 – 4.18 and Tables 4.7 – 4.9).

The crown area and plant height estimates from the LiDAR point cloud are presented for the date at which multispectral satellite imagery was acquired. Crown area estimated using the LiDAR point cloud exhibited a high degree of precision and accuracy across the different N treatments and the crops considered (Figure 4.16 and Table 4.9). The estimated crown area varies linearly, maintaining a stable one-to-one correlation with the measured values. The maximum error of estimation indicated by the SMAPE was about 15%. The range of crown area of cabbage was relatively lower, and the full range variation was not apparent, though statistically exhibiting a linear trend. Closely following the relationship observed with the crown area, the biomass estimated from the LiDAR point cloud consistently correlates with the measured biomass. Compared to the plant crown area, the error of estimation, quantified by SMAPE, is marginally lower. However, as evident from Figure 4.18, the variation of biomass as a function of N treatment exhibit overlapping pattern suggesting the potential diffusion of biomass estimations across N treatments and crops.

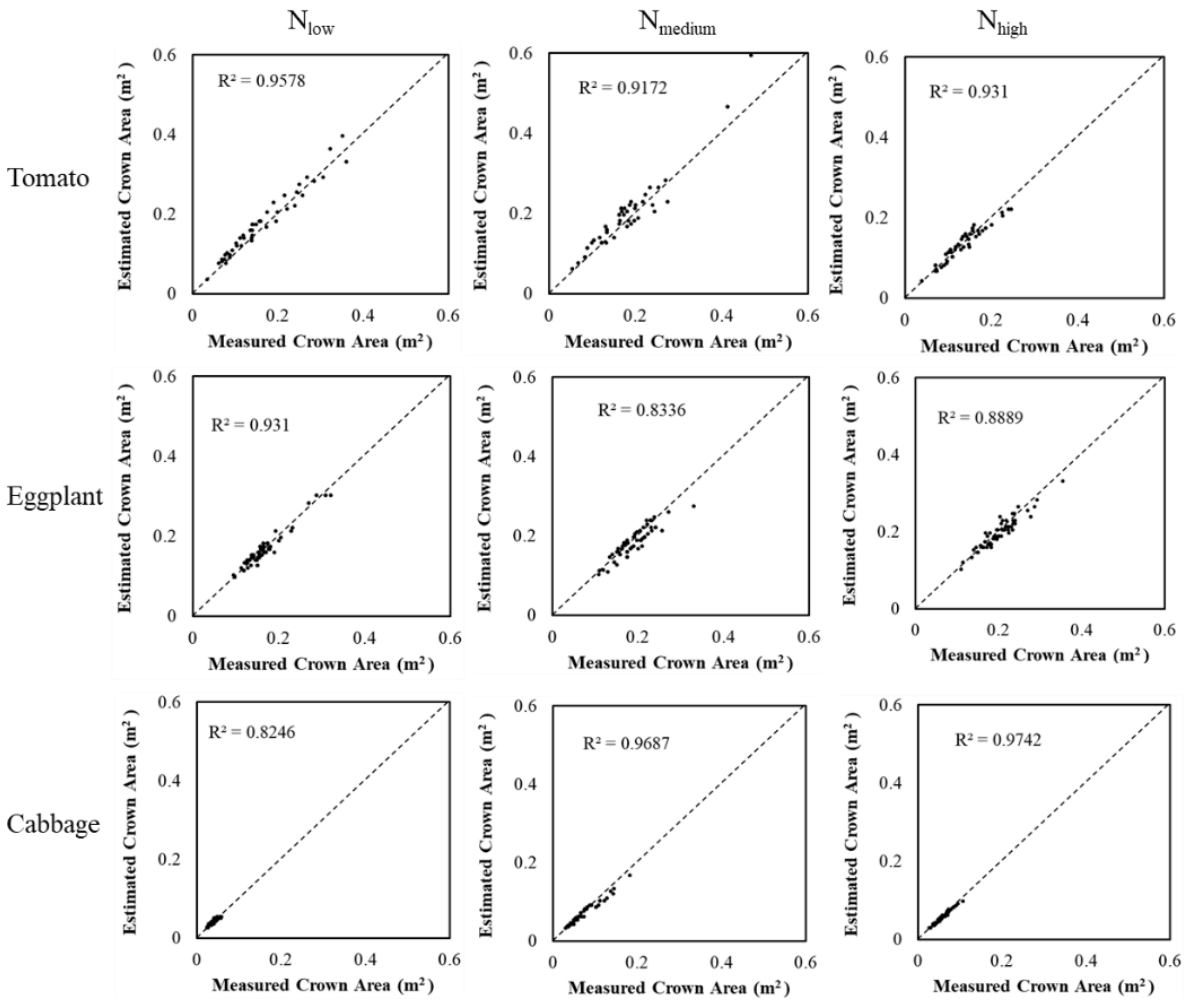

Figure 4.16: Comparison of the plant crown area estimated from LiDAR point cloud with the reference measurements.

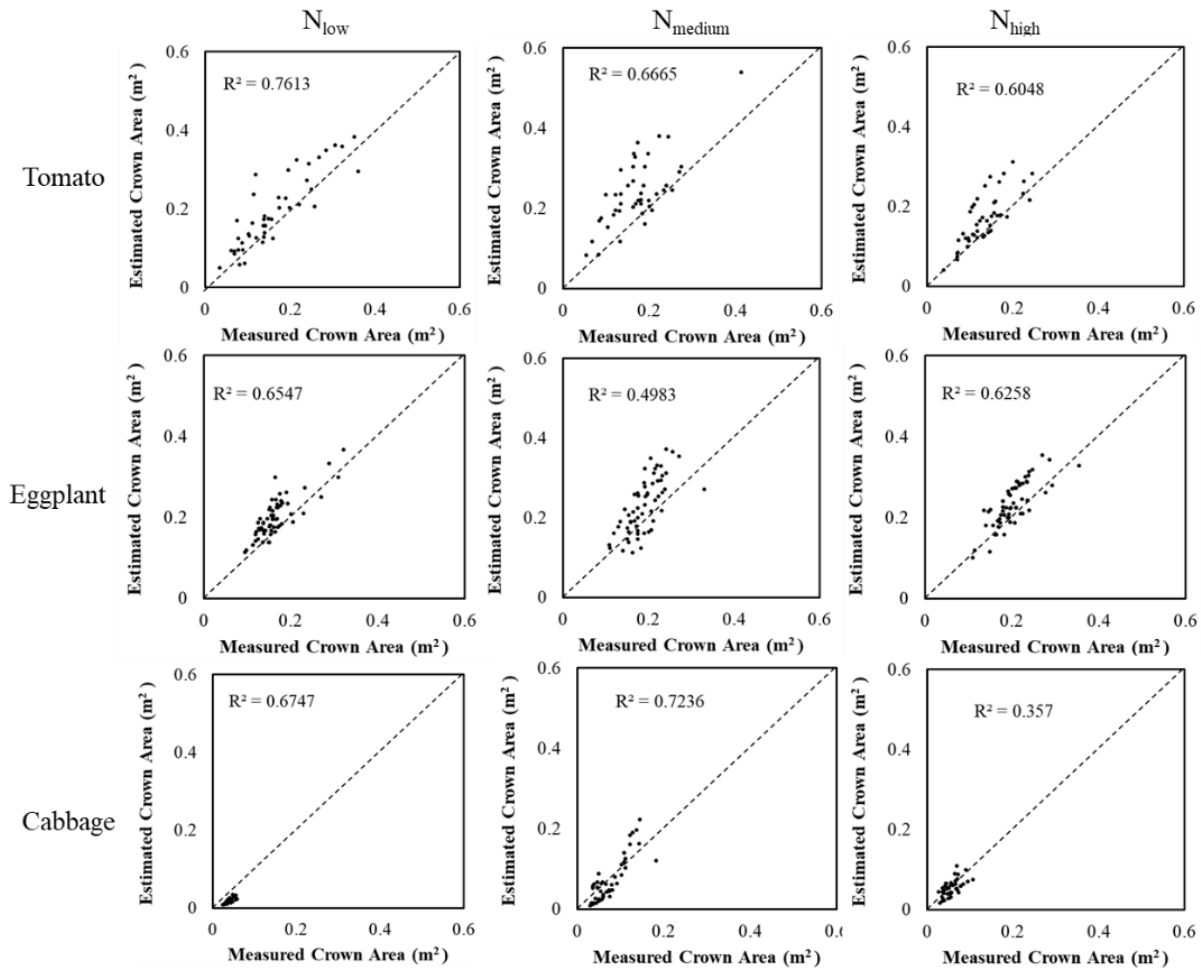

Figure 4.17: Correlation of the plant crown estimates from multispectral imagery (WorldView-III) with the reference measurements.

Compared to the results obtained with the LiDAR point cloud, the estimates of biophysical parameters from multispectral imagery show a contrasting pattern (see Figures 4.17 and 4.19). On the one hand, the crown area estimations exhibit a moderate to lower correlation with the measured crown area. The 'low' level of N treatment indicates a relatively better correlation with the measured across the three crops. Plant crown area estimation for the N treatment 'high' is rather poor. The lowest and higher error of the estimate is about 22 % and 57%, respectively.

On the other hand, the estimates of biomass using multispectral imagery show a consistently higher correlation (lowest R^2 is 0.91) with the measured biomass. They are

comparable with the estimations from the LiDAR point cloud (see Figure 4.19). However, this apparent strong correlation degrades to moderate levels of biomass estimations. The lowest and highest error of estimates is about 22% and 30%, respectively. The error is primarily the overestimation across the N treatments and crops. If the reference to the N treatment condition is relaxed, the estimation of biomass using the multispectral imagery exhibits substantially better results (Table 4.9), especially for the eggplant and cabbage.

The plant crown area and biomass estimates obtained from the fused dataset exhibit a systematically higher level of correlation and accuracy (see Figures 4.16 and 4.17, and Tables 4.7 to 4.9). Compared to the contrasting behaviour of extremely large overestimations of plant crown area and substantial underestimation of biomass from the multispectral imagery, the results of biophysical characterization using the fused dataset exhibit a consistent one-to-one trend across the crops and N treatments. The variation of estimates from the fused dataset for both the plant crown area and biomass is similar to the variation of the estimates from the LiDAR point cloud. Continuing the pattern observed with the LiDAR point cloud or multispectral imagery, the biomass estimates from the fused dataset also show considerable overlapping in the estimates for different N treatments. Overall, the estimation of plant crown and biomass from the fused dataset exhibit marginal to substantial improvements compared to the better estimates from the LiDAR point cloud.

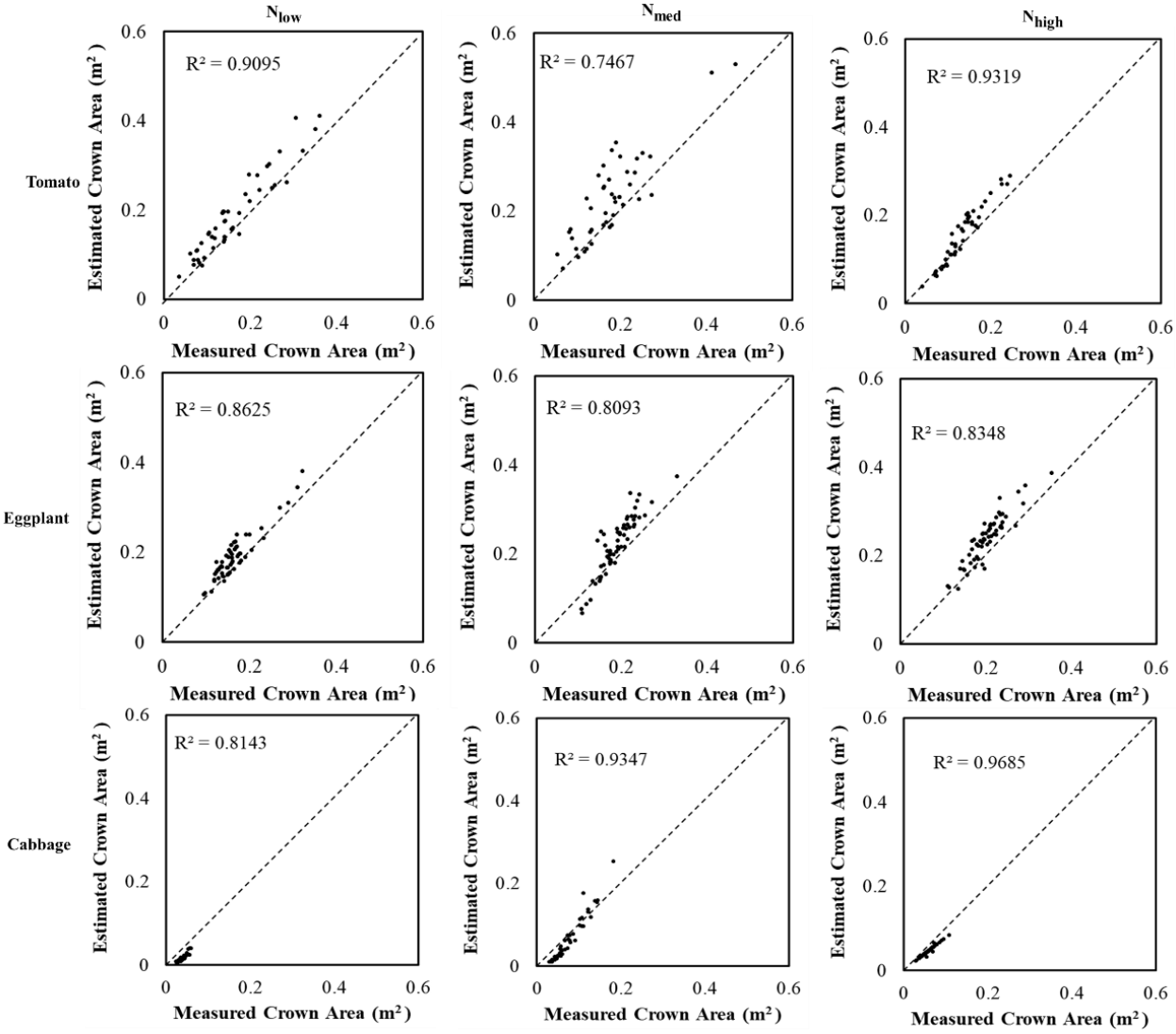

Figure 4.18: Comparison of the plant crown estimates obtained from the fusion of multispectral imagery (WorldView-III) and LiDAR point cloud with the reference measurements.

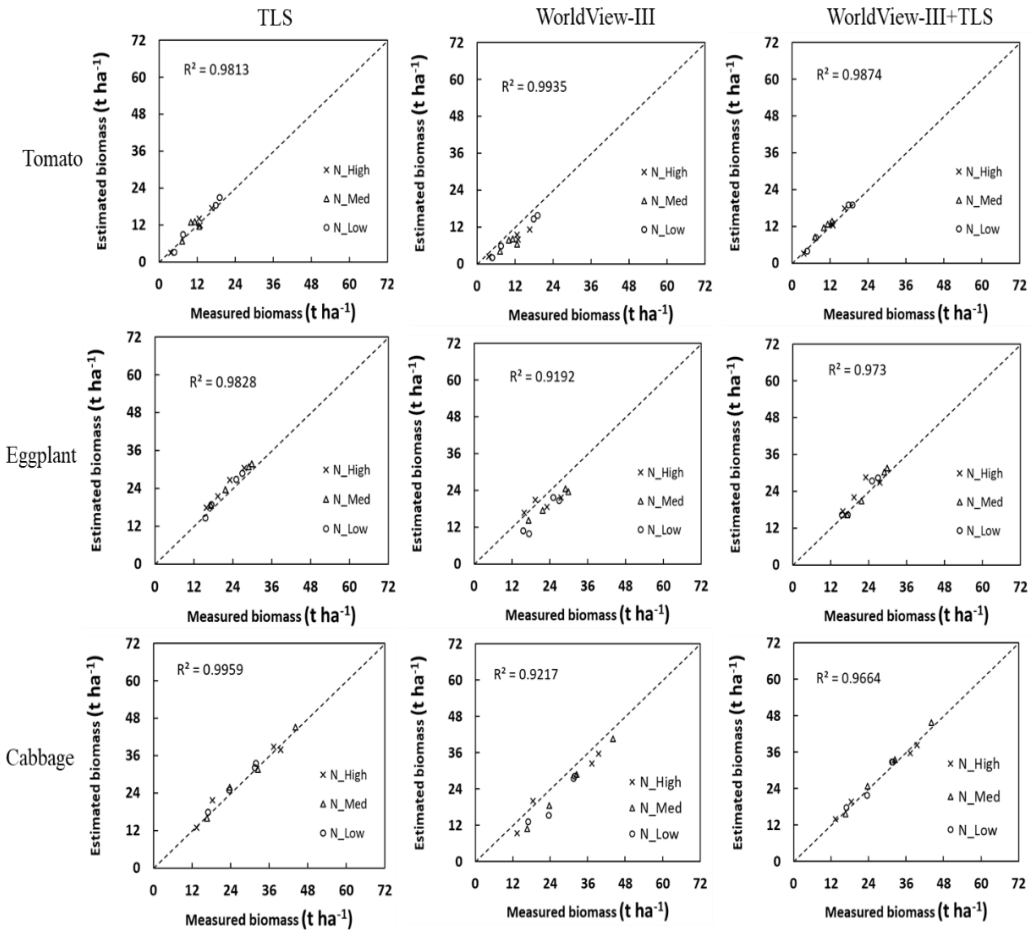

Figure 4.19: Comparison of the biomass estimates obtained from LiDAR point cloud, multispectral imagery (WorldView-III) and combination dataset generated by the fusion of multispectral imagery and LiDAR point cloud with the reference measurements.

Table 4.7: The overall accuracy and error (SMAPE) plant crown area estimates for different N treatments from the remote sensing datasets considered. The measured crown area is also included for ready reference.

Crop	Measured Crown Area (m^2)		Estimated Crown Area (m^2)	Remote sensing data type								
				TLS			WorldView-III			WorldView-III + TLS		
				Mean	Accuracy (%)	SMAPE (%)	Mean	Accuracy (%)	SMAPE (%)	Mean	Accuracy (%)	SMAPE (%)
Tomato	L	0.163		0.175	88.32	11.68	0.191	72.74	27.26	0.188	80.02	19.98
	M	0.179		0.194	84.17	15.83	0.248	63.78	36.22	0.226	70.11	29.89
	H	0.134		0.132	90.35	9.65	0.166	69.31	30.69	0.154	80.36	19.64
Eggplant	L	0.169		0.167	92.85	7.15	0.204	77.69	22.31	0.195	83.48	16.52
	M	0.198		0.191	90.36	9.64	0.242	72.67	27.33	0.228	81.99	18.01
	H	0.211		0.205	92.4	7.6	0.245	81.05	18.95	0.248	82.32	17.68
Cabbage	L	0.039		0.04	90.25	9.75	0.016	42.9	57.1	0.016	67.44	32.56
	M	0.076		0.07	85.95	14.05	0.071	56.23	43.77	0.06	71.15	28.85
	H	0.057		0.054	92.28	7.72	0.053	67.47	32.53	0.044	75.01	24.99

Table 4.8: Summary statistics of overall accuracy, prediction error (SMAPE) of the biomass estimated for different N treatments from the remote sensing datasets considered. For ready reference, measured biomass values are also presented. Negative values of SMAPE indicate the error of underestimation.

Crop	Measured Biomass (t ha-1)		Estimated biomass (t ha^{-1})	Remote sensing data type								
				TLS			WorldView-III			WorldView-III + TLS		
				Mean	Accuracy (%)	SMAPE (%)	Mean	Accuracy (%)	SMAPE (%)	Mean	Accuracy (%)	SMAPE (%)
Tomato	L	12.35		12.90	95.76	4.24	9.60	77.75	22.25	12.57	98.21	-1.79
	M	11.85		12.55	94.42	5.58	8.22	69.38	30.62	13.10	90.42	-9.58
	H	11.52		11.61	99.19	-0.81	7.76	67.39	32.61	11.62	99.10	-0.90
Eggplant	L	21.26		22.25	95.57	-4.43	15.81	74.35	25.65	22.13	96.08	-3.92
	M	24.44		26.25	93.12	-6.88	19.98	81.72	18.28	24.78	98.63	-1.37
	H	21.46		24.10	89.07	-10.93	19.48	90.73	9.27	23.75	90.38	-9.62
Cabbage	L	25.97		27.12	95.76	-4.24	21.05	81.05	18.95	26.28	98.84	-1.16
	M	29.22		29.63	98.65	-1.35	24.73	84.60	15.40	29.93	97.66	-2.34
	H	27.19		27.83	97.70	-2.30	24.40	89.75	10.25	26.90	98.95	1.05

Table 4.9: Summary of the biomass estimation when there is no specific reference to N treatment. The estimated biomass is compared against the mean of the measured biomass. The SMAPE value in the negative sign indicates the error of underestimation.

Crop	Measured biomass (t ha^{-1})	Estimated biomass (t ha^{-1})	Remote sensing data source								
			TLS			WorldView-III			WorldView-III + TLS		
			Mean	Accuracy (%)	SMAPE (%)	Mean	Accuracy (%)	SMAPE (%)	Mean	Accuracy (%)	SMAPE (%)
Tomato	11.40		11.85	96.05	-3.95	7.99	70.09	29.91	11.94	95.26	-4.74
Eggplant	22.39		24.20	91.92	-8.08	18.42	82.27	17.73	23.55	94.82	-5.18
Cabbage	27.40		28.19	97.12	-2.88	23.39	85.36	14.64	27.70	98.91	-1.09

To understand the relevance of inherent variability in the field conditions, the mean and standard deviation of the measured biomass values are plotted for different N levels (Figure 15). The measured biomass exhibits substantial variations across the N treatments and crops (Figure 15). The intra-crop biomass variation was more than the inter-crop biomass, thereby blurring the predictive boundaries of the non-parametric discrimination models used for fusion and estimation of biomass.

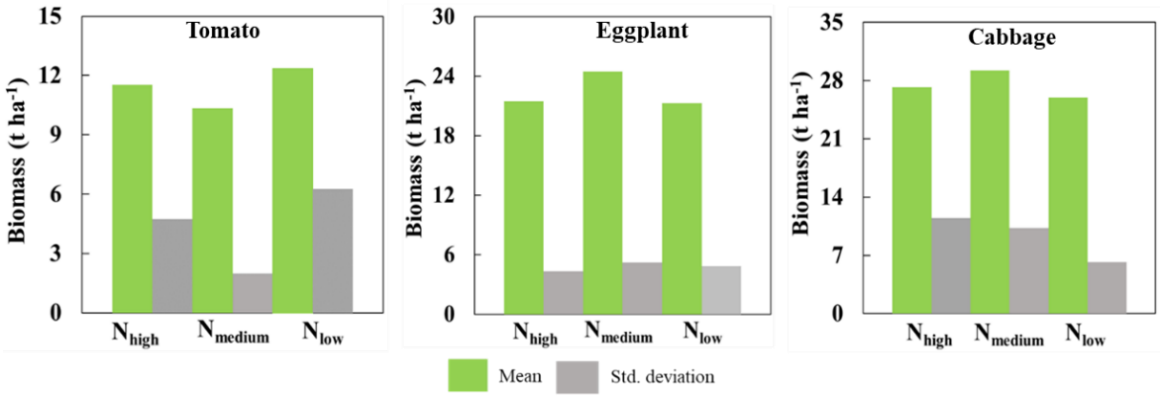

Figure 4.18: First-order statistical representation of the measured biomass across the N treatments.

4.4 Potential of deep learning for fusion-based classification of crops at different N levels

A deep convolution neural network was used for the classification of the crops with explicit reference to different levels of N. The idea was to evaluate if there is any discernible improvement in the discrimination of the crops considering the implicit nature of nutrient effects on the crop growth. Especially the apparent confusion that was observed with the classification of the crops using the RF algorithm at the object level, in which within in crop confusion was prevailing at the N level, was expected to be solved with the deep learning-based approach at the pixel-level. Results of the validation of the deep CNN based classification of the fused dataset are shown in Figure 4.19 and Table 4.10.

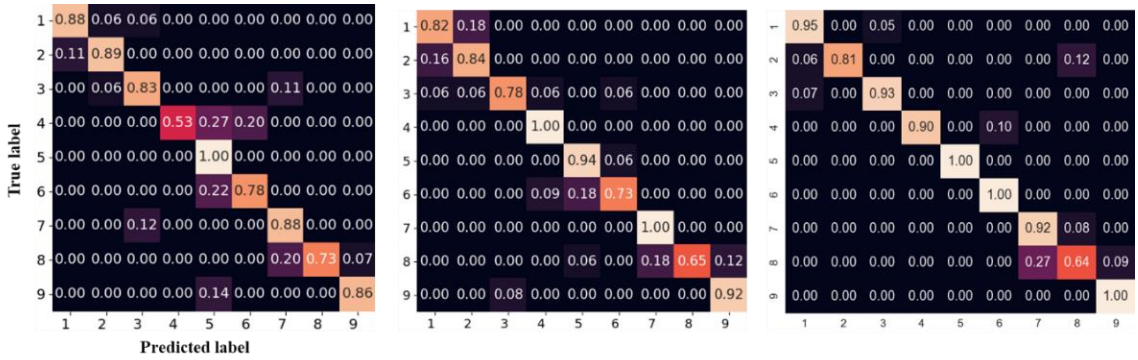

(a) (b) (c)

Figure 4.19: Confusion matrix showing the deep CNN based classification of crops using data (a) WorldView-III, (b) LiDAR point cloud, and (c) WorldView-III + LiDAR point cloud. The nine classes corresponding to the labels numbered from 1 to 9 are eggplant medium, eggplant low, eggplant high, tomato medium, tomato low, tomato high, cabbage medium, cabbage low, cabbage high, respectively.

For comparative performance, the deep CNN model has also been applied on WorldView-III and LiDAR point cloud independently. As evident from Table 4.10, the classification performance of the deep CNN compared to the RF algorithm indicates two distinct features. The first observation is that the overall accuracy of crop classification with explicit reference to N level with independent datasets WorldView-III and LiDAR point cloud has improved substantially. The second observation is that the overall accuracy of the classification of the fused dataset is higher, with an accuracy of 92%, and is only comparable with that of the RF-based classification. However, a remarkable observation of the classification of the fused dataset using deep CNN is that between crop discrimination has increased while exhibiting the moderate level of within crop confusion, particularly at the medium level of N. Cabbage at low and high N levels were identified as tomato, and there is an inherent confusion between tomato within its N levels. The apparent misclassification of the cabbage as tomato would have been due to the spectral confusion resulting from the WorldView-III dataset. As evident from the quality of classification is relatively poor with the

WorldView-III dataset across the crops, the trend is similar to that of RF-based classification. However, as evident from Figure 4.19b, the deep CNN exhibits a distinctly higher classification accuracy level with the LiDAR point cloud supporting the improvement of between-crop discrimination from the fused dataset. These observations support the prominence of the LiDAR point cloud derived structural features in discriminating crops based on N. Summarizing the deep CNN-based classification performance, an improvement of 10.5% and 7.5% is observed for the LiDAR WorldView-III datasets independently. This observation supports the premise that deep CNN based classification models exploit the spectral-geometrical features of the fused dataset produced by integrating WorldView-III and LiDAR point cloud.

Table 4.10: Summary of the accuracy estimates of the classification of crops at different N levels using deepCNN approach. For comparison accuracy estimates from the RF classifier are also presented.

Classifier	**Data type**	**Kappa Coefficient (%)**	**Overall accuracy (%)**
DCNN	WorldView-III + LiDAR point cloud	91.1	92.1
	LiDAR point cloud	83.9	85.5
	WorldView-III	80.6	82.9
RF	WorldView-III + LiDAR point cloud	92.1	93.1
	LiDAR point cloud	79.3	76.2
	WorldView-III	68.96	64.5

4.5 DL based temporal framework for predicting crop structural parameters (Objective 4)

The plant height and crown area were predicted using three different deep learning models. The first two types of predictions are obtained from LSTM and GRU architectures, respectively. The third model we name as 'TemporalCropNet' is a hybrid architecture of deep learning framework, which was generated based on the symbiotic combination of LSTM and GRU models. Results are presented for each of the three models. The temporal plant height and crown area prediction obtained from the LSTM model is shown in Figure 4.20. As evident from Figure 4.20, the prediction ability of LSTM is rather stagnant and indicate no response to the substantial variations in the structural parameters across different ranges and dates of the data acquisition. However, the major limitation is not the lack of predictive response to the training-induced learning capability of LSTM but the magnitude of the structural parameter predicted. As illustrated in Figure 4.20 for plant crown area, the LSTM model does predict the structural parameters considering the spatial variation of the corresponding across different growth stages. The quantity of predicted value is only one half of the quantity of the measured values, further calibrated with TLS estimates, especially, the prediction of relatively lower values of the crown area or plant height is of non-responsive kind from the LSTM model. This inconsistency in prediction is further corroborated by the logarithmic deviation metric computed for the prediction from the LSTM model as shown in Figure 4.21.

Figure 4.21 represented the logarithmic deviation of the height (Figure 4.21(a-c)) and crown area (Figure 4.21(d-e)) measurements derived from LiDAR point cloud and predicted using TemporalCropNet. The direction of predicted values of the crown area or plant height is indicated from L_d metric is rather monotonically decreasing, showing the lack of any responsive learning in the model prediction. The systematically looking distribution of points

with a crossover of direction at midway (Figure 4.21) suggests that the predicted values are not in tune with the measured values of the structural parameters considered. For the predicted height in Figure 4.21, even though there are numerous positive and negative deviations, most of the predictions are prone to negative estimation. Also, the extend of the deviation (L_d) are mostly distributed from -0.2 to 0.2. Similarly, the log deviation depicts a considerable over and under estimation for tomato crop. In the case of cabbage and eggplant, the number of samples which have undergone both the estimations are mostly near $L_d = 0$, precisely between -0.1 and +0.1. A contrasting pattern is visible in the case of the crown area. Here, many samples are in the direction of overestimation and extend of deviation is also greater than the height parameter.

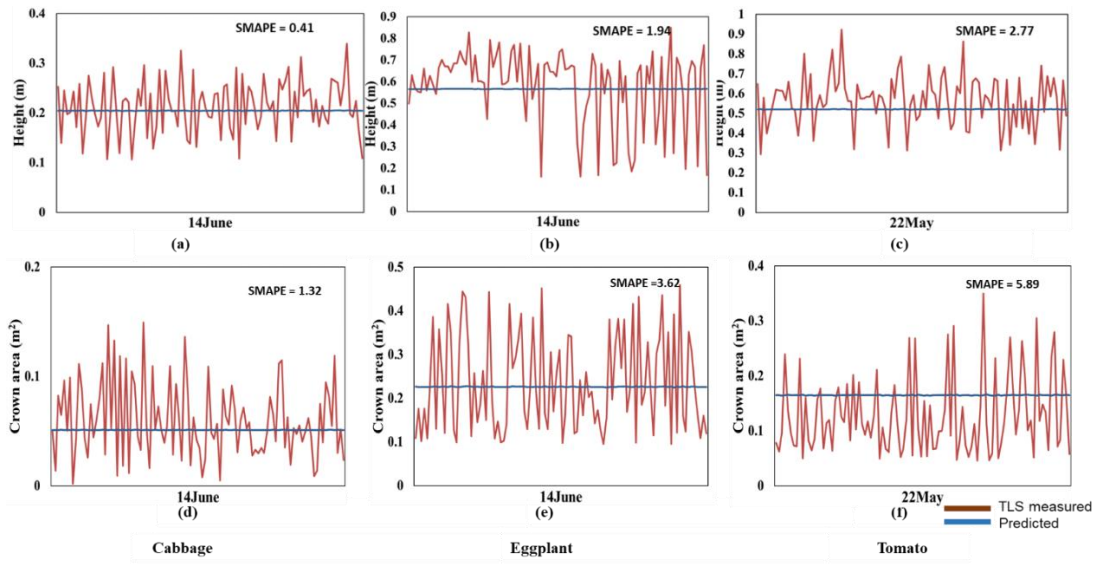

Figure 4.20: Predicted and TLS measured height and crown area plots for LSTM model the crops: cabbage (a, d), eggplant (b, e), and tomato (c, f).

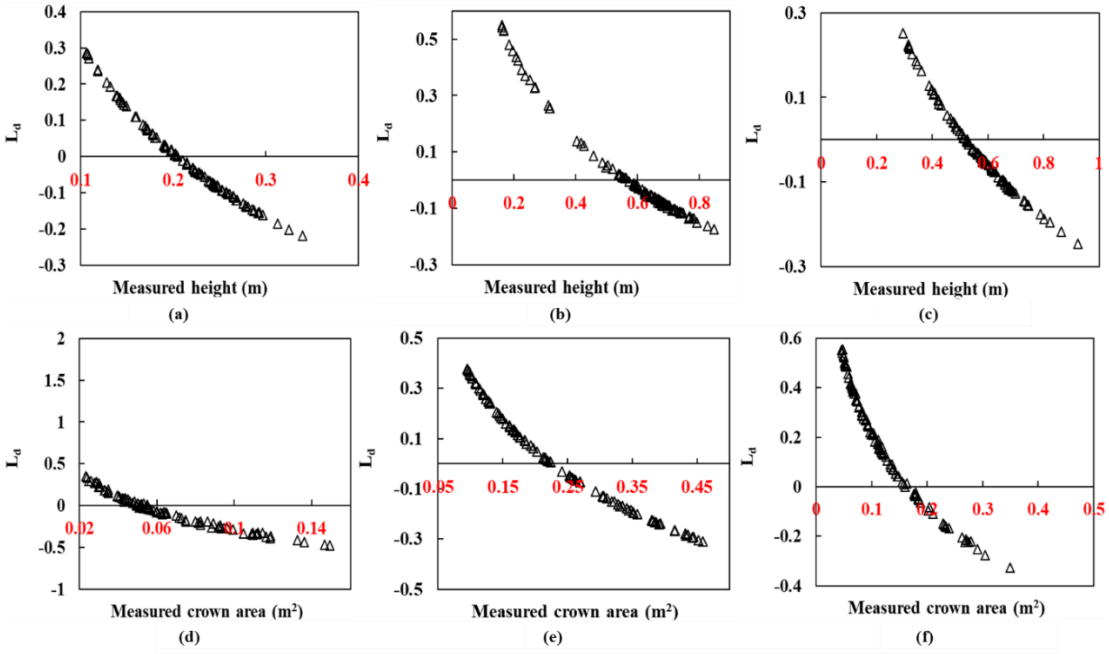

Figure 4.21: Logarithm deviation (L_d) between the measured and predicted height (a-c), and crown areas (d–f) for the baseline model LSTM showing the over and under estimations in the prediction.

The results of the prediction of the crop structural parameters from the GRU models are shown in Figure 4.22. As seen from the Figure, the nature of predictions of the crop structural parameters for the GRU model closely follows the predictions from the LSTM model. At the overall level during the entire crop growth stage, the predictions are slightly dynamic in tune with the direction of variations of the measured values. However, the variations in the predicted values are limited by local gradients to the extent that most of the predictions at the lower values of the structural parameters are almost static. This lack of structural prediction is also evident in the values of L_d metric (Figure 4.23). The complementary LSTM and GRU-based predictions are mainly in the change in direction of predictions at different plant growth stages (Figures 4.24 and Figure 4.25).

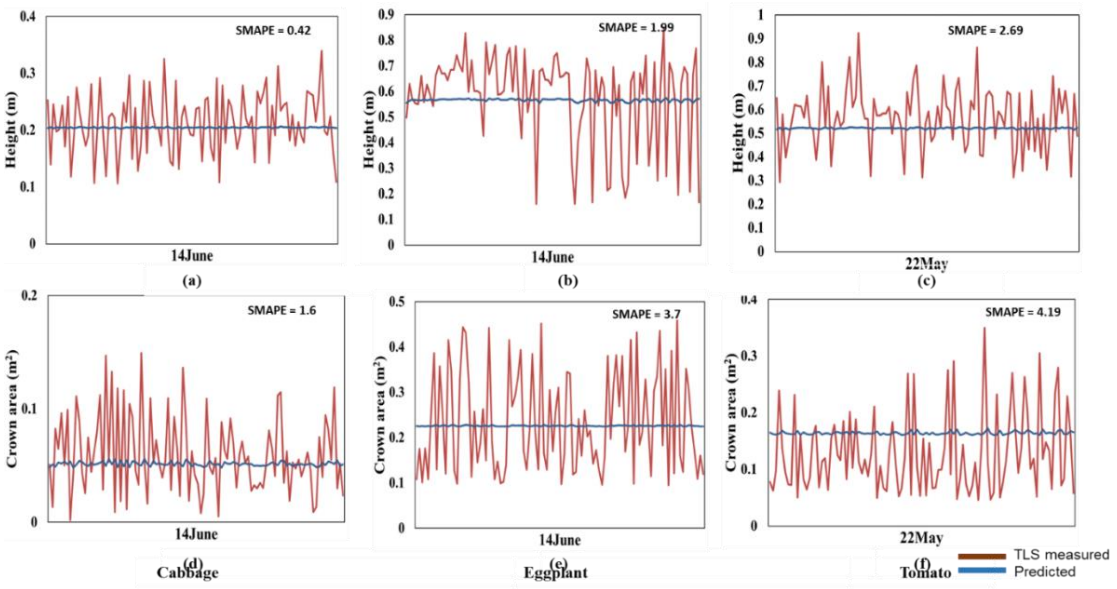

Figure 4.22: Predicted and TLS measured height and crown area plots for GRU model the crops: cabbage (a, d), eggplant (b, e), and tomato (c, f).

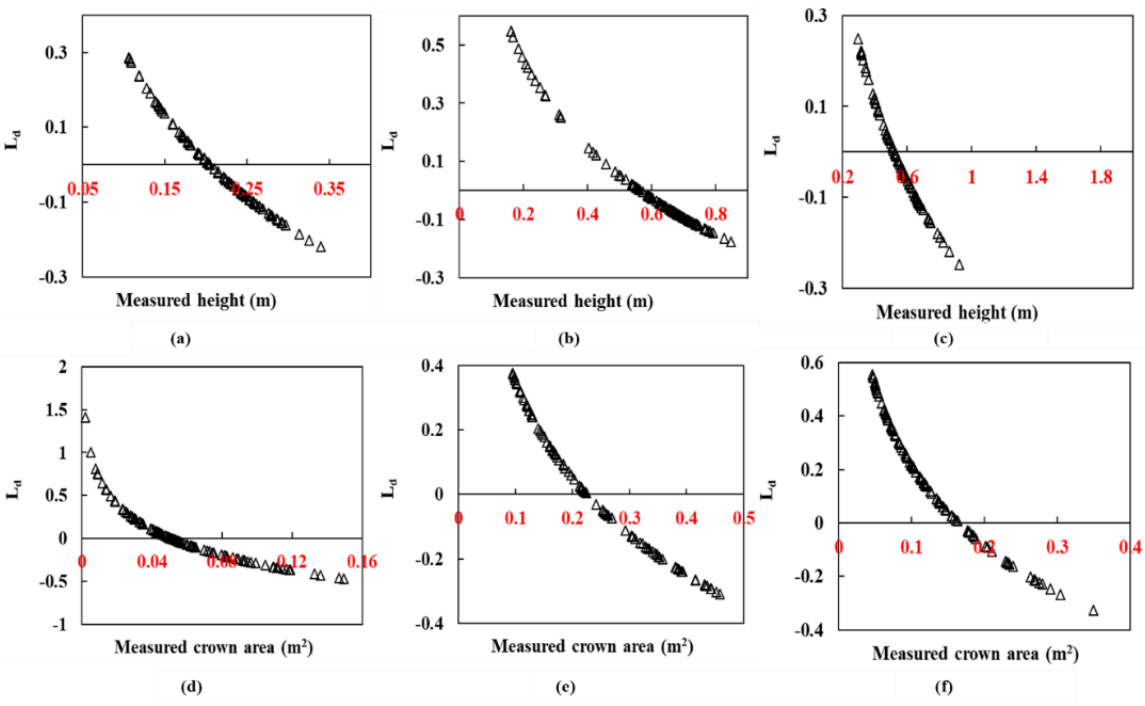

Figure 4.23: Logarithm deviation (L_d) between the measured and predicted height(a-c), and crown areas (d–f) for the baseline model GRU showing the over and under estimations in the prediction.

The results of the temporal prediction of structural parameters from the hybrid RNN model – TemporalCropNet are presented in Figure 4.24. The directional variation of the predicted values vis-à-vis to the measured values are presented in Figure 4.25. The predicted values of both the structural parameters considered are fairly closer to the measured values across the growth stages, as indicated in Figure 4.24. However, when the tomato crop is at the harvesting stage, the quality of prediction of the crown area is slightly lesser in precision compared to the measured values. The trend of the prediction across the crops is supported by the directional dependency of the predicted values as indicated by the L_d metric (Figure 4.25). The predicted crown area and plant heights are slightly overestimated at the lower range of the measured values. The predictions are slightly underestimated at the upper ranges of the measured values. The predictions match almost one-to-one when the measured values are in the intermediate ranges. The variations of the predictions across different crops, as indicated by the SMAPE, show a slightly different pattern by the magnitude of the error. Converting the relative values of the estimate through the absolute percentage error, the error margin of the predicted values is between 5 to 12%.

Comparing the performance of the TemporalCropNet with the results from LSTM or GRU, it can be summarized that the prediction of crop structural parameters is viable and depends upon the sophistication of the deep model and the inherent ability to derive the complimentary nature of the two different types of architecture considered in this work. The correlation of predicted and the TLS point cloud-based estimation of the plant height are shown in Figure 4.24. As evident from Figure 4.20, The error assessment computed using SMAPE is 0.01 (Figure 4.24(d)) for cabbage and 0.04 (Figure 4.24(f)), which exhibits a minimal error rate for predicting the crop height. However, for the crown area, the mean absolute error percentage is 0.4, 0.8 and 2 higher respectively for cabbage, eggplant and tomato.

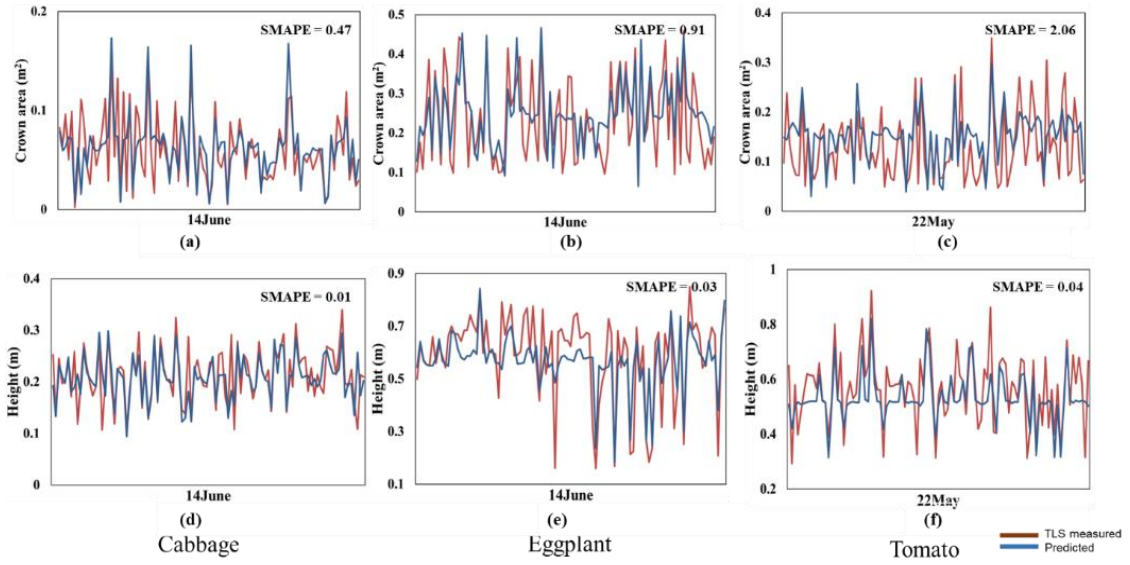

Figure 4.24: Measured and predicted plot of crown area and height for cabbage, eggplant and tomato for proposed TemporalCropNet.

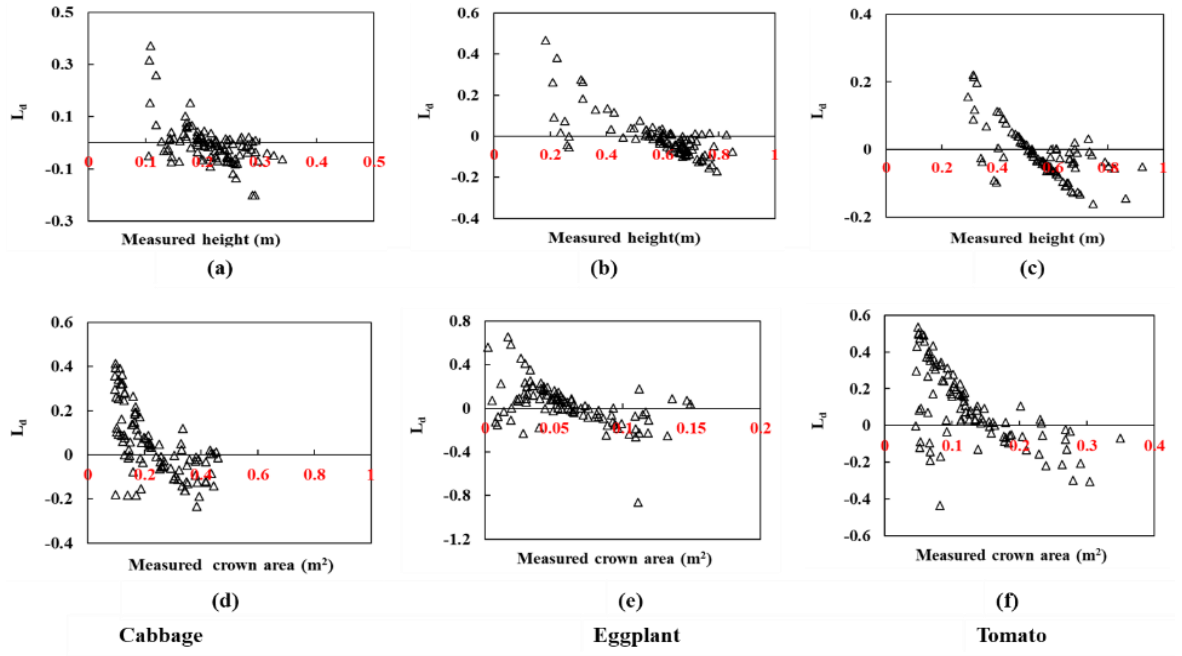

Figure 4.25: Logarithm deviation (L_d) of the crown area showing the over and under estimation of the crops for the proposed TemporalCropNet.

Interestingly, the same trend is visible for height and crown area prediction at different levels of N, where the error is calculated between the in-situ measurements and the LiDAR point cloud derived parameters. Figure 4.25 shows the logarithmic deviation of the height

(Figure 4.21(a-c)) and crown area (Figure 4.25(d-e)) measurements derived from LiDAR point cloud and predicted using TemporalCropNet. For the predicted height in Figure 4.25, even though there are numerous positive and negative deviations, more predictions are prone to negative estimation. Also, the extent of the deviation (L_d) is mostly distributed from -0.2 to 0.2. Similarly, the log deviation depicts a considerable over and under estimation for tomato crop. For cabbage and eggplant, the number of samples which have undergone both the estimations are mostly near $L_d = 0$ precisely between -0.1 and +0.1. A contrasting pattern is visible in the case of the crown area. Here, many samples are in the direction of overestimation and extend of deviation is also greater than the height parameter. Compared to Figure 4.25 of the TemporalCropNet, L_d values are systematically over and under estimated in all six cases, which shows the inefficiency of the baseline LSTM and GRU models (Figures 4.21, 4.23) in predicting the crown area. A similar trend is exhibited by the baseline models, LSTM and GRU, in predicting the height values (Figures 4.21, 4.23). Likewise, a systematic positive and negative deviation are observed, which extends from 0.5 to 0.3.

Since the variation of the crown area values is negligibly small for the baseline models, a closer look at the measured and predicted crown area for LSTM is provided in Figure 4.26. In this Figure, we can actually observe a visible height variation when the predicted value is plotted individually, as in Figure 4.26b. But the extent of the values for the predicted crown area is marginal. Hence in Figure 4.20 the predicted parameters appear as a line. This shows that both the baseline models fail to capture the inherent temporal growth pattern of the crops.

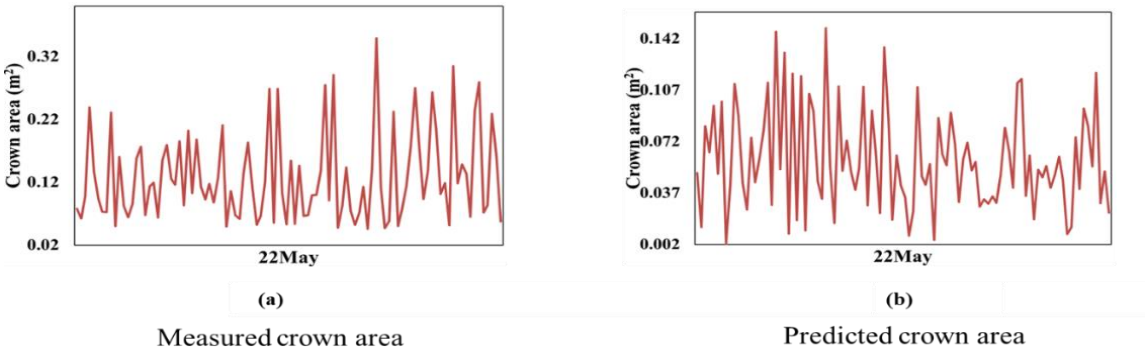

Figure 4.26: Variation of crown area values using baseline LSTM method.

The prediction of temporal growth parameters such as height and crown area for horticulture crops has not yet been addressed in the literature, especially using LiDAR point cloud. This is a strong motivation for carrying out such studies and understanding the crop dynamics, temporal growth pattern and correlation among data, subtle crop changes through that. Another important aspect of this study is to evaluate the temporal dependency that exists within a field that follows intercrop farming practices. The concept of combining LSTM-GRU layers is the systematic approach that is followed for CNN models where several convolutional and fully connected layers are connected in a sequential manner for a better structure for various kinds of classification tasks tends to derive non-linear temporal dependencies. We can embed several hidden layers for LSTM and GRU layers; in this experiment, the number of units of LSTM and GRU layers is set to 50. The number of epochs used for training is 400 epochs with a batch size of 50. A combined representative model of LSTM-GRU can learn the temporal dependency in the data in a much better way than the individual LSTM, GRU models. The baseline models failed to learn the pattern of the crop growth and the development of the canopy areas as the crop grow and mature.

CHAPTER 5

DISCUSSION

Prelude

In this chapter, we present a detailed discussion of the observations, key insights and the implications of the understanding gained. Based on the results, there are several potential new insights and clarifications of the thought processes forming the state-of-the-art in the relevant subject. The nature of the results, with specific relevance to the methods and parameters considered presented in the previous chapter, is elaborate in this chapter. Broadening the analytical observations implicitly presented in the results, this chapter elaborates on the broad impact of the key insights, referring to the relevant literature and potential future implications and connecting with the remote sensing application in precision agriculture. For ease of reference, content in this chapter is presented objective wise, explicitly referring to the sub-tasks in each objective.

5.1 Estimation of the biophysical parameters using TLS point cloud

The potential of airborne LiDAR point clouds for estimating various structural and biophysical parameters such as tree height, canopy cover, and biomass has been successfully demonstrated (Khosravipour et al., 2014; Olsoy et al., 2014; Adao et al., 2017). Recent studies (Friedli et al., 2016; Jimenez-Berni et al., 2018) have attempted to apply the LiDAR point cloud to field crops such as maize, barley, paddy rice, and oat. Crop biophysical characteristics such

as height and biomass have been estimated with an R^2 of ≥ 0.8. Studying vegetable crops with different temporal dynamics of height and yield characteristics and their relation to different N levels is vital for optimal nutrient management and agro-ecological balance. Compared to patch-based field crops such as barley, paddy rice, and wheat, which do not have individual canopy structural attributes, vegetable crops exhibit a complicated geometrical relationship with TLS point clouds. Generally, a shorter plant height (the observed average cabbage height in our study is 18 cm) and individual plant structural attributes need to be preserved in the point cloud.

5.1.1 Estimation of plant height

Our results support the potential of applying the TLS point cloud for estimating vegetable crop height at the plant level. At the overall growth stage level, estimated plant heights for the vegetable crops considered were accurate and followed the magnitude of the reference measurements. Our results confirm the observations made by Bendig et al. (2014), even though their study used barley as the test crop. On the same experimental field used in our study, plant height estimates of Moeckel et al. (2018) using synthetic point cloud generated from the UAV-based stereo RGB imagery documented the possibility of height retrievals for vegetable crops. Plots with high N have substantially higher plant heights compared to low N plots. However, analyses of the error and the direction of deviation measures (SMAPE, L_d) and the qualitative assessment of the spread of the plant level height, crown area, and biomass across the possible ranges indicate that different crops can be quantitatively described using TLS point cloud across growth phases. However, the specific question of matching crop structural attributes to different N levels could not be addressed, given the significant variation in crop growth at our study site.

5.1.2 Estimation of plant crown area

Apart from plant height, the crown area is a vital plant characteristic that can be used to estimate other functional biophysical and structural parameters such as biomass and leaf area index. We have retrieved the crown area at the plant level from the multi-date TLS point cloud based on the innovative application of adaptive filtering and marker-controlled segmentation approaches. Our results indicate an unambiguous retrieval of the crown area at the plant level to be consistent with growth at particular sampling dates and N levels. However, plants treated with medium N exhibited substantial variations. Overall, the strong correlation (R^2 = 0.81 to 0.96) and the relatively low percentage deviation error (maximum SMAPE of 13.6 for crops treated with low, and high levels of nitrogen; Figure 4.4) consistent across sampling dates, indicate the potential of TLS point clouds adapted for the estimation of the crown area. A distinct advantage of delineating plant crowns using this methodology is the possibility of automatic counting plant numbers at the field level. Such automated plant counts help assess the impact of massive crop losses due to heavy rainfalls or severe pests. As a surrogate variable, plant counting coupled with the mean crown area can be directly used for predicting biomass or yield. The ability to derive unambiguously individual plant crowns and counting of plants from TLS diminishes with advanced growth stages for vegetable crops such as tomato. This is due to the mixing of plant components, lodging, and uneven horizontal growth.

5.1.3 Estimation of biomass and the effect of different N levels

Our results show that using plant height and crown area as independent variables, estimation of biomass using TLS point cloud is accurate for the three different vegetable crops considered. However, the assessment carried out to test the discriminability of the estimations for different N levels yielded ambiguous results owing to the wider within plot variations of

crops' growth resulting in a lack of distinct patterns in the reference measurements of plant height and biomass. As evident from Figures 4.6 and 4.7, the TLS point cloud processing methods used in this work allowed a close matching between the measured and predicted biomass across the entire growing season and combing different N levels for all three crops studied. The deviation of the estimations of plant height, crown area, and biomass is across sampling dates affected by the N level applied. While plant height is overestimated for tomato and eggplant for most of the growing period, plant height of cabbage indicates no such specific pattern concerning sampling date. With a further generalization of the cyclic patterns observed for plant height of cabbage (Figure 4.5), the temporal behaviour of crown area measurements follows skewed cyclic patterns for all three vegetable crops (Figure 4.5).

Complementing the strengths of plant height and crown area, the SVR based modelling of biomass with the plant height and crown area as the predictor variables allowed consistent and accurate biomass predictions (Figures 4.6) across sampling dates and vegetable type. The logarithmic deviation measure shows systemic patterns in the estimated amounts of biomass by sampling date and indicates different amounts of biomass for different sampling dates from the accuracy of prediction as indicated by overestimation or underestimation. This observation supports that TLS estimation of crown area accounts for different plant architecture and paves the way for tracking the biomass accumulation in the horizontal growth direction of the crops. We, therefore, recommend further validation of the possibility of crown area retrievals from the TLS point cloud for other crops and sites.

5.2 Crop discrimination at plant level using deep CNN and the performance of the CropPointNet architecture developed

Technological approaches for plant-level crop discrimination and phenotyping are vital for precision crop monitoring. Semantic segmentation and classification in 3D perspective are common processes in the application of LiDAR point cloud data for crop discrimination. We have implemented an improved deep learning convolutional neural network architecture, 'CropPointNet', for the segmentation and classification of TLS point cloud to discriminate three different vegetable crops (cabbage, tomato, and eggplant). The unorganized and discrete point cloud of the crops in the original 3D perspective were processed for semantic segmentation and classification of the vegetable crops at the plant level. This was implemented by adapting and improving a recently reported deep learning convolutional neural network (CNN) architecture (PointNet) developed for the segmentation of common indoor objects with low-density point clouds generated in a typical computer vision application.

The deep CNN model, "CropPointNet", has improved training strategy for handling high-density point clouds such as the TLS point cloud used in this study and compact-guided feature mapping architecture for faster convergence and error handling ability. The performance of the 3D semantic object-based classification of the crops was assed rigorously using a host of statistical and non-parametric accuracy estimation measures both at the overall and per-class level. Besides, the results from the CropPointNet model were compared with that of two recent deep CNN models, PointNet and DGCNN. Results suggest the possibility of plant-level discrimination of the crops chosen with an overall accuracy of 81%. The accuracy of the crop discrimination by the CropPointNet model is superior and statistically significant. At the individual crop level, we observe that the soil and plant structure substantially influences the accuracy and spatial conformity of the crops. The CropPointNet and DGCNN models

consistently discriminated the cabbage and eggplant crops with accuracy close to 90%. As evident from Figures 4.8 and 4.9, a point cloud of the plots of tomato suffered a massive loss of point cloud in the ground filtering process. As a result, the quality of tomato crop classification was relatively inferior, even though the CropPointNet model performed relatively better compared to the PointNet and DGCNN models. Relating to the state-of-the-art in this evolving domain of remote sensing technologies for plant-level segmentation and classification, we describe the significance of the results in the following sub-sections.

There have been some works in the literature on the classification of crops using the LiDAR point cloud. Weiss et al. (2010) and Weiss and Biber (2011) reported laboratory experiments on the plant species classification in 3D LiDAR point cloud using multiple supervised machine learning algorithms. They reported the best overall accuracy of 98% from the Logistic Model Trees algorithm. In a similar study, Paulus et al. (2013, 2014) analyzed a 3D LiDAR point cloud to classify different plant organs (leaf, stem) of grapevines and barley plants using a statistical surface-feature approximation of histogram using a robust estimation technique, RANSAC. These studies suggest the successful discrimination of plant organs with an accuracy of about 96%. Similar to the TLS instrument used for data acquisition used in our experiment, Murray et al. (2020) have quantified the plant structure of orchids. They suggest superior results from the TLS point cloud and are better than the results from proximal photogrammetry. In Jin et al. (2018), the authors applied a recurrent convolutional neural network (R-CNN) based deep learning model to segment the TLS point cloud of maize plants. The methodology employed a region growing procedure on the 2D depth imagery obtained from the conversion of the 3D point height into intensity before applying the R-CNN deep learning model for segmentation. The best estimates of Precision and Recall estimates are about 93%.

Despite using different methods of classification and crop type, these studies have demonstrated the successful plant level segmentation and classification of crops using LiDAR point cloud with accuracies comparable or slightly better than our results. However, the principal difference and contribution of this research are the comprehensive experimental setup and evaluating a potential automated method for object-based crop classification. The state-of-the-art studies, including the afore-cited, have acquired point cloud data under a controlled experimental design – mostly indoor or laboratory-controlled with smooth soil surfaces and involving only one or a few crop species or plant organs. Further expanding the state-of-the-art, our study has been carried out on multiple crops under open natural environmental conditions subjected to the crop growth, soil, and surface landscape variability common to operational regional agricultural practices. Our results, thus, present a broader spectrum of the potential and challenges of applying 3D LiDAR remote sensing data for object-based crop classification from a realistic landscape perspective.

5.2.1 Spatial filtering and crop point cloud generation

Unlike the indoor scene dataset, the crops are affected by various outdoor factors such as terrain undulation, soil background, wind, and other agricultural infrastructure elements. Therefore, the data must be pre-processed before ingestion into the deep neural network for training. The complex tasks in pre-processing are ground filtration and a normalized surface. The nature of soil preparation for planting crops determines the critical separation line between soil and plant point cloud. For example, soil ridges and furrows in our study have created a continuous undulation of the soil surface, complicating the ground filtering process and demanding human intervention. When the rise of the soil ridges is comparable to the height of crops, the ground filtering process leads to the loss of point cloud of plants. We observe that

the filtering approach has wrongly identified about 15% of the point cloud of the crop plants as ground points. Additional features that reduce the quality of point cloud are the plant or patch level agricultural infrastructure, such as drip irrigation pipes and support sticks for minimizing plant lodging. This support system for tomato and lack of distinct height profile with crop plants has enhanced the overlap in the height of crop plants and non-crop geometrical features. Faithful retrieval of the point cloud of the crops in the filtering process has yielded only about 50% of the point cloud for tomato. The lack of distinct canopy architecture of the tomato crop at the fully grown stage and the reduced density point cloud of tomato crop are the primary reasons for the low accuracy of the crop discrimination. However, the relatively consistent and higher scores of the non-parametric accuracy metrics (Table 4.4) indicate two distinct features of the crop classification. First, the reasonably well discrimination of the crops indicated by the confusion matrix based on the overall accuracy is supported with a similar level of perception. Second, in contrast to the relatively low accuracies shown (Table 4.2), the quality of discrimination of the non-crop classes is also high (0.79 and better for some classes) and comparable to that of the crops.

Compared to the estimate of sampling-based computation of the accuracy metrics (Table 4.2), estimates from the plant-to-plant matching based accuracy measures emphasize the number of correct predictions. The apparent differences in the accuracy estimates of crop and non-crop categories are due to the uncertainties in the ground filtering. The estimates of the IoU which quantify the crop plant-to-plant level conformity between the predicted and ground truth suggest relatively higher discrimination of the crops with the mean IoU (mIoU) scores exceeding 50% by all the three models (see Table 4.6) (72.78%, 64.28%, and 52.94% respectively). However, by the stability in the discrimination of both crop and non-crop information classes, the CropPointNet model meets the accuracy thresholds (see Table 4.6).

The substantial changes in the accuracy of the tomato crop suggest the need for choosing an appropriate discrimination model for crop classification under skeletal point density.

5.2.2 Significance of the shape of crop plant canopy

The deep learning models' ability to predict crop patterns at the scale of individual plant objects in the 3D point cloud has also been affected by the shape of the crop canopy (see Figure. 4.8, 4.9). While the apparent uniform spatial distribution and higher accuracy of cabbage and eggplant suggest fair discrimination, the relatively lower classification accuracy and the substantial gaps in the spatial distribution of the tomato crop indicate the models' sensitivity to the crop canopy. The cabbage plant has a specific geometrical structure with a compact spherical mass of smooth or dense-leaved heads enfolded over each other. Due to this, all three models are effective in identifying the crop. In the case of tomato, due to irregular canopy shape and lodging at the mature growth stage, the stalk overlaps with neighbouring plants. This overlapping further enhances the confusion in the crops' geometrical features, leading to sub-optimal feature learning in the discrimination model. As a result, tomato was confused partly with eggplant and residual soil ridges leading to lower classification accuracies by the PointNet and DGCNN models. However, compared to the performance of the PointNet and DGCNN models, the CropPointNet model indicates a relatively better accuracy for the tomato crop due to the reduction of false positives from the residual soil ridges.

5.3 Crop discrimination at plant \ patch level with explicit reference to N levels: fusion of LiDAR point cloud and multispectral satellite imagery

High-resolution remote sensing has been extensively used to map and monitor crops at regional to national scales. In most studies, the typical mapping unit has been a crop field of several hectares. This perspective scale is appropriate for deriving overall estimates such as crop area, type and potential yield and general crop health in countries and landscapes where the average field size is several hectares. In most developing countries such as India, the average field size is less than one hectare, and the agricultural landscapes are very heterogeneous and are covered by a range of crops and phenological cycles. Further, the soils are highly variable by available nutrients. Chemical nutrients have been applied extensively without reference to plant availability and demands, resulting in loss of soil fertility and causing severe eutrophication. Forming part of the baseline dynamic data on the crops at the management unit of variance in the field, mapping, and biophysical quantification at the plant or patch level has promising applications in precision agriculture. This part of the study has been undertaken, evaluating the potential for plant or patch level information extraction for three different field vegetable crops. The hypothesis tested is ‘‘whether the synergistic fusion of multispectral imagery and LiDAR point cloud allows nutrient specific vegetable crop discrimination and biophysical quantification at the plant or patch level?”.

5.3.1 Crop discrimination at plant or patch level

The crop discrimination has been approached by considering the object-based classification of the vegetable crops using the dataset generated by the pixel-level fusion of multispectral imagery and LiDAR point cloud and compared with the base datasets independently. The two levels of crop discrimination – the fine classification with reference to N treatment and the coarse level classification without considering N treatment indicate a new level of opportunity and challenge for remote sensing application for plant or patch level information extraction. Compared to the results obtained from LiDAR point cloud, the quality of crop discrimination from the multispectral imagery, with explicit reference to N treat, is relatively poor. The best accuracy of classification is about 68%.

Supporting the premise that structural features are vital for crop discrimination at a fine level, the quality of crop discrimination from the fused dataset is very high and is consistent across the crops and treatments. The best accuracy of classification is about 92%, which is about 30% and 20% higher compared to the results from multispectral imagery and LiDAR point cloud, respectively. This observation indicates the possibility of patch-level crop classification with explicit reference to N treatment. The improved results also suggest the complementary of spectral and geometrical features, thereby illustrating the distinct benefits of fusion of multispectral imagery and LiDAR point cloud for crops mapping.

In contrast, the classification of crops without reference to the N treatment indicates a fairly higher accuracy for both the multispectral imagery and LiDAR point cloud independently. The difference in accuracy between the classification results from the multispectral imagery and LiDAR point cloud is marginal (about 5%). However, the accuracy of classification results from the fused dataset shows substantial improvement over both the base datasets.

5.3.2 Biophysical characterization

The retrieval of two biophysical parameters, plant crown area and biomass, belonging to two distinct categories, show two different patterns. Due to the destructive harvesting method used for ground measurement of biomass, the number of samples used for validation is limited. In contrast, as is possible without destructive harvesting, the plant crown area has been sampled extensively for ground measurements and used for validation. The plant height has not been used for comparison of the results from LiDAR point cloud and multispectral imagery as plant height is not retrievable from single multispectral imagery.

The estimates of the plant crown area, a tangible structural parameter, exhibit different levels of correlation with measured values and vary both in magnitude and direction based on the data used. When LiDAR point cloud in the retrieval, the plant crown area exhibits a very close relationship with the measured values. The estimated values reflect the crop type and N treatment as observed from measured values. For the case of retrieval from the multispectral imagery, the quality of crown area degraded substantially, and the strength of correlation varied between 65 to 76% for the instances of crops with N treatments ‘low’ and ‘medium’. However, the correlation is rather poor for the case of N treatment ‘high’. Except for the case of cabbage treated with ‘low’ N, the estimated values of crown area substantial overestimations. This also indicates the possibility of soil background and open-canopy gaps in the tomato and eggplant, thereby causing some of the pixels filtered out as belonging to non-plant in the image processing stage. The possibility of plant lodging with further skewed spatial spread on the soil also reduces the effective crown area is in the purview of the satellite sensor’s instantaneous field of view (IFOV). Interestingly, the results from the fused dataset exhibit an unusual pattern. On the one hand, the estimates of crown area are consistent and better than the estimates from the multispectral imagery (see Table 4.7). However, on the other hand, the quality of estimation degraded substantially, with the error of estimation between 20 % and 28%. This contrasts with

the observation that the accuracy of crown area estimation from LiDAR point cloud is very high, and the maximum error of estimation is about 15% (see Table 4.7). The reduction in the accuracy of the estimation with the fused dataset indicates the substantial influence of confused-spectral features in modelling the crown area. This observation points out the possibility of destructive interference of spectral and geometrical features for several plant objects, thereby suggesting the caution for data fusion applicability.

The estimates of biomass from the three different datasets exhibit a distinct trend compared with the crown area. The best performance observed LiDAR point cloud for the crown area has continued with the biomass estimation, further reducing the most probable error of estimation to less than 5%. Contrasting with the relatively lower performance, the accuracy of estimation from the fused dataset is substantially higher than the accuracy of estimation from the LiDAR point cloud across the crops and N. Exhibiting a somewhat similar trend, the accuracy of biomass estimation from the multispectral imagery also has improved substantially, with the error of estimation of between 10 and 30%. This observation also supports the premise that a combination of spectral and geometrical features is vital for plant biophysical description.

However, the distinction of biomass estimates with explicit N treatment is unclear from all three datasets (see Figure 4.17). In addition, there are only marginal changes in the accuracy of biomass estimations without explicit reference to N treatments (see Table 4.9). One of the pertinent reasons can be ascribed to the field level crop growing conditions and the variations of the crop growth across different plots. The intra-crop biomass variation is more than the inter-crop biomass, thereby blurring the predictive boundaries of the non-parametric discrimination models used for fusion and estimation of biomass (Figure 4.18). In addition, extreme weather phenomena such as rains cause the nutrient transport from one N treatment

site to another, influencing the biomass accumulations and degrading the functional limits of crop growth profile.

5.4 Scope for improved crop discrimination: DL based fusion of multispectral data and LIDAR point cloud

Deep machine learning approaches have been rapidly expanding into the application base of remote sensing by offering a common methodological framework for building the models and transfer across space and time. A range of problems related to data analyses such as classification, prediction, regression, clustering, and data engineering such as data fusion, super-resolution, multi-modal data integration has been explored. The fusion of spectral data (multispectral and hyperspectral) and LiDAR point cloud acquired from the ground, airborne and satellite platforms have been explored in the last few years. The studies have mainly reported on the fusion of data- spectral and LiDAR point cloud for improved classification of land use/land cover, buildings' footprints generation, and the classification of forest tree species (e.g. Singh et al., 2012; Ahmed et al., 2015; Garcia et al., 2018; Li et al., 2020). Our exploration of the deep machine learning approach for the fusion of satellite-based multispectral imagery and the terrestrial LiDAR point cloud for the classification of vegetable crops with explicit reference to N levels is distinct. The challenges are: (i) objects are crop plants of relatively short height and lack sturdy shape and profile, and (ii) response to N levels, which can be further influenced by various soil and environmental factors.

Compared to the results obtained from the RF-based traditional machine learning approach, the nature of the classification performance can be explained from two distinct perspectives: (i) discrimination performance within and between crops and (ii) crop discrimination sensitivity to different N levels. The accuracy of the crop discrimination, irrespective of the N status, is comparable with the best-case performance of the results obtained by data fusion using the RF algorithm. However, a significant performance improvement obtained from the deep CNN based data fusion is increased within-crop accuracy

by 10%. With reference to the discrimination sensitive to N level, the results from the deep CNN based fused imagery are only marginally better.

Contrasting with the results obtained from the fused dataset, the deep CNN has exhibited substantially higher performance on the independent datasets of multispectral (WorldView-III) and LiDAR point cloud. The results are consistent across the crops with and without reference to the N status. Compared to the classification results from the WorldView-III, the overall accuracy of classification from the LiDAR point cloud is higher. This observation establishes the prominence of plant structural features for crop discrimination at the plant/patch level. Although the different versions and model architectures of the deep learning methods available in the recent literature offer various levels of sophistication and performance improvements, we can draw two stable inferences: (i) the performance of the deep machine learning method for the data fusion of multispectral (WorldView-III) and LiDAR point cloud is higher for crop discrimination, and (ii) the discrimination with explicit reference to N status is comparable to that of the RF algorithm.

5.5 DL framework for the prediction of crop structural parameters

Providing spatial estimates of tangible or intangible parameters of different landscape elements (e.g. buildings, trees, crops, soils, water bodies, etc.) has been one of the primary applications of remote sensing data. A host of statistical, machine learning and fast-emerging deep machine learning approaches have been explored extensively. The general process followed across different domains is to provide spatially distributed reference measurements at some locations in the study site covered by the remote sensing data and build a classification or regression model for generating spatial maps of the parameters of interest. As described in the literature review, estimation of the parameters related to vegetation, generally called

biophysical characterization, has been extensively studied during the last three decades. At the scale of individual vegetation elements, especially trees in the urban landscape and forest environment, delineation and structural characterization are increasing attempted with LiDAR point cloud employing deep machine learning methods (Wu et al., 2015; Aubry-Kientz et al., 2019; Calders et al., 2020). The successful generation of geographically extensive coverage maps of vegetation heights (Lang et al., 2019; Weinstein et al., 2021) and tree crown area canopy affirm the promising combination of deep learning models and LiDAR point cloud. Apart from applying to a different domain of vegetable crops, exploring the potential of the combination of LiDAR point cloud and deep machine learning models for estimation of plant-level structural parameters at different growth stages is a distinct feature of research carried out in this thesis. Given the limitations and functional constraints of different deep machine learning methods, the generation of hybrid models broadly within the context of ensemble modelling has been considered a viable option. Broadly related to this perspective, the application of two different deep machine learning models – LSTM and GRU, and the hybrid model generated, 'TemporalCropNet' is aimed at expanding the horizon of the single state 'estimation' of biophysical parameters to 'prediction' thereby enabling the predictive maps of crop growth profiles for advanced crop management.

The performance of 'predicted' values of two important crop structural parameters – plant height and the crown area has been compared with the ground truth reference values measured throughout the crop growing season. Analyzing the results obtained from the base models (LSTM and GRU) and the proposed hybrid model 'TemporalCropNet' suggests crucial insights. The quality of the predictions of structural parameters from the LSTM is poor because the magnitude of prediction is less than one half of the actual value. Further, the LSTM model is non-responsive to the variation of structural parameters both at the lower and higher-level values. While following the general trend of the predictions from the LSTM, results from the

GRU suggest the existence of a stepped gradient in the predictions indicating the dominance of local features in the predictions of GRU. As a result, the point-on-point plot of structural parameters (Figures 4.20 and 4.22) of the predicted with the LiDAR point cloud-based values show a limited extent of the predicted values by amplitude and direction. The proposed 'TemporalCropNet' has exploited the complementary functional performance of the LSTM and GRU, thereby offering 'predictions' of crop structural parameters at plant level closely matching with the TLS LiDAR point cloud-based values. The 'TemporalCropNet' is developed and implemented for predicting plant level height and crown area. As the model is based on an open architecture with the flexibility to ingest different ranges of values, the method can be extended to predict crops' other biophysical parameters.

CHAPTER 6

SUMMARY AND CONCLUSION

The ever-evolving remote sensing techniques and the demands for precision agriculture require the development of tools and contemporary techniques for information retrieval at the plant/ patch level. Motivated by this, the thesis has considered three crucial aspects of precision agriculture in remote sensing applications: (i) estimation of biophysical parameters of the crops at high resolution. (ii) crop discrimination at plant/patch level, and (iii) temporal prediction of crop structural parameters. These key aspects form the basis of the overarching aim of the thesis. The aim was formulated into four objectives: (1) multi-temporal estimation of biophysical parameters of agricultural crops at different levels of nitrogen using TLS point cloud. (2) to develop a deep learning-based methodology for multi-crop point cloud classification of agricultural crops, (3) examining the potential of integration of TLS point cloud with high-resolution multispectral satellite data for crop discrimination and biophysical characterization at different N levels, and (4) to develop a temporal framework to predict crop structural parameters.

Estimating the biophysical parameters of the vegetable crops at varying N levels using 3D TLS point cloud data at the plant level seems viable. There is a stable agreement between the estimated and measured parameters. Substantial variability in plant height across different N treatments is also evident. Estimating crown area and its combination with plant height for modelling biomass using SVR has given a consistent level of prediction for all N levels and all the crops considered. The extraction of height and crown area measurements for individual plants (object-oriented marker-controlled watershed segmentation) exhibit a good agreement

with the reference measurements. An improved 2D DCNN model "CropPointNet" capable of ingesting the point clouds directly to the architecture for segmentation and classification has been developed. The proposed CropPointNet can handle high-density point clouds. The performance of the 3D semantic object-based classification of the crops was assed rigorously using a host of statistical and non-parametric accuracy estimation measures both at the overall and per-class level. Besides, the results from the CropPointNet model were compared with the other two deep CNN models, PointNet and DGCNN. Results suggest the possibility of plant-level discrimination of the crops chosen with an overall accuracy of 81%. The accuracy of the crop discrimination by the CropPointNet model is superior and statistically significant. At the individual crop level, the soil and plant structure substantially influence the accuracy and spatial conformity of the crops. The CropPointNet and DGCNN models have consistently discriminated the cabbage and eggplant crops with accuracy close to 90%.

Two approaches have been explored related to evaluating the potential of fusing LiDAR point cloud and multispectral imagery for crop discrimination and biophysical parameter estimation at different N levels. The ensemble-based method (Random Forest) is used for feature-based classification. The results have been compared against these two different datasets discretely. The classification accuracy of the fused dataset is 92% which is 20% greater than the individual sensors. For the pixel-level classification, a DCNN model has been developed. In comparison to the RF classifier, which needs handcrafted features as input to the model, the DL based model has better accuracy rates remarkably better accuracy rates for LiDAR and WorldView-III datasets. When classified using the RF algorithm, the quality of improvement with the fused datasets is not substantial when compared to the accuracies from the independent datasets. In contrast, the improvement in the accuracy of the biomass and plant crown area estimates using the fused dataset is substantial and consistent across the different cases considered. The error estimate SMAPE observed for crown area varies from 16.5% to

32.5% for the combined dataset and recorded negative values for the error estimation of biomass which indicates the error of underestimation.

Based on the crop plants' structural attributes at past growth stages, prediction of the future structural parameters of the crops at the crop patch/plant level has been attempted first time, to the best of our literature review. To this end, an LSTM-GRU integrated deep learning-based model named 'TemporalCropNet' has been developed for prediction at the individual plant lev66el. The structural parameters are derived from the CHM developed from the LiDAR point cloud during the crops' key phenological growth stages. The predicted values are compared with the actual LiDAR point cloud derived values. Compared to the baseline LSTM, GRU models, TemporalCropNet can predict the crop growth parameters with a very low error rate, especially for plant height (SAMPE = 0.02). The model can capture the temporal dependency for the given date of the crop growth.

6.1 Conclusions

Based on the critical observations noted, the following conclusions are drawn.

- LIDAR point cloud from TLS offers plant/patch level biophysical characterization of crops using LiDAR point cloud. It can be a potential terrestrial remote sensing technique catering to the needs of precision agriculture.
- Compared to plant height, plant crown area is the better indicator of crop growth under different N levels across various growth stages. Biomass estimates obtained by 6including the crown area and the plant height in the prediction model are accurate across the growing seasons and N levels.
- The potential of TLS based LiDAR point cloud for crop discrimination at patch/plant level is promising. The deep learning model adopted in this thesis, 'CropPointNet'

classifies structurally different crops with an overall accuracy of 90%. This model is amenable for generalizing to apply on other field crops. The quality of the crop discrimination is relatively less when viewed from the sensitivity to different N levels.

- Object-based classifications of the crops using LiDAR point cloud and high-resolution multispectral imagery independently and by fusion suggest that spectral information is vital for achieving stable crop discriminations with explicit reference to different N levels.

- If crop discrimination without reference to N levels is the goal, then LiDAR point cloud alone can offer the classification performance with better accuracy. On the other hand, if the requirement is crop discrimination with explicit reference to N level, spectral data needs to be combined with the LiDAR point cloud.

- A novel modelling exploration of the temporal LiDAR point cloud, using deep machine learning, suggests the in-advance prediction of plant/patch level crop structural parameters (plant height and crown area). The predictions of the deep machine learning model ‘‘TemporalCropNet’, developed based on the ensemble integration of the LSTM and GRU models, closely match the estimates from the TLS point cloud, especially for the advanced growth stages of the crops.

6.2 Challenges and Limitations

- Acquiring quality 3D point cloud for field crops is affected by the agriculture infrastructure and soil preparation. In the experimental site, we acquired several scans of TLS from different views for forming the LiDAR point clouds of crops. However, acquiring LiDAR point clouds from multiple perspectives is a challenge in a practical

farming landscape of extensive areal extent. The point cloud filtering and classification methods are sensitive to the quality of geometrical view of the plant-object formation in the LiDAR point clouds.

- Irrespective of the quality of the equipment used for acquiring LiDAR point cloud acquisition and the nature of crops' growth profiles, rapid changes in environmental/weather factors like winds cause the crop plants to deflect the pulses away.
- Vegetable crops exhibit a complicated geometrical relationship with point cloud compared to cereal crops. Sensitivity of the estimations of vegetable crop biophysical characteristics, specific to N levels, may also be influenced by unpredictable events, such as changes in N availability due to heavy rainfall, run-off etc.
- The learning-based classification or prediction models, including the deep learning models CropPointNet, CropTemporalNet developed in this thesis, are partially sensitive to the crops' phenological stage. With fine tuning of method based parameters, it is expected that the same models can be extended onto farmer's field and up scaled to larger geographical locations.

CHAPTER 7

MAJOR THESIS CONTRIBUTION AND DIRECTION OF FUTURE WORK

This thesis has undertaken studies, developed methods, and algorithmic process flow on three important aspects of RS technology application in agriculture - estimation of some important functional biophysical parameters, classification of crops at plant level, and prediction of crop height, and crown area using statistical, ML and DL techniques.

- Explored the potential of high-density terrestrial laser scanning for the retrieval of plant-level crop height and crown area and further estimated crops' biomass across the growing seasons and under different nitrogen treatments.
- A Deep CNN based model named as "CropPointNet" has been developed for the plant levelclassification of LiDAR point cloud for vegetable crops.
- Established that high-density LiDAR point cloud alone, even though very dense, will not be sufficient to discriminate crops with sensitivity to nitrogen levels.
- Traditional machine learning, and deep learning methods have been explored for the fusion of LiDAR and WorldView-III satellite imagery for the object-based classification of crops, reference to N levels.
- A crop growth stage prediction model "TemporalCropNet", based on stacked RNN based deep learning architectures (GRU and LSTM), has been developed and applied for plant-level crop height and crown area prediction.

7.1 Future Scope of the Work

The work accomplished in this thesis can be extended as summarised below.

- The methods and algorithms developed in this thesis have been implemented on vegetable crops. For understanding the transfer characteristics of the models, studies are to be conducted on other row crops with and without characteristic canopy shapes.
- The multispectral data used in this thesis is satellite imagery. For better spatial resolution compatibility with LiDAR point cloud, we recommend acquiring multispectral imagery from airborne or UAV-based platforms simultaneously with the LiDAR point cloud acquisition.
- The DL based prediction model "TemporalCropNet" has the potential to serve as a generic framework for the prediction of crop structural parameters well before the establishment of crops and is a valuable tool for pre-planning agronomic management interventions. This model needs to be validated across different cropping systems with considering different crops and phenological stages.

LIST OF PUBLICATIONS

Journal Articles

1. Reji, J., Nidamanuri, R.R., Ramiya, A.M., Astor, T., Wachendorf, M. and Buerkert, A., 2021. Multi-temporal estimation of vegetable crop biophysical parameters with varied nitrogen fertilization using terrestrial laser scanning. *Computers and Electronics in Agriculture*, *184*, p.106051.

2. Jayakumari, R., Nidamanuri, R.R. and Ramiya, A.M., 2021. Object-level classification of vegetable crops in 3D LiDAR point cloud using deep learning convolutional neural networks. *Precision Agriculture*, pp.1-17.

3. Nidamanuri, R.R., Jayakumari, R., Ramiya, A.M., Astor, T., Wachendorf, M. and Buerkert, A., 2022. Integration of very high resolution WorldView-III and TLS LiDAR data for vegetable crop discrimination. *Biosystems Engineering*, *222*, pp.177-195.

4. Jayakumari, R., Nidamanuri, R.R., 2023. High-resolution multispectral imagery and LiDAR point cloud fusion for the discrimination and biophysical characterisation of vegetable crops at different levels of nitrogen [submitted: Applied SoftComputing]

5. Reji J, Nidamanuri RR., 2023. Deep ealrning based fusion of LiDAR point cloud and multispectral imagery for crop classification sensitive to nitrogen level [submitted: Information Fusion]

Conference proceedings

1. Reji J, Nidamanuri RR and Ramiya A.M,2020. Integration of World View –III and terrestrial LiDAR for horticulture crop discrimination. IEEE India Geoscience and Remote Sensing Young Researchers Conclave 2020. *Won best oral presentation award.*

2. Reji J, Nidamanuri RR., 2023. Deep Learning based fusion of LiDAR point cloud and multispectral imagery for crop classification sensitive to nitrogen level. International Conference on Machine Intelligence for GeoAnalytics and Remote Sensing, 2023.

REFERENCES

‘

Adam, E., Mutanga, O., Abdel-Rahman, E.M. and Ismail, R., 2014. Estimating standing biomass in papyrus (Cyperus papyrus L.) swamp: exploratory of in situ hyperspectral indices and random forest regression. *International Journal of Remote Sensing*, *35*(2), pp.693-714.

Adam, E., Mutanga, O. and Rugege, D., 2010. Multispectral and hyperspectral remote sensing for identification and mapping of wetland vegetation: a review. *Wetlands Ecology and Management*, *18*(3), pp.281-296.

Adao, T., Hruska, J., Padua, L., Bessa, J., Peres, E., Morais, R., Sousa, J.J., 2017. Hyperspectral imaging: A review on UAV-based sensors, data processing and applications for agriculture and forestry. Remote Sensing 9, 1–31.

Ahmed, O.S., Franklin, S.E., Wulder, M.A. and White, J.C., 2015. Characterizing stand-level forest canopy cover and height using Landsat time series, samples of airborne LiDAR, and the Random Forest algorithm. *ISPRS Journal of Photogrammetry and Remote Sensing*, *101*, pp.89-101.

Aubry-Kientz, M., Dutrieux, R., Ferraz, A., Saatchi, S., Hamraz, H., Williams, J., Coomes, D., Piboule, A. and Vincent, G., 2019. A comparative assessment of the performance of individual tree crowns delineation algorithms from ALS data in tropical forests. *Remote Sensing*, *11*(9), p.1086.

Axelsson, P., 2000. DEM generation from laser scanner data using adaptive TIN models. *International archives of photogrammetry and remote sensing*, *33*(4), pp.110-117.

Baatz, M., 2000. Multiresolution segmentation: an optimization approach for high quality multi-scale image segmentation. *Angewandte geographische informationsverarbeitung*, pp.12-23.

Battude, M., Al Bitar, A., Morin, D., Cros, J., Huc, M., Sicre, C.M., Le Dantec, V. and Demarez, V., 2016. Estimating maize biomass and yield over large areas using high spatial and temporal resolution Sentinel-2 like remote sensing data. *Remote Sensing of Environment*, *184*, pp.668-681.

Becker-Reshef, I., Justice, C., Sullivan, M., Vermote, E., Tucker, C., Anyamba, A., Small, J., Pak, E., Masuoka, E., Schmaltz, J. and Hansen, M., 2010. Monitoring global croplands with coarse resolution earth observations: The Global Agriculture Monitoring (GLAM) project. Remote Sensing, 2(6), pp.1589-1609.

Benomar, L., DesRochers, A. and Larocque, G.R., 2011. Changes in specific leaf area and photosynthetic nitrogen-use efficiency associated with physiological acclimation of two hybrid poplar clones to intraclonal competition. *Canadian journal of forest research*, *41*(7), pp.1465-1476.

Belgiu, M. and Drăguţ, L., 2016. Random forest in remote sensing: A review of applications and future directions. *ISPRS journal of photogrammetry and remote sensing*, *114*, pp.24-31.

Bellocchi, G., Rivington, M., Donatelli, M. and Matthews, K., 2011. Validation of biophysical models: issues and methodologies. *Sustainable Agriculture Volume 2*, pp.577-603.

Bendig, J., Bolten, A., Bennertz, S., Broscheit, J., Eichfuss, S. and Bareth, G., 2014. Estimating biomass of barley using crop surface models (CSMs) derived from UAV-based RGB imaging. *Remote sensing*, *6*(11), pp.10395-10412.

BEUCHER, S., 1993. The Morphological Approach to Segmentation: The Watershed Transformation. *Mathematics of Morphology in Image Processing*, pp.433-482.

Biskup, B., Scharr, H., Schurr, U. and Rascher, U.W.E., 2007. A stereo imaging system for measuring structural parameters of plant canopies. *Plant, cell & environment*, *30*(10), pp.1299-1308.

Blaschke, T., 2010. Object based image analysis for remote sensing. *ISPRS journal of photogrammetry and remote sensing*, *65*(1), pp.2-16.

Breiman, L., 2001. Random forests. *Machine learning*, *45*, pp.5-32.

Camps-Valls, G., Shervashidze, N. and Borgwardt, K.M., 2010. Spatio-spectral remote sensing image classification with graph kernels. *IEEE Geoscience and Remote Sensing Letters*, *7*(4), pp.741-745.

Calders, K., Adams, J., Armston, J., Bartholomeus, H., Bauwens, S., Bentley, L.P., Chave, J., Danson, F.M., Demol, M., Disney, M. and Gaulton, R., 2020. Terrestrial laser scanning in forest ecology: Expanding the horizon. *Remote Sensing of Environment*, *251*, p.112102.

Chang, S., Lee, U., Hong, M.J., Jo, Y.D. and Kim, J.B., 2021. Time-series growth prediction model based on U-Net and machine learning in Arabidopsis. *Frontiers in Plant Science*, p.2454.

Chao, Z., Liu, N., Zhang, P., Ying, T. and Song, K., 2019. Estimation methods developing with remote sensing information for energy crop biomass: A comparative review. *Biomass and Bioenergy*, *122*, pp.414-425.

Chawade, A., van Ham, J., Blomquist, H., Bagge, O., Alexandersson, E. and Ortiz, R., 2019. High-throughput field-phenotyping tools for plant breeding and precision agriculture. *Agronomy*, *9*(5), p.258.

Chlingaryan, A., Sukkarieh, S. and Whelan, B., 2018. Machine learning approaches for crop yield prediction and nitrogen status estimation in precision agriculture: A review. *Computers and electronics in agriculture*, *151*, pp.61-69.

Claverie, M., Demarez, V., Duchemin, B., Hagolle, O., Ducrot, D., Marais-Sicre, C., Dejoux, J.F., Huc, M., Keravec, P., Béziat, P. and Fieuzal, R., 2012. Maize and sunflower biomass estimation in southwest France using high spatial and temporal resolution remote sensing data. *Remote Sensing of Environment*, *124*, pp.844-857.

Clark, M.L., Roberts, D.A., Ewel, J.J., and Clark, D.B., 2011. Estimation of tropical rain forest aboveground biomass with small-footprint lidar and hyperspectral sensors. *Remote Sensing of Environment*, 115: 2931–2942.

Cloutis, E.A., Connery, D.R., Major, D.J. and Dover, F.J., 1996. Airborne multi-spectral monitoring of agricultural crop status: effect of time of year, crop type and crop condition parameter. *Remote Sensing*, *17*(13), pp.2579-2601.

Colaço, A.F., Molin, J.P. and Rosell-Polo, J.R., 2019. Spatial variability in commercial orange groves. Part 1: canopy volume and height. *Precision Agriculture*, *20*(4), pp.788-804.

Corcoran, J.M., Knight, J.F. and Gallant, A.L., 2013. Influence of multi-source and multi-temporal remotely sensed and ancillary data on the accuracy of random forest classification of wetlands in Northern Minnesota. *Remote Sensing*, *5*(7), pp.3212-3238.

Erudel, T., Fabre, S., Houet, T., Mazier, F. and Briottet, X., 2017. Criteria comparison for classifying peatland vegetation types using in situ hyperspectral measurements. *Remote Sensing*, *9*(7), p.748.

Ehlert, D., Adamek, R., Horn, H.J., 2009. Laser rangefinder-based measuring of crop biomass under field conditions. Precision Agriculture 10, 395–408.

Eitel, J.U., Magney, T.S., Vierling, L.A., Brown, T.T. and Huggins, D.R., 2014. LiDAR based biomass and crop nitrogen estimates for rapid, non-destructive assessment of wheat nitrogen status. *Field Crops Research*, *159*, pp.21-32.

Feng, L., Raza, M.A., Li, Z., Chen, Y., Khalid, M.H.B., Du, J., su, W., Wu, X., Song, C., Yu, L. and Zhang, Z., 2019. The influence of light intensity and leaf movement on

photosynthesis characteristics and carbon balance of soybean. *Frontiers in plant science*, *9*, p.1952.

Fieber, K.D., Davenport, I.J., Tanase, M.A., Ferryman, J.M., Gurney, R.J., Becerra, V.M., Walker, J.P., and Hacker, J.M., 2015. Validation of canopy height profile methodology for small-footprint full-waveform airborne LiDAR data in a discontinuous canopy environment. ISPRS Journal of Photogrammetry and Remote Sensing, 104: 144–157.

Forkuor, G., Hounkpatin, O. K. L., Welp, G., & Thiel, M., 2017. High Resolution Mapping of Soil Properties Using Remote Sensing Variables in South-Western Burkina Faso: A Comparison of Machine Learning and Multiple Linear Regression Models. *PLoS ONE*, *12*(1), e0170478. http://doi.org/10.1371/journal.pone.0170478.

Franco, M. and Kelly, C.K., 1998. The interspecific mass–density relationship and plant geometry. *Proceedings of the National Academy of Sciences*, *95*(13), pp.7830-7835.

Friedli, M., Kirchgessner, N., Grieder, C., Liebisch, F., Mannale, M. and Walter, A., 2016. Terrestrial 3D laser scanning to track the increase in canopy height of both monocot and dicot crop species under field conditions. *Plant methods*, *12*, pp.1-15.

García, M., Saatchi, S., Ustin, S. and Balzter, H., 2018. Modelling forest canopy height by integrating airborne LiDAR samples with satellite Radar and multispectral imagery. *International journal of applied earth observation and geoinformation*, *66*, pp.159-173.

Ganguly, S., Nemani, R.R., Zhang, G., Hashimoto, H.,Milesi, C., Michaelis, A., and Dungan, J.L., 2012.Generating global leaf area index from Landsat:Algorithm formulation and demonstration. Remote Sensing of Environment, 122, 185–202. doi:10.1016/j.rse.2011.10.032.

Goel, P., Prasher, S., Landry, J.-A., Patel, R., Viau, A., Miller, J., 2003. Estimation of crop biophysical parameters through airborne and field hyperspectral remote sensing. Transactions of the American Society of Agricultural Engineers 46, 1235 – 1246.

Großkinsky, D.K., Svensgaard, J., Christensen, S. and Roitsch, T., 2015. Plant phenomics and the need for physiological phenotyping across scales to narrow the genotype-to-phenotype knowledge gap. *Journal of experimental botany*, *66*(18), pp.5429-5440.

Guo, Y., Bennamoun, M., Sohel, F., Lu, M. and Wan, J.,2014. 3d object recognition in cluttered scenes with local surface features: a survey. Trans. PAMI, 36(11):2270– 2287.

Guan, Z., Abd-Elrahman, A., Fan, Z., Whitaker, V.M. and Wilkinson, B., 2020. Modeling strawberry biomass and leaf area using object-based analysis of high-resolution images. *ISPRS Journal of Photogrammetry and Remote Sensing*, *163*, pp.171-186.

Hackel, T., Wegner, J.D. and Schindler, K., 2016. Fast semantic segmentation of 3D point clouds with strongly varying density. *ISPRS annals of the photogrammetry, remote sensing and spatial information sciences*, *3*, pp.177-184.

He, Y., Liang, B., Yang, J., Li, S. and He, J., 2017. An iterative closest points algorithm for registration of 3D laser scanner point clouds with geometric features. *Sensors*, *17*(8), p.1862.

Hoffmeister, D., Waldhoff, G., Curdt, C., Tilly, N., Bendig, J. and Bareth, G., 2013. Spatial variability detection of crop height in a single field by terrestrial laser scanning. In *Precision agriculture'13* (pp. 267-274). Wageningen Academic Publishers, Wageningen.

Hosoi, F., Omasa, K., 2009. Estimating vertical plant area density profile and growth parameters of a wheat canopy at different growth stages using three-dimensional portable LIDAR imaging. ISPRS Journal of Photogrammetry and Remote Sensing 64, 151–158.

Hosoi, F. and Omasa, K., 2006. Voxel-based 3-D modeling of individual trees for estimating leaf area density using high-resolution portable scanning lidar. *IEEE transactions on geoscience and remote sensing*, *44*(12), pp.3610-3618.

Huang, J., Gómez-Dans, J.L., Huang, H., Ma, H., Wu, Q., Lewis, P.E., Liang, S., Chen, Z., Xue, J.H., Wu, Y. and Zhao, F., 2019. Assimilation of remote sensing into crop growth models: Current status and perspectives. *Agricultural and Forest Meteorology*, *276*, p.107609.

Huang, J. and You, S., 2016, December. Point cloud labelling using 3d convolutional neural network. In 2016 23rd International Conference on Pattern Recognition (ICPR) (pp. 2670-2675). IEEE.

Hunt, E.R., Hively, W.D., Fujikawa, S.J., Linden, D.S., Daughtry, C.S. and McCarty, G.W., 2010. Acquisition of NIR-green-blue digital photographs from unmanned aircraft for crop monitoring. *Remote Sensing*, *2*(1), pp.290-305.

Ienco, D., Gaetano, R., Interdonato, R., Ose, K. and Minh, D.H.T., 2019, July. Combining Sentinel-1 and Sentinel-2 Time Series via RNN for object-based land cover classification. In *IGARSS 2019-2019 IEEE International Geoscience and Remote Sensing Symposium* (pp. 4881-4884). IEEE.

Jaderberg, M., Simonyan, K., Zisserman, A. and Kavukcuoglu, K., 2015. Spatial transformer networks. *arXiv preprint arXiv:1506.02025*.

Jin, S., Su, Y., Song, S., Xu, K., Hu, T., Yang, Q., Wu, F., Xu, G., Ma, Q., Guan, H. and Pang, S., 2020. Non-destructive estimation of field maize biomass using terrestrial lidar: an evaluation from plot level to individual leaf level. *Plant Methods*, *16*, pp.1-19.

Jin, S., Su, Y., Gao, S., Wu, F., Hu, T., Liu, J., Li, W., Wang, D., Chen, S., Jiang, Y. and Pang, S., 2018. Deep learning: individual maize segmentation from terrestrial lidar data using faster R-CNN and regional growth algorithms. *Frontiers in plant science*, *9*, p.866.

Jha, S.S., Manohar Kumar, C.V.S.S. and Nidamanuri, R.R., 2021. Flexible atmospheric compensation technique (FACT): a 6S based atmospheric correction scheme for remote sensing data. *Geocarto International*, *36*(1), pp.28-46.

Jimenez-Berni, J.A., Deery, D.M., Rozas-Larraondo, P., Condon, A.T.G., Rebetzke, G.J., James, R.A., Bovill, W.D., Furbank, R.T. and Sirault, X.R., 2018. High throughput determination of plant height, ground cover, and above-ground biomass in wheat with LiDAR. *Frontiers in plant science*, *9*, p.237.

Jones, T.J., Coops, N.C., and Sharma, T., 2010. Assessing the utility of airborne hyperspectral and LiDAR data for species distribution mapping in the coastal Pacific Northwest, Canada. *Remote Sensing of Environment*, 114: 2841–2852.

Kayad, A., Sozzi, M., Gatto, S., Marinello, F. and Pirotti, F., 2019. Monitoring within-field variability of corn yield using Sentinel-2 and machine learning techniques. *Remote Sensing*, *11*(23), p.2873.

Khan, A., Hansen, M.C., Potapov, P., Stehman, S.V. and Chatta, A.A., 2016. Landsat-based wheat mapping in the heterogeneous cropping system of Punjab, Pakistan. *International Journal of Remote Sensing*, *37*(6), pp.1391-1410.

Khosravipour, A., Skidmore, A.K., Isenburg, M., Wang, T., Hussin, Y.A., 2014. Generating pit-free canopy height models from airborne lidar. Photogrammetric Engineering & Remote Sensing 80, 863–872. doi:10.14358/PERS.80.9.863.

Kjaer, K.H. and Ottosen, C.O., 2015. 3D laser triangulation for plant phenotyping in challenging environments. *Sensors*, *15*(6), pp.13533-13547.

Klukas, C., Chen, D. and Pape, J.M., 2014. Integrated analysis platform: an open-source information system for high-throughput plant phenotyping. *Plant physiology*, *165*(2), pp.506-518.

Lang, N., Schindler, K. and Wegner, J.D., 2019. Country-wide high-resolution vegetation height mapping with Sentinel-2. *Remote Sensing of Environment*, *233*, p.111347.

Lowphansirikul, C., Kim, K.S., Vinayaraj, P. & Tuarob, S., 2019. 3D Semantic segmentation of large-scale point-clouds in urban areas using deep learning. In *Proceedings of the IEEE 11th International Conference on Knowledge and Smart Technology*, 23-26 Jan. 2019, Phuket, Thailand. 10.1109/KST.2019.8687813.

Li, W., Niu, Z., Shang, R., Qin, Y., Wang, L. and Chen, H., 2020. High-resolution mapping of forest canopy height using machine learning by coupling ICESat-2 LiDAR with Sentinel-1, Sentinel-2 and Landsat-8 data. *International Journal of Applied Earth Observation and Geoinformation*, *92*, p.102163.

Li, C. R. Q., Su, H., & Guibas, L. J., 2018. PointNet++. Proceedings of the IEEE Computer Society Conference on Computer Vision and Pattern Recognition, 7652–7660. https://doi.org/10.1109/CVPR.2018.00798.

Li, Z. and Chen, Z., 2011, July. Remote sensing indicators for crop growth monitoring at different scales. In *2011 IEEE International Geoscience and Remote Sensing Symposium* (pp. 4062-4065). IEEE.

Li, L., Zhang, Q. and Huang, D., 2014. A review of imaging techniques for plant phenotyping. *Sensors*, *14*(11), pp.20078-20111.

Li, W., Weiss, M., Waldner, F., Defourny, P., Demarez, V., Morin, D., Baret, F., 2015. A generic algorithm to estimate LAI, FAPAR and FCOVER variables from SPOT4_HRVIR and landsat sensors: Evaluation of the consistency and comparison with ground measurements.Remote Sensing, 7(12), 15494–15516. doi:10.3390/rs71115494.

Lichti, D.D., 2002. Ground-based laser scanners: operation, systems and applications. *Geomatica*, *56*(1), pp.21-33.

Lin, T., Zhong, R., Wang, Y., Xu, J., Jiang, H., Xu, J., Ying, Y., Rodriguez, L., Ting, K.C. and Li, H., 2020. DeepCropNet: a deep spatial-temporal learning framework for county-level corn yield estimation. *Environmental Research Letters*, *15*(3), p.034016.

Lin, Y., 2015. LiDAR: An important tool for next-generation phenotyping technology of high potential for plant phenomics?. *Computers and electronics in Agriculture*, *119*, pp.61-73.

Liu, Y., Piramanayagam, S., Monteiro, S.T. and Saber, E., 2019. Semantic segmentation of multisensor remote sensing imagery with deep ConvNets and higher-order conditional random fields. *Journal of Applied Remote Sensing*, *13*(1), p.016501.

Lu, D., Chen, Q., Wang, G., Liu, L., Li, G. and Moran, E., 2016. A survey of remote sensing-based aboveground biomass estimation methods in forest ecosystems. *International Journal of Digital Earth*, *9*(1), pp.63-105.

Lumme, J., Karjalainen, M., Kaartinen, H., Kukko, A., Hyyppä, J., Hyyppä, H., Jaakkola, A. and Kleemola, J., 2008. Terrestrial laser scanning of agricultural crops. *Int. Arch. Photogramm. Remote Sens. Spat. Inf. Sci*, *37*, pp.563-566.

Luo, S., Liu, W., Zhang, Y., Wang, C., Xi, X., Nie, S., Ma, D., Lin, Y. and Zhou, G., 2021. Maize and soybean heights estimation from unmanned aerial vehicle (UAV) LiDAR data. *Computers and Electronics in Agriculture*, *182*, p.106005.

Madec, S., Baret, F., De Solan, B., Thomas, S., Dutartre, D., Jezequel, S., Hemmerlé, M., Colombeau, G. and Comar, A., 2017. High-throughput phenotyping of plant height: comparing unmanned aerial vehicles and ground LiDAR estimates. *Frontiers in plant science*, *8*, p.2002.

Malhi, Y., Jackson, T., Patrick Bentley, L., Lau, A., Shenkin, A., Herold, M., Calders, K., Bartholomeus, H. and Disney, M.I., 2018. New perspectives on the ecology of tree

structure and tree communities through terrestrial laser scanning. *Interface Focus*, *8*(2), p.20170052.

Marcial-Pablo, M.D.J., Gonzalez-Sanchez, A., Jimenez-Jimenez, S.I., Ontiveros-Capurata, R.E. and Ojeda-Bustamante, W., 2019. Estimation of vegetation fraction using RGB and multispectral images from UAV. *International journal of remote sensing*, *40*(2), pp.420-438.

Mariotto, I., Thenkabail, P.S., Huete, A., Slonecker, E.T. and Platonov, A., 2013. Hyperspectral versus multispectral crop-productivity modeling and type discrimination for the HyspIRI mission. *Remote Sensing of Environment*, *139*, pp.291-305.

Maurer, T., 2013. How to pan-sharpen images using the gram-schmidt pan-sharpen method–A recipe.

McNairn, H., Kross, A., Lapen, D., Caves, R. and Shang, J., 2014. Early season monitoring of corn and soybeans with TerraSAR-X and RADARSAT-2. *International Journal of Applied Earth Observation and Geoinformation*, *28*, pp.252-259.

Meij, B.V.D., Kooistra, L., Suomalainen, J., Barel, J.M. and Deyn, G.B.D., 2017. Remote sensing of plant trait responses to field-based plant–soil feedback using UAV-based optical sensors. *Biogeosciences*, *14*(3), pp.733-749.

Moeckel, T., Dayananda, S., Nidamanuri, R.R., Nautiyal, S., Hanumaiah, N., Buerkert, A. and Wachendorf, M., 2018. Estimation of vegetable crop parameter by multi-temporal UAV-borne images. *Remote Sensing*, *10*(5), p.805.

Murray, J., Fennell, T.H., Blackburn, G.A., Whyatt, J.D. & Li, B., 2020. The novel use of proximal photogrammetry and terrestrial LiDAR to quantify the structural complexity of orchard trees. Precision Agriculture, 21, 473–483.

Mutanga, O. and Skidmore, A.K., 2004. Hyperspectral band depth analysis for a better estimation of grass biomass (Cenchrus ciliaris) measured under controlled laboratory conditions. *International journal of applied earth observation and geoinformation*, *5*(2), pp.87-96.

Næsset, E., 2002. Predicting forest stand characteristics with airborne scanning laser using a practical two-stage procedure and field data. *Remote sensing of environment*, *80*(1), pp.88-99.

Næsset, E. and Bjerknes, K.O., 2001. Estimating tree heights and number of stems in young forest stands using airborne laser scanner data. *Remote sensing of Environment*, *78*(3), pp.328-340.

Nebiker, S., Annen, A., Scherrer, M. and Oesch, D., 2008. A light-weight multispectral sensor for micro UAV—Opportunities for very high resolution airborne remote sensing. *Int. Arch. Photogramm. Remote Sens. Spat. Inf. Sci*, *37*(B1), pp.1193-1200.

Nevavuori, P., Narra, N., Linna, P. and Lipping, T., 2020. Crop Yield Prediction Using Multitemporal UAV Data and Spatio-Temporal Deep Learning Models. *Remote Sensing*, *12*(23), p.4000.

Nidamanuri, R.R., Zbell, B., 2011. Normalized spectral similarity score (NS3) as an efficient spectral library searching method for hyperspectral image classification. IEEE Journal of Selected Topics in Applied Earth Observations and Remote Sensing, 4, 226–240.

Nidamanuri, R.R. and Zbell, B., 2010. Normalized Spectral Similarity Score (NS^3) as an Efficient Spectral Library Searching Method for Hyperspectral Image Classification. *IEEE Journal of Selected Topics in Applied Earth Observations and Remote Sensing*, *4*(1), pp.226-240.

Nidamanuri, R.R., Garg, P.K., Ghosh, S.K., 2007. Development of an agricultural crops spectral library and classification of crops at cultivar level using hyperspectral data. Precision Agriculture, 8, 173–185.

Niemeyer, J., Rottensteiner, F. and Soergel, U., 2014. Contextual classification of lidar data and building object detection in urban areas. *ISPRS journal of photogrammetry and remote sensing*, *87*, pp.152-165.

Nie, S., Wang, C., Dong, P. and Xi, X., 2016. Estimating leaf area index of maize using airborne full-waveform lidar data. *Remote Sensing Letters*, *7*(2), pp.111-120.

Olsoy, P.J., Glenn, N.F. and Clark, P.E., 2014. Estimating sagebrush biomass using terrestrial laser scanning. *Rangeland Ecology & Management*, *67*(2), pp.224-228.

Otsu, K., Pla, M., Duane, A., Cardil, A. and Brotons, L., 2019. Estimating the threshold of detection on tree crown defoliation using vegetation indices from UAS multispectral imagery. *Drones*, *3*(4), p.80.

Pask, A., Pietragalla, J., Mullan, D. and Reynolds, M.P., 2012. Physiological breeding II: a field guide to wheat phenotyping.

Paulus, S., Dupuis, J., Riedel, S. and Kuhlmann, H., 2014. Automated analysis of barley organs using 3D laser scanning: An approach for high throughput phenotyping. *Sensors*, *14*(7), pp.12670-12686.

Paulus, S., Dupuis, J., Mahlein, A.K. and Kuhlmann, H., 2013. Surface feature based classification of plant organs from 3D laserscanned point clouds for plant phenotyping. *BMC bioinformatics*, *14*(1), pp.1-12.

Phattaralerphong, J. and Sinoquet, H., 2005. A method for 3D reconstruction of tree crown volume from photographs: assessment with 3D-digitized plants. *Tree Physiology*, *25*(10), pp.1229-1242.

Popescu, S.C., Wynne, R.H., 2004. Seeing the trees in the forest: using lidar and multispectral data fusion with local filtering and variable window size for estimating tree height. Photogramm. Eng. Remote Sens. 70, 589–604. https://doi.org/10.14358/PERS.70.5.589.

Poorter, H., Niklas, K.J., Reich, P.B., Oleksyn, J., Poot, P. and Mommer, L., 2012. Biomass allocation to leaves, stems and roots: meta-analyses of interspecific variation and environmental control. *New Phytologist*, *193*(1), pp.30-50.

Pedergnana, M., Marpu, P.R., Dalla Mura, M., Benediktsson, J.A. and Bruzzone, L., 2013. A novel technique for optimal feature selection in attribute profiles based on genetic algorithms. *IEEE Transactions on Geoscience and Remote Sensing*, *51*(6), pp.3514-3528.

Pirotti, F., 2010. IceSAT/GLAS waveform signal processing for ground cover classification: state of the art. *Italian Journal of Remote Sensing*, *42*(2), pp.13-26.

Poenaru, V., Badea, A., Cimpeanu, S.M. and Irimescu, A., 2015. Multi-temporal multi-spectral and radar remote sensing for agricultural monitoring in the Braila Plain. *Agriculture and Agricultural Science Procedia*, *6*, pp.506-516.

Pound, M.P., French, A.P., Murchie, E.H. and Pridmore, T.P., 2014. Automated recovery of three-dimensional models of plant shoots from multiple color images. *Plant physiology*, *166*(4), pp.1688-1698.

Peerbhay, K.Y., Mutanga, O. and Ismail, R., 2015. Random forests unsupervised classification: The detection and mapping of solanum mauritianum infestations in plantation forestry using hyperspectral data. *IEEE Journal of Selected Topics in Applied Earth Observations and Remote Sensing*, *8*(6), pp.3107-3122.

Qi, C.R., Su, H., Mo, K. & Guibas, L. J., 2017. PointNet: Deep learning on point sets for 3D classification and segmentation. In: *Proceedings - 30th IEEE Conference on Computer Vision and Pattern Recognition, CVPR 2017*. 77–85. doi:10.1109/CVPR.2017.16

Qi, C. R., Yi, L., Su, H., Guibas, L. J., 2017. Pointnet++: Deep hierarchical feature learning on point sets in a metric space. Advances in Neural Information Processing Systems, 5099–5108.

Ramoelo, A., Cho, M.A., Mathieu, R., Madonsela, S., Van De Kerchove, R., Kaszta, Z. and Wolff, E., 2015. Monitoring grass nutrients and biomass as indicators of rangeland quality and quantity using random forest modelling and WorldView-2 data. *International journal of applied earth observation and geoinformation*, *43*, pp.43-54.

Rosell, J.R. and Sanz, R., 2012. A review of methods and applications of the geometric characterization of tree crops in agricultural activities. *Computers and electronics in agriculture*, *81*, pp.124-141.

Saha, K.K., Tsoulias, N., Weltzien, C. and Zude-Sasse, M., 2022. Estimation of vegetative growth in strawberry plants using mobile LiDAR laser scanner. *Horticulturae*, *8*(2), p.90.

Sahoo, R.N., Ray, S.S. and Manjunath, K.R., 2015. Hyperspectral remote sensing of agriculture. *Current Science*, pp.848-859.

Seok, K.H., Cho, D., Hwang, C. and Shim, J., 2010, June. Support vector quantile regression using asymmetric e-insensitive loss function. In *2010 2nd International Conference on Education Technology and Computer* (Vol. 1, pp. V1-438). IEEE.

Shelestov, A., Kolotii, A., Camacho, F., Skakun, S., Kussul, O., Lavreniuk, M., &Kostetsky, O., 2015. Mapping of biophysical parameters based on high resolution EO imagery for JECAM test site in Ukraine. In Geoscience and Remote Sensing Symposium (IGARSS), 2015 IEEE International (pp. 1733–1736). IEEE.

Shwetank, S., Jain, K. and Bhatia, K., 2012. Development of digital spectral library and supervised classification of rice crop varieties using hyperspectral image processing. *Asian Journal of Geoinformatics*, *11*(3).

Shim, J.Y, and Chang, H.H., 2011. Support vector quantile regression using asymmetric ε-insensitive loss function. Communications for Statistical Applications and Methods 18, 165–170.

Singh, B.M., Komal, C. and Victorovich, K.A., 2020. Crop growth monitoring through Sentinel and Landsat data based NDVI time-series. Компьютерная оптика, 44(3).

Singh, K.K., Vogler, J.B., Shoemaker, D.A. and Meentemeyer, R.K., 2012. LiDAR-Landsat data fusion for large-area assessment of urban land cover: Balancing spatial resolution, data volume and mapping accuracy. *ISPRS Journal of Photogrammetry and Remote Sensing*, *74*, pp.110-121.

Skakun, S., Franch, B., Vermote, E., Roger, J.C., Becker-Reshef, I., Justice, C. and Kussul, N., 2017. Early season large-area winter crop mapping using MODIS NDVI data, growing degree days information and a Gaussian mixture model. *Remote Sensing of Environment*, *195*, pp.244-258.

Soilán Rodríguez, M., Lindenbergh, R., Riveiro Rodríguez, B. and Sánchez Rodríguez, A., 2019. Pointnet for the automatic classification of aerial point clouds.

Sritarapipat, T., Rakwatin, P. and Kasetkasem, T., 2014. Automatic rice crop height measurement using a field server and digital image processing. *Sensors*, *14*(1), pp.900-926.

Su, H., Maji, S., Kalogerakis, E. and Learned-Miller, E., 2015. Multi-view convolutional neural networks for 3d shape recognition. In *Proceedings of the IEEE international conference on computer vision* (pp. 945-953).

Tchapmi, L., Choy, C., Armeni, I., Gwak, J. and Savarese, S., 2017, October. Segcloud: Semantic segmentation of 3d point clouds. In *2017 international conference on 3D vision (3DV)* (pp. 537-547). IEEE.

Tesfamichael, S.G., Van Aardt, J.A.N. and Ahmed, F., 2010. Estimating plot-level tree height and volume of Eucalyptus grandis plantations using small-footprint, discrete return lidar data. *Progress in physical Geography*, *34*(4), pp.515-540.

Tetteh Kwasi Nuer, A., Agbeko, D., Worlali, S., Mwangi Thiga, M., Ndogo Ndungu, S., Wangari Mutiga, M. and Babcock, L.H., 2018. *Why Invest in ICTs for agriculture?*. CTA.

Thenkabail, P.S., Lyon, J.G. and Huete, A., 2018. Advances in hyperspectral remote sensing of vegetation and agricultural crops. In *Fundamentals, Sensor Systems, Spectral Libraries, and Data Mining for Vegetation* (pp. 3-37). CRC Press.

Thenkabail, P.S. and Lyon, J.G. eds., 2016. *Hyperspectral remote sensing of vegetation*. CRC press.

Thenkabail, P.S., Mariotto, I., Gumma, M.K., Middleton, E.M., Landis, D.R. and Huemmrich, K.F., 2013. Selection of hyperspectral narrowbands (HNBs) and composition of hyperspectral twoband vegetation indices (HVIs) for biophysical characterization and discrimination of crop types using field reflectance and Hyperion/EO-1 data. *IEEE Journal of Selected Topics in Applied Earth Observations and Remote Sensing*, *6*(2), pp.427-439.

Tilly, N., Hoffmeister, D., Cao, Q., Huang, S., Lenz-Wiedemann, V., Miao, Y. and Bareth, G., 2014. Multitemporal crop surface models: accurate plant height measurement and biomass estimation with terrestrial laser scanning in paddy rice. *Journal of Applied Remote Sensing*, *8*(1), p.083671.

Tong, H., Maxwell, T., Zhang, Y. and Dey, V., 2012. A supervised and fuzzy-based approach to determine optimal multi-resolution image segmentation parameters.

Tilly, N., Aasen, H. and Bareth, G., 2015. Fusion of plant height and vegetation indices for the estimation of barley biomass. *Remote Sensing*, *7*(9), pp.11449-11480.

Van Der Meij, B., Kooistra, L., Suomalainen, J., Barel, J.M., De Deyn, G.B., 2017. Remote sensing of plant trait responses to field-based plant-soil feedback using UAV-based optical sensors. Biogeosciences 14, 733–749.

Vapnik, V., 1998. Statistical Learning Theory: New York etc.

Varfolomeev, I., Yakimchuk, I. and Safonov, I., 2019. An application of deep neural networks for segmentation of microtomographic images of rock samples. *Computers*, *8*(4), p.72.

Verrelst, J., Rivera, J.P., Moreno, J. and Camps-Valls, G., 2013. Gaussian processes uncertainty estimates in experimental Sentinel-2 LAI and leaf chlorophyll content retrieval. *ISPRS journal of photogrammetry and remote sensing*, *86*, pp.157-167.

Vincent, L. and Soille, P., 1991. Watersheds in digital spaces: an efficient algorithm based on immersion simulations. *IEEE Transactions on Pattern Analysis & Machine Intelligence*, *13*(06), pp.583-598.

Walter, J.D., Edwards, J., McDonald, G. and Kuchel, H., 2019. Estimating biomass and canopy height with LiDAR for field crop breeding. *Frontiers in plant science*, *10*, p.1145.

Wang, Y., Wu, G., Deng, L., Tang, Z., Wang, K., Sun, W. and Shangguan, Z., 2017. Prediction of aboveground grassland biomass on the Loess Plateau, China, using a random forest algorithm. *Scientific reports*, *7*(1), p.6940.

Wang, L., Gong, P. and Biging, G.S., 2004. Individual tree-crown delineation and treetop detection in high-spatial-resolution aerial imagery. *Photogrammetric Engineering & Remote Sensing*, *70*(3), pp.351-357.

Weinstein, B.G., Marconi, S., Bohlman, S.A., Zare, A., Singh, A., Graves, S.J. and White, E.P. 2021. A remote sensing derived data set of 100 million individual tree crowns for the national ecological observatory network. *Elife*, *10*, p.62922.

Weiss, U., Biber, P., Laible, S., Bohlmann, K. and Zell, A., 2010, December. Plant species classification using a 3D LIDAR sensor and machine learning. In *2010 Ninth International Conference on Machine Learning and Applications* (pp. 339-345). IEEE.

Weiss, U. and Biber, P., 2011. Plant detection and mapping for agricultural robots using a 3D LIDAR sensor. *Robotics and autonomous systems*, *59*(5), pp.265-273.

Wehr, A. and Lohr, U., 1999. Airborne laser scanning—an introduction and overview. *ISPRS Journal of photogrammetry and remote sensing*, *54*(2-3), pp.68-82.

Whitehead, K. and Hugenholtz, C.H., 2014. Remote sensing of the environment with small unmanned aircraft systems (UASs), part 1: A review of progress and challenges. *Journal of Unmanned Vehicle Systems*, *2*(3), pp.69-85.

Whiting, M.L., Ustin, S.L., Zarco-Tejada, P., Palacios-Orueta, A. and Vanderbilt, V.C., 2006, September. Hyperspectral mapping of crop and soils for precision agriculture. In *Remote Sensing and Modeling of Ecosystems for Sustainability III* (Vol. 6298, p. 62980B). International Society for Optics and Photonics.

Wu, J., Yao, W., Choi, S., Park, T. and Myneni, R.B., 2015. A comparative study of predicting DBH and stem volume of individual trees in a temperate forest using airborne waveform LiDAR. *IEEE Geoscience and Remote Sensing Letters*, *12*(11), pp.2267-2271.

Yang, F., Liao, D., Wu, X., Gao, R., Fan, Y., Raza, M.A., Wang, X., Yong, T., Liu, W., Liu, J. and Du, J., 2017. Effect of aboveground and belowground interactions on the intercrop yields in maize-soybean relay intercropping systems. *Field Crops Research*, *203*, pp.16-23.

Yousefhussien, M., Kelbe, D.J., Ientilucci, E.J. and Salvaggio, C., 2018. A multi-scale fully convolutional network for semantic labeling of 3D point clouds. *ISPRS journal of photogrammetry and remote sensing*, *143*, pp.191-204.

Zhang, C., Yang, G., Jiang, Y., Xu, B., Li, X., Zhu, Y., Lei, L., Chen, R., Dong, Z. and Yang, H., 2020. Apple tree branch information extraction from terrestrial laser scanning and backpack-lidar. *Remote Sensing*, *12*(21), p.3592.

Zhongyang, Z., Yinglei, C., Xiaosong, S., Xianxiang, Q., Li, S., 2018. Classification of LiDAR Point Cloud based on Multiscale Features and PointNet. pp. 1–7. https://doi.org/10.1109/IPTA.2018.8608120

Zhou, X., Zheng, H.B., Xu, X.Q., He, J.Y., Ge, X.K., Yao, X., Cheng, T., Zhu, Y., Cao, W.X. and Tian, Y.C., 2017. Predicting grain yield in rice using multi-temporal vegetation indices from UAV-based multispectral and digital imagery. *ISPRS Journal of Photogrammetry and Remote Sensing*, *130*, pp.246-255.

***